



**TITLE:**                    **Impedance dynamics of mobile phones influenced by user interaction**

**PROJECT PERIOD:**

January, 2009 – June, 2009

**PROJECT GROUP:**

Group 1111

**MEMBERS:**

Célia Saïssset  
Pierre-Rémi Travers

**SUPERVISORS:**

Gert Pedersen  
Mauro Pelosi

**ABSTRACT**

Interactions between the human body and the personal communications are a nowadays a crucial point. Until now, studies are largely focused on the electromagnetic fields fading due to the head and the body being in the vicinity. However, it has been shown that the impact of the hand has been underestimated. Recent investigations [7], lead on the different user hand grip styles and shapes, give the possibility to examine interactions between hand models and mobile antennas.

This thesis intends to investigate the influence of the usual hand-hold position on different dual-band PIFAs antennas using the Finite-Difference-Time-Domain (FDTD) method.

The simulation analysis is based on both mismatch and absorption loss providing a comparison of performance for five types of PIFAs. Six hand models are used and different positions of the antenna are investigated. It is shown that the antenna efficiency is significantly altered owing to the hand and finger position. The antenna behaviour is described for all different configurations and some of them present

**PUBLICATIONS:**            5

**NUMBER OF PAGES:**    77

**DELIVERED :**                3 June 2009

# PREFACE

---

This report was written during the 10<sup>th</sup> semester in Mobile Communication carried out at the Department of Electronic Systems, Aalborg University, Denmark.

The purpose of this thesis is to investigate the effect of the hand on the performance of the handset antennas. The report consists of 4 main chapters. The contents, list of figures, tables, abbreviations and symbols are presented in order for the sake of reading convenience. References within the text are given as numbers within square brackets and they are listed at the end of this report.

We would like to express our recognition to our supervisors Gert Pedersen and Mauro Pelosi for their guidance and disponibility throughout this project.

Aalborg University  
June 3<sup>th</sup>, 2009

---

Célia Saïssset

---

Pierre-Rémi Travers

# CONTENTS

PREFACE.....	2
CONTENTS.....	3
LIST OF FIGURES .....	6
LIST OF TABLES.....	8
LIST OF ABBREVIATIONS.....	9
LIST OF SYMBOLS .....	10
CHAPTER 1: INTRODUCTION.....	12
1.1. PROBLEM DEFINITION .....	12
1.2. THESIS PURPOSE.....	13
1.3. REPORT OUTLINE .....	13
CHAPTER 2: TECHNICAL BACKGROUND .....	14
2.1. MAIN ANTENNAS PARAMETERS .....	14
2.1.1. Radiation Patterns .....	14
2.1.2. Antenna Impedance.....	15
2.1.3. Directivity.....	16
2.1.4. Antenna Efficiency .....	17
2.1.4.1. Total Radiated Power .....	18
2.1.4.2. Radiation Efficiency .....	18
2.1.4.3. VSWR .....	19
2.1.4.4. Mismatch and Reflection Loss .....	20
2.1.5. Gain.....	20
2.1.6. Bandwidth.....	21
2.1.7. Quality Factor.....	21
2.1.8. Specific Absorption Rate (SAR) .....	22
2.2. ELECTRICALLY SMALL ANTENNA .....	23
2.2.1. Small antennas' fundamental limitations .....	24
2.2.2. Different Small Antennas .....	25
2.2.2.1. External Antennas .....	25
2.2.2.2. Internal Antennas .....	26
2.3. INFLUENCE OF THE USER HAND ON MOBILE PHONE .....	29
2.4. FINITE DIFFERENCE TIME DOMAIN METHOD .....	31
2.4.1. Maxwell's Equations in 3D .....	31
2.4.2. The Yee Algorithm.....	33
2.4.2.1. The principle .....	33
2.4.2.2. Finite-Difference Expressions for Maxwell's Equations in 3D .....	34
2.4.3. Numerical stability .....	36
2.4.4. Numerical dispersion .....	36
2.4.5. Absorbing Boundary Conditions (ABC). .....	37
2.4.5.1. Berenger Perfectly Matched Layer .....	37
2.4.6. FD-TD applied for the Antenna Analysis .....	39
2.4.6.1. The FD-TD formulation for an antenna .....	39
2.4.6.2. Electronic circuit fundamentals .....	40
2.4.6.3. Excitation Source .....	41

<b>CHAPTER 3: SIMULATIONS</b>	<b>42</b>
<b>3.1. SENSITIVITY ANALYSIS</b>	<b>42</b>
3.1.1. Number of time steps	42
3.1.2. PML thickness	43
3.1.3. The Computational domain size	43
3.1.4. Conclusion	43
<b>3.2. BASIC HANDSET ANTENNAS</b>	<b>44</b>
3.1.5. The Monopole	44
3.1.5.1. <i>The effect of the feed position</i>	44
3.1.5.2. <i>The effect of the ground plane</i>	44
3.1.5.3. <i>Hand influence</i>	44
3.1.6. The PIFA	46
3.2.1.1. <i>Introduction of a short circuit element</i>	46
3.2.1.2. <i>Influence of the gap between the ground plane and the plate</i>	46
3.2.1.3. <i>Length and width configuration of the Plate</i>	46
3.2.1.4. <i>Ground Plane dimensions</i>	46
3.2.1.5. <i>Short circuit width effects</i>	46
3.2.1.6. <i>Feed size effects</i>	47
3.2.1.7. <i>Short position</i>	47
3.2.1.8. <i>Feed position</i>	47
3.2.1.9. <i>Introduction of a variable capacitor</i>	47
3.2.1.10. <i>Hand effect</i>	47
3.2.2. Comparison PIFA/Monopole	48
<b>3.3. HAND INFLUENCE ON MOBILE PHONE ANTENNA</b>	<b>49</b>
3.3.1. PIFA1 Profile	50
3.3.1.1. <i>Design Description</i>	50
3.3.1.2. <i>Performance in free space</i>	50
3.3.1.3. <i>Hands Influence on the antenna performances</i>	51
3.3.2. PIFA2 Profile	53
3.3.2.1. <i>Design Description</i>	53
3.3.2.2. <i>Performance in free space</i>	53
3.3.2.3. <i>Hands Influence on the antenna performances</i>	54
3.3.3. PIFA3 Profile	56
3.3.3.1. <i>Design description</i>	56
3.3.3.2. <i>Performance in free space</i>	56
3.3.3.3. <i>Hands Influence on the antenna performances</i>	57
3.3.4. PIFA4 Profile	60
3.3.4.1. <i>Design description</i>	60
3.3.4.2. <i>Performance in free space</i>	60
3.3.4.3. <i>Hands Influence on the antenna performances</i>	61
3.3.5. FICA Profile	63
3.3.5.1. <i>Design description</i>	63
3.3.5.2. <i>Performance in free space</i>	63
3.3.5.3. <i>Hands Influence on the antenna performances</i>	64
<b>3.4. HAND INFLUENCE BENCHMARK ON FIVE DUAL-BAND ANTENNAS</b>	<b>66</b>
3.4.1. Introduction	66
3.4.2. The different antenna models	66
3.4.3. Simulations and measurements in talk position	67
3.4.3.1. <i>Simulations setup</i>	67
3.4.3.2. <i>Results and Comparative study</i>	67
3.4.4. Benchmark conclusion	72
<b>CHAPTER 4: CONCLUSION</b>	<b>75</b>
<b>4.1. GENERAL CONCLUSION</b>	<b>75</b>
<b>4.2. FUTURE WORK</b>	<b>76</b>

<b>REFERENCES .....</b>	<b>77</b>
<b>APPENDICES A: SENSITIVITY ANALYSIS .....</b>	<b>79</b>
<b>APPENDICES B: BASIC HANDSET ANTENNA .....</b>	<b>82</b>
<b>APPENDIX C: THE HAND MODELS .....</b>	<b>90</b>
<b>APPENDIX D: HAND INFLUENCE ON FIVE PIFAS .....</b>	<b>91</b>
<b>APPENDIX E: COMPARATIVE STUDY .....</b>	<b>96</b>
<b>APPENDIX D: FREQUENCY BANDS USED IN WIRELESS PERSONAL COMMUNICATIONS.....</b>	<b>102</b>

# LIST OF FIGURES

FIGURE 1 : (A) RADIATION LOBES AND BEAMWIDTHS OF AN ANTENNA PATTERN. (B) LINEAR PLOT OF POWER PATTERN AND ITS ASSOCIATED LOBES AND BEAMWIDTHS [8] .....	14
FIGURE 2 : TRANSMITTING ANTENNA AND ITS EQUIVALENT CIRCUIT. [8].....	16
FIGURE 3 : REFERENCE TERMINALS AND LOSSES OF AN ANTENNA [8] .....	17
FIGURE 4 : “DEPICTION OF A, THE RADIUS OF AN IMAGINARY SPHERE CIRCUMSCRIBING THE MAXIMUM.....	23
FIGURE 5 : TELESCOPIC WHIP ANTENNA.....	26
FIGURE 6 : STUBBY ANTENNA PROTECTED BY A PLASTIC HOUSING .....	26
FIGURE 7 : CONFIGURATION OF TWO INTERNAL ANTENNAS: (A) PLANAR MONOPOLE ANTENNA AND (B) PIFA. [8] .....	27
FIGURE 8 : DETAILS OF THE PLANAR INVERTED ANTENNA.....	27
FIGURE 9 : (A) BANDWIDTH OF THE PIFA WHEN SHORT-CIRCUIT PLATE.....	29
FIGURE 10 : TARGET VALUES FOR PHANTOM HAND MATERIAL, FROM THE AVERAGE PERMITTIVITY AND CONDUCTIVITY OF DRY AND MOISTENED PALM SKIN. [28].....	30
FIGURE 11 : (A) SCHEMATIC DRAWING SHOWING THE COMPUTATIONAL .....	33
FIGURE 12 : VARIATION OF THE NUMERICAL PHASE VELOCITY WITH WAVE PROPAGATION ANGLE IN A TWO DIMENSIONAL FD-TD GRID FOR THREE GRID RESOLUTION [31].....	37
FIGURE 13 : TWO DIMENSIONAL GRID STRUCTURE [36].....	38
FIGURE 14 : ANTENNA CONFIGURATION IN THE COMPUTATIONNAL DOMAIN [8] .....	39
FIGURE 15 : DETAIL FOR THE NEAR FIELD TO THE FAR FIELD TRANSFORMATION [8] .....	39
FIGURE 16: ANTENNA EXCITATION [8] .....	40
FIGURE 17: TIME STEPS ALTERATION ANALYSIS.....	43
FIGURE 18: MONOPOLE ANTENNA SURROUNDED BY A BASIC BRICK DESIGN .....	45
FIGURE 19: LOSSES COMPARISON ACCORDING TO THE SIX HAND MODELS.....	49
FIGURE 20: PIFA1 DESIGN .....	50
FIGURE 21: PIFA1 SMITH CHART      FIGURE 22: RETURN LOSS PLOT OF THE PIFA1.....	51
FIGURE 23: PIFA1 MISMATCH AND ABSORPTION LOSS WITH HAND MODELS FOR BOTH FREQUENCIES .....	51
FIGURE 24: PIFA1 TOP/BOTTOM MISMATCH AND ABSORPTION LOSS COMPARISON AT 900MHZ.....	52
FIGURE 25: PIFA1 TOP/BOTTOM MISMATCH AND ABSORPTION LOSS COMPARISON AT 1900MHZ.....	52
FIGURE 26: PIFA2 DESIGN .....	53
FIGURE 27: RETURN LOSS COMPARISON PLOT BETWEEN PIFA1 AND PIFA2      FIGURE 28: PIFA2 VS.PIFA1 SMITH CHART.....	54
FIGURE 29: PIFA2 MISMATCH AND ABSORPTION LOSS WITH HAND MODELS FOR BOTH FREQUENCIES .....	54
FIGURE 30: PIFA2 TOP/BOTTOM MISMATCH AND ABSORPTION LOSS COMPARISON AT 900MHZ.....	55
FIGURE 31: PIFA2 TOP/BOTTOM MISMATCH AND ABSORPTION LOSS COMPARISON AT 2000MHZ.....	55
FIGURE 32: PIFA3 DESIGN .....	56
FIGURE 33: RETURN LOSS AND SMITH CHART PLOT OF THE PIFA3 .....	57
FIGURE 34: PIFA3 MISMATCH AND ABSORPTION LOSS FOR BOTH FREQUENCIES.....	57
FIGURE 35: PIFA3 TOP/BOTTOM MISMATCH AND ABSORPTION LOSS COMPARISON AT 900MHZ.....	58
FIGURE 36: PIFA3 NEAR FIELD RADIATION IN THE ZX PLAN AT 1900MHZ.....	58
FIGURE 37: PIFA3 TOP/BOTTOM MISMATCH AND ABSORPTION LOSS COMPARISON AT 1900MHZ.....	59
FIGURE 38: RETURN LOSS PLOT OF THE PIFA4      FIGURE 39: SMITH CHART OF THE PIFA4.....	61
FIGURE 40: PIFA4 MISMATCH AND ABSORPTION LOSS FOR BOTH FREQUENCIES.....	61
FIGURE 41: PIFA4 TOP/BOTTOM MISMATCH AND ABSORPTION LOSS COMPARISON AT 900MHZ.....	62
FIGURE 42: PIFA4 TOP/BOTTOM MISMATCH AND ABSORPTION LOSS COMPARISON AT 1800MHZ.....	62
FIGURE 43: FICA DESIGN .....	63
FIGURE 44: RETURN LOSS PLOT OF THE FICA      FIGURE 45: SMITH CHART OF THE FICA.....	64
FIGURE 46: FICA MISMATCH AND ABSORPTION LOSS FOR BOTH FREQUENCIES.....	64
FIGURE 47: FICA TOP/BOTTOM MISMATCH AND ABSORPTION LOSS COMPARISON AT 900MHZ.....	65
FIGURE 48: FICA TOP/BOTTOM MISMATCH AND ABSORPTION LOSS COMPARISON AT 1800MHZ.....	65
FIGURE 49: OVERALL RETURN LOSS ILLUSTRATION FOR THE FIVE ANTENNAS .....	66
FIGURE 50: MISMATCH(A) AND ABSORPTION(B) LOSSES COMPARISON BETWEEN THE HAND MODELS.....	68
FIGURE 51: ANTENNAS ANALYSIS BASED ON THE GRIP STYL.....	69
FIGURE 52: ANTENNAS ANALYSIS BASED ON THE INDEX POSITION.....	70
FIGURE 53: MISMATCH(A) AND ABSORPTION(B) LOSSES ANALYSIS ACCORDING TO THE FREQUENCY RANGE .....	70

FIGURE 54: MISMATCH(A) AND ABSORPTION(B) LOSSES ANALYSIS ACCORDING TO THE ANTENNA POSITION ..... 71

FIGURE 55: (A) HAND POSITION (FROM ONE TO SIX) AND (B) INDEX POSITION (LEFT, MIDDLE AND RIGHT) IMPACT ON MISMATCH AND ABSORPTION LOSS MERGED ..... 72

FIGURE 56 : (A) GRIP STYLE (FIRM AND SOFT) AND (B) ANTENNA POSITION (BOTTOM AND TOP) IMPACT ON MISMATCH AND ABSORPTION LOSS MERGED ..... 72

FIGURE 57 : THE GLOBAL ANTENNA POSITION AND GRIP STYLE IMPACT ..... 73

FIGURE 58 : THE GLOBAL PERFORMANCE AT DIFFERENT FREQUENCIES ..... 73

FIGURE 59 : THE GLOBAL PERFORMANCE OF THE PIFAS ..... 74

FIGURE 60: BASIC PIFA DESIGN ..... 79

FIGURE 61: TIME STEPS NUMBER INFLUENCE ON THE RETURN LOSS ..... 80

FIGURE 62: PML THICKNESS INFLUENCE ON THE RETURN LOSS ..... 80

FIGURE 63: COMPUTATIONAL DOMAIN SIZE INFLUENCE ON THE RETURN LOSS ..... 81

FIGURE 64: BASIC MONOPOLE DESIGN ..... 82

FIGURE 65: FEED SIZE INFLUENCE ..... 83

FIGURE 66: GROUND PLANE SIZE INFLUENCE ..... 84

FIGURE 67: FEED SOURCE POSITION INFLUENCE ..... 85

FIGURE 68: MISMATCH AND ABSORPTION LOSS RESULTS ..... 85

FIGURE 69: BASIC PIFA DESIGN ..... 86

FIGURE 70: MISMATCH AND ABSORPTION LOSS WITH HAND MODELS ..... 89

FIGURE 71: OVERVIEW OF WIRELESS BANDS WIDELY USED IN WIRELESS PERSONAL COMMUNICATIONS ..... 102

# LIST OF TABLES

---

TABLE 1 : PARAMETERS OF THE FDTD	43
TABLE 2 : THE FD-TD PARAMETERS USED IN THE SIMULATIONS	44
TABLE 3 : THE FD-TD PARAMETERS USED IN THE SIMULATIONS	49
TABLE 4: PIFA1 PERFORMANCE IN FREE SPACE	50
TABLE 5: PIFA2 PERFORMANCE IN FREE SPACE	53
TABLE 6: PIFA3 PARAMETERS	56
TABLE 7: PIFA3 PERFORMANCE IN FREE SPACE	56
TABLE 8: PIFA4 PARAMETERS	60
TABLE 9: PIFA4 PERFORMANCE IN FREE SPACE	60
TABLE 10 :FICA PARAMETERS	63
TABLE 11 : FICA PERFORMANCE IN FREE SPACE	63
TABLE 12 : PIFAS DESIGNS	66
TABLE 13 : PIFAS PERFORMANCE IN FREE SPACE	67
TABLE 14: ELECTRIC PROPERTIES OF THE HAND MODELS	67
TABLE 15: GRAPH LEGENDS	68
TABLE 16: REFERENCE PIFA PARAMETERS	79
TABLE 17 : RESULTS FOR THE NUMBER OF TIME STEPS	79
TABLE 18: PML THICKNESS RESULTS	80
TABLE 19: DOMAIN SIZE RESULTS	81
TABLE 20 : FEED POSITION EFFECTS ON THE MONOPOLE	83
TABLE 21: EFFECTS OF THE GROUND PLANE SIZE ON THE MONOPOLE	83
TABLE 22: PERFORMANCE OF THE MONOPOLE IN FREE SPACE	84
TABLE 23 : BRICK HAND EFFECTS ON THE MONOPOLE	84
TABLE 24: EFFECTS OF THE HAND MODELS ON THE MONOPOLE	85
TABLE 25 : SHORT EFFECTS ON THE PIFA	86
TABLE 26: GAP GROUND PLANE/PLATE EFFECTS ON THE PIFA	87
TABLE 27 : PLATE CONFIGURATION EFFECTS ON THE PIFA	87
TABLE 28 : SHORT SIZE EFFECTS ON THE PIFA	87
TABLE 29: FEED SIZE EFFECTS ON THE PIFA	87
TABLE 30: SHORT POSITION EFFECTS ON THE PIFA	88
TABLE 31: FEED POSITION EFFECTS ON THE PIFA	88
TABLE 32: CAPACITOR VALUE EFFECTS ON THE PIFA	88
TABLE 33: CAPACITOR POSITION EFFECTS ON THE PIFA	88
TABLE 34: GROUND PLANE DIMENSION EFFECTS ON THE PIFA	89
TABLE 35: HAND EFFECTS ON THE PIFA	89
TABLE 36: HAND MODELS	90
TABLE 37: PIFA1 PERFORMANCE AT THE TOP	91
TABLE 38: PIFA1 PERFORMANCE AT THE BOTTOM	91
TABLE 39: PIFA2 PERFORMANCE AT THE TOP	92
TABLE 40: PIFA1 PERFORMANCE AT THE BOTTOM	92
TABLE 41: PIFA1 PERFORMANCE AT THE TOP	93
TABLE 42: PIFA1 PERFORMANCE AT THE BOTTOM	93
TABLE 43: PIFA1 PERFORMANCE AT THE TOP	94
TABLE 44: PIFA1 PERFORMANCE AT THE BOTTOM	94
TABLE 45: PIFA1 PERFORMANCE AT THE TOP	95
TABLE 46: PIFA1 PERFORMANCE AT THE BOTTOM	95

# LIST OF ABBREVIATIONS

---

<i>FBW<sub>v</sub></i>	Fractional Matched Bandwidth VSWR
ABC	Absorbing Boundary Conditions
BW	Bandwidth
Dc	Direct Current
EM	Electromagnetic (fields)
FD-TD	Finite Domain Time Difference
FICA	Folded Inverted Conformal Antenna
Fig.X	Figure Numbered “X”
Eq.X	Equation Numbered “X”
GSM	Global System for Mobile Communications (or God Saved my Life ☺ )
IFA	Inverted-F Antenna
ML	Mismatch Loss
MTE	Mobile Telecommunication Equipment
NFFF	Near-field to Far-field
PDA	Personal Digital Assistant
PEC	Perfect Electric Conductor
PIFA	Planar Inverted Folded Antenna
PML	Perfectly Matched Layer
RF	Radio Frequency
RL	Return Loss
SAM	Standard Anthropomorphic Model
SAR	Specific Absorption Rate
TM	Transverse Magnetic
TRP	Total Radiated Power
TS	Time Step
UMTS	Universal Mobile Telecommunications System
VSWR	Voltage Standing Wave Ratio

# LIST OF SYMBOLS

---

$\beta$	Bandwidth
$\Delta x$	x-directed space increment
$\Delta y$	y-directed space increment
$\Delta z$	z-directed space increment
$\Delta t$	Unit time step
$\varepsilon$	Electric Permittivity
$\varepsilon_r$	Electric relative Permittivity
$\varepsilon_0$	Permeability in free-space
$\sigma$	Electric conductivity
$\sigma^*$	Magnetic conductivity
$\lambda$	Wavelength
$\alpha$	Radius of an imaginary sphere circumscribing the maximum dimension of the antenna
$\mu$	Magnetic Permeability
$\mu_0$	Permeability in free-space
$\rho$	Density
$\Gamma$	Voltage reflection coefficient
$\omega$	Angular frequency
$\vec{B}$	Magnetic flux density
$c$	Speed of light in free space
$D$	Directivity
$\vec{D}$	Electric flux density
$\vec{A}, \vec{F}$	potential vectors
$\vec{E}$	Electric field
$e_0$	Antenna efficiency
$e_c$	Conduction efficiency
$e_d$	Dielectric efficiency
$e_r$	Reflection efficiency
$e_{cd} = \eta_r$	Radiation efficiency
$f$	Frequency
$f_r$	Resonant frequency
$\vec{J}$	Electric current density
$G$	Gain
$G_{abs}$	Absolute Gain
$\vec{H}$	Magnetic field

$H$	Height between the ground plane and the PIFA patch
$k$	Free space wavenumber
$L_1$	Length of the antenna patch
$L_2$	Width of the antenna patch
$\vec{M}$	Magnetic current density
$P_A$	Accepted power by the antenna
$P_{available}$	Total available power from the source
$P_{loss}$	Power consumed in the load or the imperfect conductor
$P_{rad}$	Total radiated power
$Q$	Quality factor
$Q_{lb}$	Low Band Quality Factor
$R_A$	Antenna resistance
$R_r$	Radiation resistance
$R_g$	Generator resistance
$R_l$	Loss resistance
$S_{11}$	Return Loss
$U$	Radiation intensity
$v_p$	Numerical phase velocity
$W$	Width of the short cut element of a PIFA
$X_A$	Antenna reactance
$X_g$	Generator reactance
$Z_A$	Antenna impedance
$Z_{in}$	Input impedance
$Z_0$	Characteristic impedance

# CHAPTER 1: INTRODUCTION

---

## 1.1. Problem definition

During the last fifteen years, mobile communications have been developed in a very significant way. Nowadays, mobile handsets are multimedia, being able to make and receive calls, take photos, play some music and so on. Technologies have been focused not only on functionalities, but also on design and aesthetics of the handsets. Size and weight are the two main parameters that industry managed to reduce, providing smarter designed devices. This aggressive market is now expecting more attractive applications from these “everyday’s life” devices, since people are carrying their mobile phone almost all the time. More than a simple medium to make a call, mobile phones are now used as entertainment devices, making life easier or more enjoyable. In the near future, using their own handset, people will be able to watch some high definition video programs, to get a broadband connection and so on. Applications are virtually unlimited as long as the devices have the capabilities to provide such type of services.

Among any hardware part in a handset, the antenna is a key element regarding to the mobile telecommunication equipment (MTE). A lot of improvements have been made during these last years. For instance, these days it is really rare to find a mobile with an external monopole despite it being frequently used only ten years ago. Usage of these new internal antennas has increased both performances and possibilities to produce a nice looking mobile phone. Due to aforementioned expected applications that require better data rate transfers’, optimization of the communication link between antennas and base station are essentials.

These new demands coupled to the wavelength at which mobile handsets are working at represent a real challenge to keep antenna small. Moreover, in today’s environment, devices have to operate at more than only one frequency. For example, an antenna can cover two separate frequency bands that encompass few mobile band standards. All these facts added together are making the task of designing small antenna really tough, however, hopefully it can be helped by new computer-assisted techniques. To acquire reliable results when simulating new antenna designs, one of the most used computational algorithms implemented in the simulators is called Finite Domain Time Difference (FD-TD). Based on the Yee’s algorithm introduced in 1966, this method based on the Maxwell’s equations computes both the electric and magnetic field generated by antenna radiations. Thanks to the computer software simulator, simulations have become more accurate, giving the possibility to compute the radiated fields all around the antenna.

Former antenna design studies including human interactions [1, 2] have particularly focused their investigations on losses owing to the human tissues, especially caused by the user-head. Their main goal of was to determine the Specific Absorption Rate (SAR) affecting the human body. This measure evaluating the electromagnetic fields in the tissues is particularly interesting to calculate in the brain that is the first vital organ directly in the vicinity of the antenna radiations. However, recent studies [3, 4], stated that the hand effects were way larger than the head ones. In addition, the different hand positions are tuning the performances of the antenna according to [5, 6]. Two big tendencies can be pointed out concerning the hand grip styles. Mostly, is has been noticed [7] that people are either handling their mobile with their hand palm stuck to the mobile’s back, or with the finger’s extremities that leave a gap between the mobile phone and the hand palm . Therefore, it is essential to have significant data to study the hand influences on small antennas radiation.

## 1.2. Thesis Purpose

This Master thesis investigates different hand positions and shapes impacts on characteristic mobile phone antennas. The main purpose is then to analyze and point out the best antenna features when working against a human hand. To do so, simulations based on the FD-TD method are performed, being as realistic as possible using the different way to handle a mobile device observed in studies [7]. A special attention is given to the two principal sources of losses: the absorption and mismatch loss. Finally, a comparative study is led on the performances of five dual-band PIFAs when they are in the presence of the hand.

## 1.3. Report outline

The remaining part of the report is divided as follows:

- Technical background: This chapter introduces the main parameters defining an small antenna, the FD-TD method which is used for the simulations and an overview of the existing studies on the hand effects over the mobile phones.
- Simulations: In this section, the results of the simulations on the user interactions are presented and, more particularly, the hand of the user with different types and configurations of handset antennas. Results are obtained using the 3rd generation FD-TD program implemented on the Matlab software. First, a brief sensitivity analysis is led in order to define the different parameters for the simulations. Then, an investigation of the basic handset antennas which are the monopole and the PIFA is made. Next, five PIFAs antennas are described, their performances are analyzed in free space and in talk position. Finally, a comparative study of these antennas is made, focusing on their interaction with the hands and in which cases they can be reduced.

This report is concluded by a state of the achievements reached during the project, pointing up some possible fields that can be investigated for the future steps up.

# CHAPTER 2: TECHNICAL BACKGROUND

## 2.1. Main Antennas Parameters

The best way to characterize an antenna is to look at its own properties. We will particularly focus on the handset antennas which cover for instance the mobile phones, personal digital assistants (PDAs), entertainment terminals and any other pocket-size devices which communicate in a wireless network. Also, in this part, are introduced some of the most important electrical properties such as the input impedance, the gain, the mismatch and absorption loss.

### 2.1.1. Radiation Patterns

The antenna radiation pattern is defined in [8] as “a mathematical function or a graphical representation of the radiation properties of the antenna as a function of space coordinate. In most cases, the radiation pattern is determined in the far field region and is represented as a function of the directional coordinates. Radiation properties include power flux density, radiation intensity, field strength, directivity phase or polarization”.

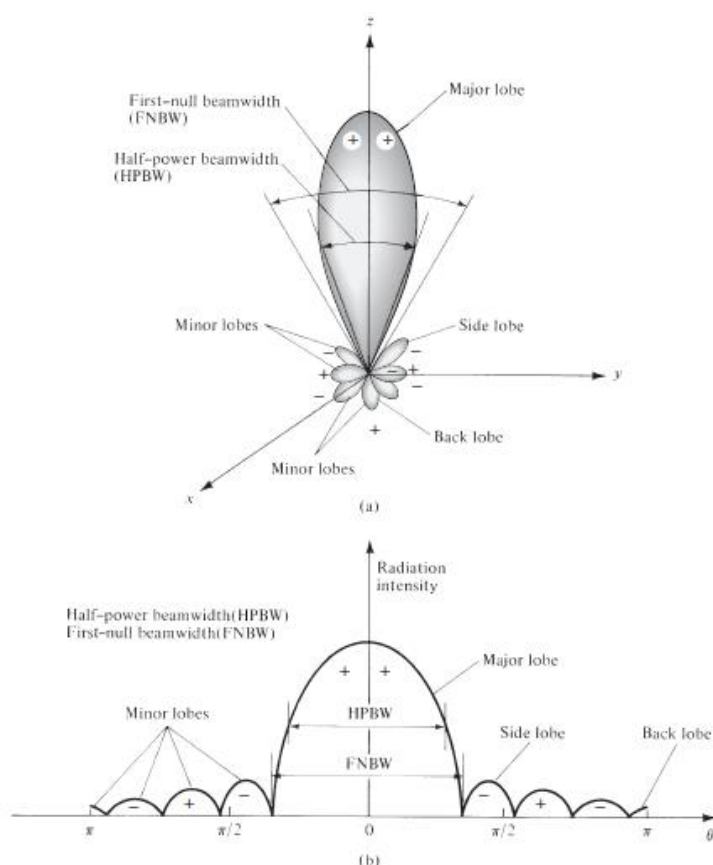


Figure 1 : (a) Radiation lobes and Beamwidths of an antenna pattern. (b) Linear plot of power pattern and its associated lobes and beamwidths [8]

Usually, this specification is pretty rare for the handset antennas since the designer has barely any control on this parameter, and, in the case of the mobile antennas, the hand or the head of the user will particularly change the radiation pattern. In addition, since the environment surrounding the communication link is permanently changing, the correlation between the mobile device and the

base station cannot be controlled. This last statement signifies that a “good” radiation pattern in accordance to a certain position  $x_1$  of the user could be altered when another position  $x_2$  of this user is considered. Therefore, there is a limited value in giving this parameter as row data.

### 2.1.2. Antenna Impedance

The antenna (input) impedance corresponds to “the impedance presented by an antenna at its terminals or the ratio of the voltage to current at a pair of terminals or the ratio of the appropriate components of the electric to magnetic field at a point.” [8]. Here, the antenna terminals which correspond to the input terminals of the antenna are designated as a-b .

The complex, frequency-dependent input impedance of the small antenna is given [8] by:

$$\boxed{Z_A(\omega) = R_A(\omega) + jX_A(\omega)} \quad (0-1)$$

where

$Z_A$  = frequency-dependant antenna impedance at terminals a-b (ohms)

$R_A$  = frequency-dependant antenna resistance at terminals a-b (ohms)

$X_A$  = frequency-dependant antenna reactance at terminals a-b (ohms)

$\omega = 2\pi f$  = radian frequency ,  $f$  = frequency (Hz)

*In the following part, a term followed by the term “( $\omega$ )” signifies that it is dependant to the frequency at which it is calculated.*

For antennas working at very low frequencies, the impedance has the same properties as a lossy capacitor [12]. Thus, the antennas resistance  $R_A$  can be divided in two components:

$$R_A(\omega) = R_r(\omega) + R_l(\omega) \quad (0-2)$$

where

$R_r$  = radiation resistance of the antenna

$R_l$  = loss resistance of the antenna

Then, assuming that the antenna is attached to a generator with internal impedance

$$Z_g(\omega) = R_g(\omega) + jX_g(\omega) \quad (0-3)$$

where

$Z_g$  = generator internal impedance (ohms)

$R_g$  = resistance of the generator impedance (ohms)

$X_g$  = reactance of generator impedance (ohms)

The maximum power is consequently delivered to the antenna when the total antenna resistance equals to the generator resistance, and when the generator reactance is the opposite of the antenna’s one:

$$\begin{aligned} R_r + R_l &= R_g \\ X_A &= -X_g \end{aligned} \quad (0.4)$$

A representation of the antenna coupled to a generator with its equivalent circuits is shown on fig.2 when it is used in the transmitting mode.

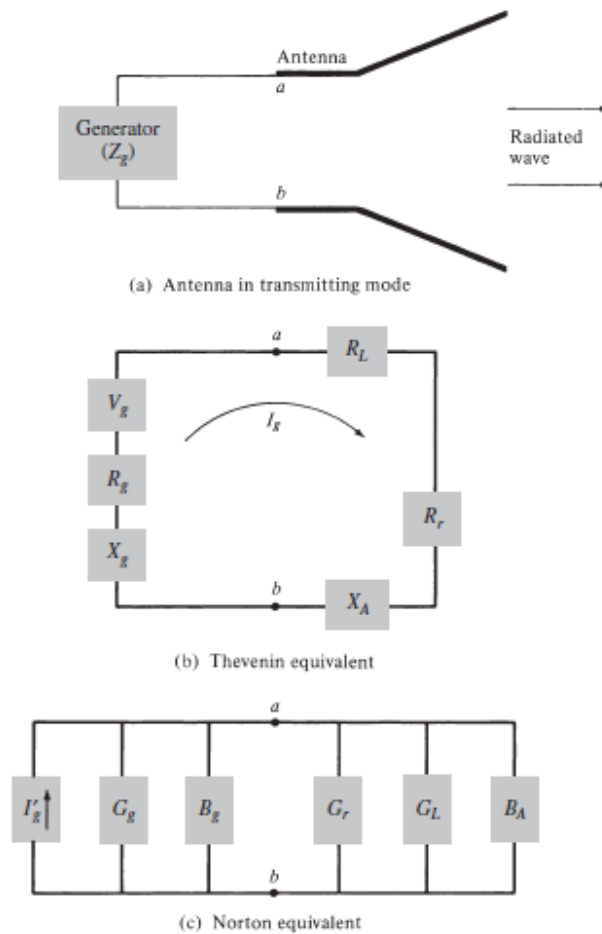


Figure 2 : Transmitting antenna and its equivalent circuit. [8]

The input impedance of an antenna is generally a function of frequency. Thus the antenna will be matched to the interconnecting transmission line and other associated equipment only within a certain bandwidth. Moreover, the input impedance of the antenna depends on many factors including its geometry, its method of excitation, and its proximity to surrounding objects.

Nb: A half wave dipole antenna has nominally a “75 ohms characteristic impedance” while a monopole has nominally a 36 ohms one. For its part, the quarter wave antenna exhibits a nominal 50 ohms impedance.

### 2.1.3. Directivity

The definition of the directivity has changed for the last thirty years and is nowadays described in [8] as: “the ratio of the radiation intensity in a given direction from the antenna to the radiation intensity averaged over all directions. The average radiation intensity is equal to the total power radiated by the antenna divided by  $4\pi$ . If the direction is not specified, the direction of maximum radiation intensity is implied.” In other terms, the directivity of a non isotropic antenna is the ratio of its radiation intensity in a given direction over that of an isotropic source:

$$D(\omega) = \frac{U(\omega)}{U_0(\omega)} \quad (0-5)$$

With  $U$  = radiation intensity ( $W / unit$  solid angle)

$U_0$  = radiation intensity of isotropic source ( $W / unit$  solid angle)

### 2.1.4. Antenna Efficiency

It has to be known that, several methods to calculate the antenna efficiency exist such as: *pattern integration method*, *Q-factor method*, and *Wheeler method* as explained in [9]. These methods have been found to make the calculation easier. Following fig.3(b), it is noticeable that several measurements can be acquired for the purpose of estimating the overall efficiency of an antenna. First of all, it is interesting to talk about the antenna efficiency  $e_0$  which not only considers losses at the input terminals but also within the antenna material. According to fig.3(b), the two main sources of losses are the reflections due to the mismatch between the transmission line and the antenna, and the  $I^2R$  losses (conduction and dielectric).

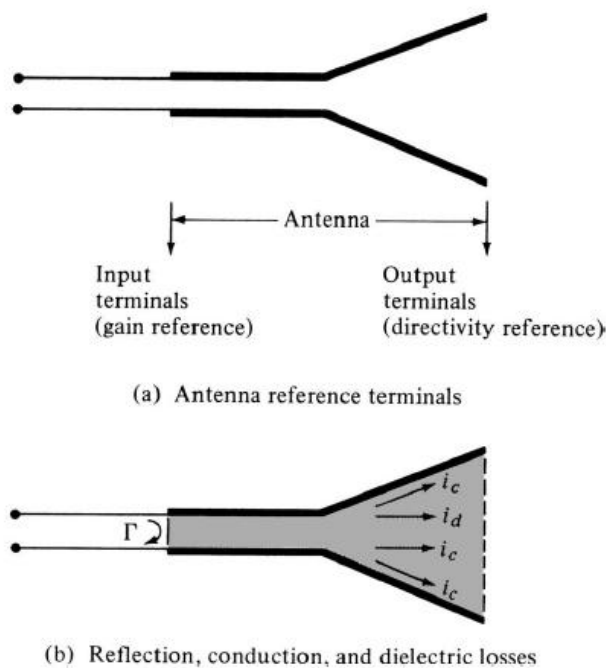


Figure 3 : Reference terminals and losses of an antenna [8]

We generally express the overall efficiency  $e_0$  as:

$$e_0(\omega) = e_r(\omega)e_c(\omega)e_d(\omega) \tag{0-6}$$

Where

$e_0(\omega)$  = total efficiency (dimensionless)

$e_r(\omega)$  = reflection (mismatch) efficiency =  $(1 - |\Gamma(\omega)|^2)$  (dimensionless)

$e_c(\omega)$  = conduction efficiency (dimensionless)

$e_d(\omega)$  = dielectric efficiency (dimensionless)

$\Gamma(\omega)$  = voltage reflection coefficient at the input terminals of the antenna

$\left[ \begin{array}{l} \Gamma(\omega) = (Z_{in}(\omega) - Z_0) / (Z_{in}(\omega) + Z_0) \text{ where } Z_{in}(\omega) = \text{antenna input impedance,} \\ Z_0 = \text{characteristic impedance of the transmission line} \end{array} \right]$

More commonly, we write the Eq. (0-5) as

$$e_0(\omega) = e_r(\omega) e_{cd}(\omega) = e_{cd}(\omega) (1 - |\Gamma(\omega)|^2) \quad (0-7)$$

Where  $e_{cd} = e_c e_d$  = antenna **radiation efficiency**, which is used to relate the gain and directivity.

#### 2.1.4.1. Total Radiated Power

This is the total power flowing from the handset when it is transmitting. Referring to the fig.3(a), we can describe the total radiated power ( $P_{rad}$ ) as a function of the total input power ( $P_A$ ) accepted by the antenna and the radiation efficiency  $e_{cd}$  mentioned previously and defined in (1-4):

$$P_{rad}(\omega) = e_{cd}(\omega) P_A(\omega) \quad (0-8)$$

It can be obtained in the far field region integrating the pointing vector over the desired surface that encloses the whole antenna [10]:

$$Prad(\omega) = \frac{1}{2} |I_0(\omega)|^2 R_r(\omega) = \frac{1}{2} \text{Re} \iint_S (E \times H^*) \cdot \hat{n} dS \quad (0-9)$$

Where E and H are the electric and magnetic intensities on the surface S.

Mathematical definition for  $P_A(\omega)$  is given as [10]

$$P_A(\omega) = P_{rad}(\omega) + P_{loss}(\omega) = \frac{1}{2} |I_0(\omega)|^2 R_r(\omega) + \frac{1}{2} |I_0(\omega)|^2 R_l(\omega) = \frac{1}{2} |I_0(\omega)|^2 (R_r(\omega) + R_l(\omega)) = \frac{1}{2} |I_0(\omega)|^2 R_A(\omega) \quad (0-10)$$

Using eq.(0-8) into (0-5) gives:

$$D = \frac{4\pi U(\omega)}{P_{rad}(\omega)} \quad (0.11)$$

#### 2.1.4.2. Radiation Efficiency

According to eq.0-7 the radiation efficiency is the product between the conduction efficiency  $e_c$  and the dielectric efficiency  $e_d$ :  $e_{cd}$ . Literature often describes the radiation efficiency (noted  $\eta_r$ ), also referred as absorption loss [15, 11], as the ratio of the total power radiated by the antenna:  $P_{rad}$  to the accepted power by the antenna at its terminals during the radiation process:  $P_A$ .

$$P_{rad}(\omega) = e_{cd}(\omega) P_A(\omega) = \eta_r(\omega) P_A(\omega) \quad (0-12)$$

$$\Leftrightarrow \eta_r(\omega) = \frac{P_{rad}(\omega)}{P_A(\omega)} \quad (0-13)$$

$$= \frac{P_A(\omega) - P_{loss}(\omega)}{P_A(\omega)} = 1 - \frac{P_{loss}(\omega)}{P_A(\omega)} \quad (0-14)$$

That is equivalent to:

$$\eta_r(\omega) = \frac{R_r(\omega)}{R_A(\omega)} = \frac{R_r(\omega)}{R_r(\omega) + R_l(\omega)} \quad (0-15)$$

And

$$\text{Absorption Loss} = -10\log(\eta_r) \quad (0-16)$$

$P_{rad}$  is proportional to  $R_r$ , the radiation resistance and  $P_A$  is proportional to  $(R_r + R_l)$ , where  $R_l$  is the loss resistance.

$P_{loss}$  is the power consumed in the load or the imperfect conductor. It can be found as:

$$P_{loss} = \frac{1}{2} |I_0|^2 R_l = \sum_{n=1}^M \text{Re}(Z_{nn}^L) |I_n|^2 \quad (0-17)$$

The radiation efficiency shows the ability of the antenna to transfer the accepted power into radiation. However, the reflection efficiency is not taken in account for the calculation of the radiation efficiency. This can be solved relating the radiated power  $P_{rad}$  to the total available power from the source  $P_{available}$  (instead of the accepted power  $P_A$ ) [11]. This statement leads to rewrite (1-6) as :

$$\eta_{total}(\omega) = \frac{P_{rad}(\omega)}{P_{available}(\omega)} = e_r(\omega) \eta_r(\omega) = (1 - |\Gamma(\omega)|^2) \eta_r(\omega) \quad (0-18)$$

#### 2.1.4.3. VSWR

The voltage standing wave ratio (VSWR) gives us a good indication of the mismatch between the antenna's impedance ( $Z_{in}$ ) and the characteristic impedance of the transmission line ( $Z_0$ ), in other terms, it shows the mismatch level of impedance between the antenna and the transmitter and the transmission line. It is defined as [8] :

$$VSWR(\omega) = \frac{1 + |\Gamma(\omega)|}{1 - |\Gamma(\omega)|} \quad (0-19)$$

With  $\Gamma$  = voltage reflection coefficient at the input terminals of the antenna

The VSWR is read as a ratio. For instance, the VSWR value 1,2:1 says that the maximum standing wave amplitude is 1,2 times greater than the minimum standing wave value.

However, there is a more explicit measure expressing "the amount of power reflected at the antenna's feed point to the incident or forward power" [12], the mismatch loss.

#### 2.1.4.4. Mismatch and Reflection Loss

Each component constituting a transmission line will contribute to the overall mismatch loss of the system. Especially in the antenna's ones, the mismatch loss is one of the main sources of error. According to the radiation efficiency part, the mismatch loss is expressed as:

$$e_r(\omega) = \text{reflection efficiency} = \text{mismatch loss} = (1 - |\Gamma(\omega)|^2) \text{ (dimensionless)}$$

which corresponds to the power delivered to the load.

However, the reflection loss (in dB) is calculated according to the mismatch loss with the formula :

$$\text{reflection loss}(\omega) = 10 \log_{10}(1 - |\Gamma(\omega)|^2) \quad (0-20)$$

Besides, it is common to characterize the mismatch loss and VSWR by the **return loss** also called  $S_{11}$  which is defined as:

$$RL(\omega) = -20 \log(|\Gamma(\omega)|) = S_{11}(\omega) \quad (0-21)$$

As the dimension of the handset antennas are becoming smaller and smaller, one of the most challenging points in designing is to minimize the VSWR over the required frequency bands. Since the mismatch loss is a component of the reflection efficiency, it is easily understandable that optimizing this parameter will amount to the same thing as optimizing the radiation efficiency. *“For most wireless, integrated device antennas, the VSWR is required to be less than 3 throughout the designated operating band(s). This is equivalent to a return loss requirement of 6 dB”* [12].

#### 2.1.5. Gain

Using the word “gain” in the mobile device world is not fully explicit and is not commonly used. It is actually more accurate to speak about the *efficiency*. However, for a general comprehension of the antenna basics, it is important to describe this other way to evaluate the performance of the antenna.

First of all, the gain in function of two major parameters of the antenna: the efficiency and the directional capabilities.

The definition of the gain of an antenna (in a given direction) is, as given in [8] : *“the ratio of the intensity, in a given direction, to the radiation intensity that would be obtained if the power accepted by the antenna were radiated isotropically. The radiation intensity corresponding to the isotropically radiated power is equal to the power accepted (input) by the antenna divided by  $4\pi$ ”*.

However, it is more common to use the **“relative gain”** that gives easier calculations. It is defined in [Balanis] as: *“the ratio of the power gain in a given direction to the power gain of a reference antenna in its referenced direction.”* (Both antennas have to get the same input power) Since the reference antenna is usually a lossless isotropic source:

$$G(\omega) = \frac{4\pi U(\omega)}{P_{in}(\omega) \text{ (lossless isotropic source)}} \text{ (dimensionless)} \quad (0-22)$$

*“When the direction is not stated, the power gain is usually taken in the direction of maximum radiation”*

IEEE standards does not include any losses in the gain calculation *“gain does not include losses arising from impedance mismatches (reflection losses) and polarization mismatches (losses).”*

Also, it can be found [8] a second type of gain, absolute gain which includes these losses, *“referred to as gain ( $G$ ) and absolute gain ( $G_{abs}$ ) that also takes into account the reflection/mismatch losses.”*

Including eq.0-6 in eq.0-19, gives:

$$\boxed{G(\omega) = e_{cd} D(\omega)} \quad (0-23)$$

Where  $D$  is the antenna's pattern directivity.

Thus, the absolute gain taking into account the reflection loss  $e_r(\omega) = (1 - |\Gamma(\omega)|^2)$  is calculated as:

$$\boxed{G_{abs}(\omega) = e_r(\omega)G(\omega) = (1 - |\Gamma(\omega)|^2)G(\omega) = e_r(\omega)e_{cd}(\omega)D(\omega) = e_r(\omega)\eta_r(\omega)D(\omega) = e_0(\omega)D(\omega)} \quad (0-24)$$

### 2.1.6. Bandwidth

The bandwidth (noted  $BW$  or  $\beta$ ) of an antenna is defined as [8]: “the range of frequencies within which the performance of the antenna, with respect to some characteristics, conforms to a specified standard.” For a handset antenna, the objective is that the bandwidth is large enough to cover the frequency bands over which the handset is expected to operate. Indeed, due to the mismatch of the antenna, a limitation criterion has to be set to define a specific bandwidth. Since every antenna does not require the same capabilities, this criterion will not be fixed, but for most of the mobile communication antenna, the limit will be ruled by the  $S_{11}$  parameter. As explained in [11] “the limit is either  $S_{11,max} = -10$  dB or  $S_{11,max} = -6$  dB at the borders of the frequency band. These two limits correspond to a power reflection of 10% and 25% respectively.

### 2.1.7. Quality Factor

The  $Q$  factor is a well defined parameter giving a good indication on the bandwidth. The value of the bandwidth is actually inversely proportional to the value of the  $Q$  factor. It is calculated for a tuned antenna at the frequency:  $f_0 \Rightarrow \omega_0 = 2\pi f_0$ . According to [8]: “The tuned antenna is one whose feed point reactance is tuned to zero at a frequency  $\omega_0$  using a single, lossless, series tuning element having a reactance  $X_S(\omega_0) = -X_A(\omega_0)$ ”.

Contrary to the bandwidth, there is a precise formula defined for the tuned antenna [10]:

$$\boxed{Q(\omega_0) = \frac{\omega_0 W(\omega_0)}{P_{in}(\omega_0)}} \quad (0-25)$$

Where  $\omega_0$  is the resonant or tuned frequency,  $W(\omega_0)$  is the internal energy, and  $P_{in}(\omega_0)$  is the power accepted by the antenna as defined in (1-9).

Typically, the  $Q$  is described in function of the bandwidth and small antennas properties. In [10], it has been found that the exact  $Q$  can be approximated as:

$$Q(\omega_0) \approx Q_z(\omega_0) = \frac{\omega_0}{2R_A(\omega_0)} \sqrt{R_A'(\omega_0)^2 + \left( X_A'(\omega_0) + \frac{|X_A(\omega_0)|}{\omega_0} \right)^2} \quad (0-26)$$

It is now convenient to find a formula relating the bandwidth and the  $Q$  that is suitable for all ranges of frequency. As it can be read in the [8]: “The definition of bandwidth suitable for this purpose is fractional matched VSWR bandwidth,  $FBW_V(\omega_0)$ , where the VSWR of the tuned antenna

is determined using a characteristic impedance,  $Z_{CH}$ , equal to the antenna's feed point resistance,  $R_A(\omega_0)$ . Fractional matched VSWR bandwidth is given by: "

$$FBW_V(\omega_0) = \frac{\omega_+ - \omega_-}{\omega_0} = \frac{\Delta f}{f_0} \propto \frac{1}{Q} \quad (0-27)$$

With  $\omega_+ = 2\pi f_h$ , the frequency above  $\omega_0 = 2\pi f_0$  and  $\omega_- = 2\pi f_l$  the frequency below  $\omega_0$ , where the VSWR is equal to any arbitrary value denoted by  $s$ . Fractional matched VSWR bandwidth and  $Q$  are related as [10]:

$$Q(\omega_0) \approx Q_B(\omega_0) = \frac{2\sqrt{\beta}}{FBW_V(\omega_0)}, \quad \sqrt{\beta} = \frac{s-1}{2\sqrt{s}} \leq 1 \quad (0-28)$$

More simply, concerning a handset antenna, the  $Q$  factor can be written in terms of the resistance and reactance part of the input impedance [13]:

$$Q(\omega) = \frac{\omega}{2R_A(\omega)} \frac{\partial(X_A(\omega))}{\partial\omega} \quad (0-29)$$

### 2.1.8. Specific Absorption Rate (SAR)

The SAR measures the amount of heat that is generated in the tissue surrounding the implant antenna. Its unit is watts per kilogram ( $W/kg$ ) and is generally taken as an average value over some portion covered by the antenna power. It is defined in [8] as:

$$SAR = \frac{\sigma}{2\rho} |E^2| \quad (0-30)$$

Where  $\sigma$  ( $S/m$ ) is the conductivity of the tissue,  $E$  ( $V/m$ ) is the electric field intensity, and  $\rho$  ( $kg/m^3$ ) is the tissue density.

We have to distinguish the limits for exposure to electromagnetism fields and maximum permitted SAR. The limits for exposure to fields are quoted in terms of power (in  $W/m^2$ ) carried by a plane wave whereas the SAR limits are not so easy to define since it relates to the power absorbed by the user's body. It is known that, the body is constituted by several layers (skin, bones, brain) which are different in terms of densities, dielectric constants, dielectric loss factor and so on. However, we can find two typical SAR limits that are:  $1.6 W/kg$  over a volume of  $1g$ , which is the limit applied to the USA, and  $2 W/kg$  over a volume of  $10g$ , which the limit is established by the European Union [14].

## 2.2. Electrically small antenna

Size of handset antennas become smaller and smaller to respond to the market demand. In correlation of that, antenna engineer have to find new solutions to design well resonating antennas in such small devices. Furthermore, it is important to distinguish two types of antenna that can be mixed up: the *electrically small antenna* (also called ESA [15]), and the *physically small antenna*. Antennas working at frequencies like 2 GHz, 3 GHz or above, with an operating wavelength of  $\lambda$  that corresponds to approximately 15cm are not considered as electrically small but as “*physically small*”. Below these frequencies, antennas will be, most of the time described as “electrically small”. Due to a certain confusion between these “electrically” and “physically small”, a well defined parameter has been settled to agree on the fact that an antenna belongs to the “electrically small” category or not. Thanks to a sphere enclosing the maximum dimension of the antenna, as shown on fig.4, one can directly say whether it is electrically small or not.

The condition that has to be fulfilled is defined as [12] :

$$k\alpha \leq 0.5 \quad (0-31)$$

Where:

-  $k = \frac{2\pi}{\lambda}$  = free space wavenumber

-  $\lambda$  = free space wavelength

-  $\alpha$  = the radius of an imaginary sphere circumscribing the maximum dimension of the antenna

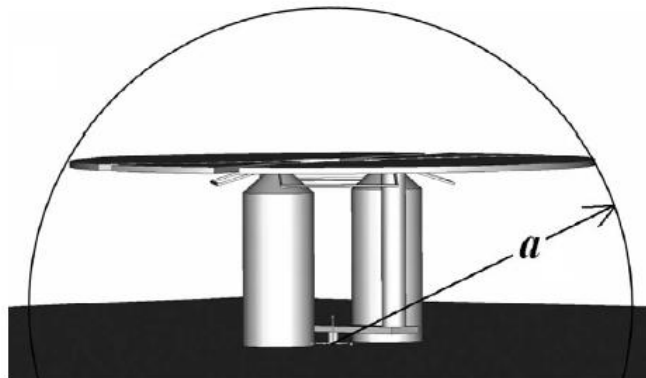


Figure 4 : “Depiction of  $\alpha$ , the radius of an imaginary sphere circumscribing the maximum dimension of an antenna. In the case of an antenna mounted at the center of a large ground plane, the value of  $\alpha$  circumscribes the “image” of the antenna within the ground plane.” [8]

Following this parameter, in the case of a monopole, the new value of  $\alpha$  would be the same as the monopole’s height. Antennas are placed here at the centre of a large ground plane which that will behave as an infinite ground plane. However, it is noticeable that this situation almost never happens in a mobile device since the antenna is often located at the top or, in some cases at the bottom of the device. Therefore, the ground plane will then have an influence on the antenna performances and should be taken in account. In other terms,  $\alpha$  should include the ground plane dimension.

Generally, speaking about space occupied by an antenna in terms of  $k\alpha$  will lay some fundamental limits on the antenna’s performance in terms of  $k\alpha$ . This amounts to saying that some performance will be limited by this factor that will be discussed further in this part.

### 2.2.1. Small antennas' fundamental limitations

Firstly, as it is mentioned in [8], for small values of  $k\alpha$ , the antennas are reaching a constant value of directivity :  $1,5 \approx 1,8dB$  for a small dipole and  $3 \approx 4,8dB$  for a small monopole. Theoretically, there is no limit to the radiation efficiency but only on the directivity as seen before. This implies that the maximum theoretical gain that can be achieved is about  $1,8dBi$  or  $4,8dBi$  for the dipole and monopole respectively. Obviously these values are not realistic since they do not take into account any losses due to the mismatch loss or the reduction of the radiation efficiency (that is dependant to the conduction and dielectric efficiency). Nevertheless, the mismatch loss is a parameter that can be corrected by adding some external components, or modifying the antenna dimensions, but, however, this will degrade the radiation efficiency. Another thing that has to be kept in mind is that tuning an antenna to different frequencies can pose a problem to keep the same  $k\alpha$ .

Secondly, small antennas operate within a narrow bandwidth because of their small dimensions. Generally, the  $Q$  factor is pretty high, due to the size of the bandwidth as they are proportionally inversed. To put it differently, there is a minimum limit of  $Q$  as it depends on the size of the operating wavelength of the antenna:  $ka$ . As stated before,  $Q$  and  $BW$  are inversely related, which means that an upper limit exists for the maximum achievable bandwidth. Thanks to the combined work done by Chu [16] and McLean [17], a formula defining the accepted lower bound on  $Q$ , (often referred to as the Chu Limit), has been deduced :

$$Q_{lb} = \eta_r \left( \frac{1}{(ka)^3} + \frac{1}{ka} \right) \quad (0-32)$$

It is important to notice that the radiation efficiency ( $\eta_r$ ) is proportional to the  $Q_{lb}$ . This corresponds to say that the  $Q_{lb}$  is decreasing with a lower  $\eta_r$ , or, equivalently, that a lossy antenna will achieve a lower  $Q_{lb}$  or a higher bandwidth. Including eq.0-31 into eq.0-27, "an upper bound on the fractional matched VSWR bandwidth can be written as" [8]

$$FBW_{vub} = \frac{1}{\eta_r} \frac{(ka)^3}{1+(ka)^2} \frac{s-1}{\sqrt{s}} \quad (0-33)$$

Besides, to find the maximum achievable bandwidth for an infinite number of external impedance matching region [16] gives the formula:

$$BW_{\infty} = \frac{1}{Q} \frac{\pi}{\ln \left( \frac{1}{|\Gamma|} \right)} \quad (0-34)$$

### 2.2.2. Different Small Antennas

During these last fifteen years, mobile design has been one of the most innovative fields. Due to the huge competition that exists between the different constructors, a lot of research and development have been performed to produce the most attractive devices. To illustrate this point, it is pretty easy to be conscious of the external improvement on the mobile design. For example it is common to see that mobile phones can fit in a pocket, with a thickness not bigger than a CD box. In addition of that, constructors have to produce devices that can transmit at different frequencies, following different technologies, with a good battery lifetime, keeping a fairly low price for this aggressive market. All these parameters gathered for such advanced devices like mobile phones represent a real challenge for designers.

One of the parts that have been investigated deeply is the antenna since it is a crucial component to get a good communication. Formerly, handset devices were mainly external, and visible for the user. The two big classes that represent these ones are the whip and stubby antennas as it is described in [19]. Nowadays, internal antennas are the most widespread for convenient and aesthetic reasons. A lot of different types have been created but the “Planar Inverted Folded Antenna (PIFA)” remains the most famous in the handset devices world. However, designing internal antennas implies to take care of the “housing effect”. Indeed, the proximity of the antenna with the other mobile components such as the loud speaker, camera, battery, and so on. All of these may have some negative effects that must be taken in account.

Lastly, a dominant factor that antenna designers have to deal with is the interaction between the antenna and the user. This particular point is relatively fussy as there is a double issue.

On the one hand, the interferences that human body, including the head and hand, is causing a really tough issue. Actually, every user is different, and handle the handset in a different way, moreover, mobile phones are not built similarly as we find some big particular types of handset like “the candy bar phone”, “the clamshell phone”, “the slide phone”. That is why, there is no exact model to predict for each case how much the user will fade the communication link (the input impedance, and radiation efficiency are the first affected by human tissues) between his own mobile and the base station. However, some studies are being conducted [7] to give antenna designers a good overview on how the users are handling their device, and according to that, how it affects the signal. Thanks to these, one can now start to investigate new antenna shapes or configuration to optimize the interaction between the antenna and the user.

On the other hand, engineers not only have to be careful about how to transmit properly the signal, but, how to lower electromagnetic field (EM) radiation in human tissues at the maximum. This particular point is discussed [20] since, the health risks is a very preoccupying field. The quantification of EM absorption in the body is done with the “Specific Absorption Rate (SAR)”. According to the different legislations, antenna designers must respect a certain amount of maximum SAR [21]. In this part, a general overview of both external and internal antennas will be given in a first time, then; the Planar Inverted Antenna (PIFA) will be studied in detail in a second time.

#### 2.2.2.1. External Antennas

External antennas were the first alternative at the beginning of mobile handset globalisation. Their simplicity and adaptability were particularly adapted at the beginning of handset development.

##### ➤ Whip Antennas

Mostly mounted on a large handset, the whip antenna is resonating with the quarter of the wavelength  $\lambda = \frac{c}{f}$ . Nevertheless, when the antenna is covering low bands, it consequently has to be longer. To solve this problem, whip antennas design can be extended or “folded up” which make

the antenna size matching with the frequency. This is inconvenient in several ways not only that it makes the handset less convenient to handle, but it adds a weakness since this mechanical part can be easily broken. In addition, the design of these antennas requires ways to be found to pull out the antenna from the mobile, but also to put in back which is tricky without dismantling the mobile.

➤ Stubby Antennas

To make whips smaller, and more robust, the single straight monopole is wound into a helix or meandered, and therefore, is protected inside a short housing. To increase its resistance, it is often built flexible.

➤ Dual Band whips and coils.

An improvement from the whip antennas is to design them as bi-band antennas. As explained in [22], *“the commonest early designs comprised whips fed by a coupling structure, but these have been replaced in most market by dual-band concentric helix-whip and non uniform helical structures”*. Both these types were really similar to the single band ones.



Figure 5 : Telescopic whip antenna



Figure 6 : Stubby antenna protected by a plastic housing

#### 2.2.2.2. Internal Antennas

Internal antennas are the most used in today's mobile handset development. Their main qualities are to be robust, without any exterior contact, plus it helps designers to conceive thinner devices with nicer shapes.

➤ Folded Monopole.

The principle is to etch a meandered monopole conductor directly on the main printed circuit board (PCB). Most of the time designed as form of T or inverted L antenna. The inverted-F antenna (IFA), a much used standard antenna, is the evolution direct of the inverted L antenna combined with a Shunt-Feeding.

➤ Planar Inverted Folded Antenna (PIFA).

The main difference with the folded monopole concerns the ground plane. Indeed, in the case of the Folded Monopole, the ground plane has to be cut out just underneath the monopole. Contrary to this last one, the PIFA, does require the ground plane underneath the patch. Following [23], this ground plane configuration *“helps block the backward RF radiation and lower the SAR values”*. The

PIFA represents nowadays the best alternative among every existing antenna thanks to its modelling capabilities and its overall efficiency.

The four main components of the PIFA are the patch, the feed pin, the short pin, and the ground plane. Modifying these ones, leaves the possibility to design well adapted antennas following different handset bandwidth.

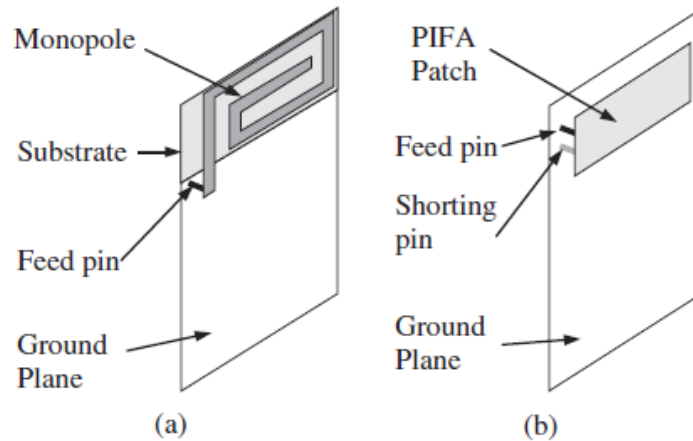


Figure 7 : Configuration of two internal antennas: (a) planar monopole antenna and (b) PIFA. [8]

A major advantage concerning the PIFA is that the dimension of the patch can be reduced, introducing the short circuit element between the feed and the ground plane. To get the best performance, it has to be placed where the electric field of the  $TM_{100}$  is equal to zero [24, 25]. In addition, using a shorting element of a smaller dimension than that of the patch, the effective inductance of the antenna increases and the resonant frequency becomes lower. In fact, to have a PIFA resonating at a low band frequency, the current distribution effective length has to be as long as possible. To take advantage of the longest length of the patch, the ratio between the length ( $L_1$ ) and the width ( $L_2$ ) of the patch, has to be as high as possible, with a shorting element small behind the dimension of the edge [15]. In other terms,  $\frac{L_1}{L_2} \geq 1$ ,  $W \ll L_1$ .

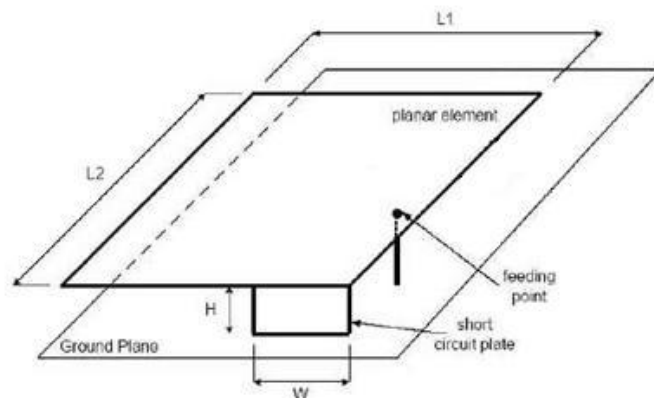


Figure 8 : Details of the Planar Inverted Antenna

- The resonant frequency

The fundamental step that has to be done when designing a new PIFA is the calculation of the patch dimension to make the antenna resonate at the right frequency.

At first, the formula relying on the plate dimensions with the wavelength was the following:

$$L_1 + L_2 = \frac{\lambda}{4} \Leftrightarrow f_r = \frac{c}{4(L_1 + L_2)} \quad (0-35)$$

Nevertheless, it does not consider the presence of the shorting plate, which gives [15] :

$$L_2 + H = \frac{\lambda}{4} \Leftrightarrow f_{r1} = \frac{c}{4(L_2 + H)}, \quad \text{for } \frac{W}{L_1} = 1 \quad (0-36)$$

Or

$$L_1 + L_2 + H = \frac{\lambda}{4} \Leftrightarrow f_{r2} = \frac{c}{4(L_1 + L_2 + H)}, \quad \text{for } W = 0 \quad (0-37)$$

And

$$L_1 + L_2 + H - W = \frac{\lambda}{4} \Leftrightarrow f_{r2} = \frac{c}{4(L_1 + L_2 + H - W)}, \quad \text{for } 0 < \frac{W}{L_1} < 1 \quad (0-38)$$

With  $c$  : the celerity in free space,  $H$  : the height between the ground plane and the patch,  $W$  : the width of the shorting element

Consequently, it is understandable that the resonant frequency is increasing with the width of the plate because of the negative sign at the denominator before  $W$ .

As it is explained in [15], the resonant frequency  $f_r$ , when  $0 < \frac{W}{L_1} < 1$ , can be approximated thanks to

the following equations :

$$f_r = r \cdot f_1 + (1-r) \cdot f_2, \quad \text{for } \frac{L_1}{L_2} \leq 1 \quad (0-39)$$

And

$$f_r = r^k \cdot f_1 + (1-r^k) \cdot f_2, \quad \text{for } \frac{L_1}{L_2} > 1 \quad (0-40)$$

With  $r = \frac{W}{L_1}$  and  $k = \frac{L_1}{L_2}$ .

- PIFA's Bandwidth

Thanks to the experiments done in [15], the height ( $H$ ) and the width ( $W$ ) of the short circuit element has some influences on the bandwidth of the antenna as it can be seen on the fig.9(a,b) where  $\Delta d$  is an element of length. Obviously, the bandwidth is not only increasing with the enhancement of  $W$  but also by raising the size ratio  $\frac{L_1}{L_2}$ . In addition of that, one can remark that the

bandwidth is higher when measuring it from a PIFA mounted on the side of portable radio housing. This can be explained by the housing effects and by the changing value of the radiation efficiency.

According to the formula, the radiation frequency is inversely proportional to the conduction and dielectric efficiency that are lowered when the antenna is positioned in the mobile.

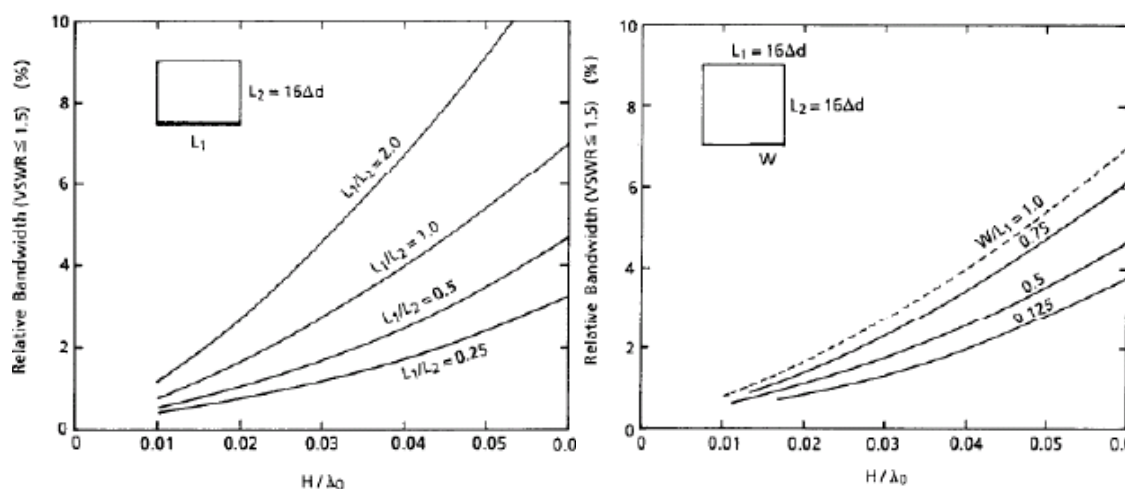


Figure 9 : (a) Bandwidth of the PIFA when short-circuit plate width is equal to  $L_1$  [15], (b) Bandwidth of the PIFA when short-circuit plate width is narrower than  $L_1$  [15]

### 2.3. Influence of the user hand on mobile phone

In the last past years, interferences between human body and radio waves has become a very serious topic. This aspect is important to investigate from two points of view. On the first hand, from the technical view, it is interesting to observe the radiation performances when the antenna is placed close to the body. On the second hand, that is the most relevant view, the amount of electromagnetic (EM) fields that are actually radiated in the human body, and especially in the head. As a general health concern, people get really involved in the results brought by studies. The most pertinent parameter to check this out is the SAR defined in section 2.1, since it quantifies the EM field in the human tissues. Some SAR limitations are already applied according to the different regulations. In Europe for example, the SAR standard is of  $2.0 \text{ mW/g}$  ( $2.0 \text{ W/kg}$ ) averaged over  $10 \text{ g}$  of tissue [26]. This specification is a real challenge to take up when confronted with other performance parameters like radiation efficiency or bandwidth. Thus some models have been designed to compute human part, head in particular.

In spite of the much used head phantom, also known as “standard anthropomorphic model” (SAM), there is still a big lack of knowledge on the hand virtualization. The foremost simulation platform that is used to simulate human tissues like skins, bones, muscles is named “SEMCAD” and is helping a lot to improve the accuracy of the results, especially for the SAR. Though, no real hand model has been really settled down so far since most of the studies were focused on the body and head influence.

The few reasons that were given to not use the hand in simulations were for instance : “*practical difficulties in specifying a unique hand holding position*”, “*with respect to SAR in the head, numerical studies suggest that not modelling the hand provides a conservative estimate*” [27] and so on.

For a lack of information on how to re-create a robust hand model, C.Gabriel, in his study about the hand virtual conception [28], finally came up with the table shown on fig.10 to express the corresponding values of the permittivity and conductivity of a phantom hand in function of the radiating frequencies.

Frequency (MHz)	$\epsilon'$	$\sigma$ (S m <sup>-1</sup> )
300	44.3	0.49
450	40.7	0.57
835	36.6	0.76
900	36.2	0.79
1450	33.8	1.07
1800	32.6	1.26
1900	32.4	1.32
1950	32.3	1.34
2000	32.1	1.37
2100	31.9	1.43
2450	31.0	1.64
3000	30.0	1.99
4000	28.5	2.70
5000	26.9	3.52
5200	26.5	3.69
5400	26.2	3.86
5600	25.9	4.03
5800	25.6	4.20
6000	25.3	4.37

Figure 10 : Target values for phantom hand material, from the average permittivity and conductivity of dry and moistened palm skin. [28]

To be able to simulate a phantom hand as realistically as possible, not only these results were essential, but some other studies showing the way people are used to handling their mobile were required. For the moment, some researches have been led at the Aalborg University [7, 29], pointing out different things.

The first main one shows that people handle a handset device with a different style between each others, and following the phone type (clamshell, candy bar...) they are using. However, two major styles are usually noted. They are called “Soft grip style” which corresponds to the hand holding “*the handset with the distal phalanges, creating a gap between the palm and the handset*” and “Firm grip style”, where “*the fingers are placed around the handset, so that while the intermediate phalanges touch its side, the distal ones reach its front region*” [7]. What is more, these two handling types strongly modify the antenna performances and have to be considered when simulating an antenna. The two most influential factors for the absorption and mismatch loss with the vicinity of the hand to the mobile underlined by those studies are:

- the index finger position on the handset device
- The height of the gap between the palm and the handset

*A representation of the different grip styles that have been found in the studies is shown on appendix C.*

## 2.4. Finite Difference Time Domain Method

The finite difference time domain (FD-TD) method is used to solve the Maxwell's equations based on the Yee's algorithm introduced in 1966. The analysis of a variety of antennas, especially for the antennas found in the mobile phone nowadays (whip, helical, PIFA or monopole antennas) is one application of the FD-TD. Contrary to the other computational algorithm known as the Moment Method, the main advantage of the FD-TD method is that it is a straightforward solution of the six-coupled field components of the Maxwell's curl equations. The electric and the magnetic field components are computed "by discretizing the Maxwell's curl equations both in time and space, and then solving the discretized equations in a time marching sequence by alternatively calculating the electric and magnetic fields in the computational domain". The purpose of this chapter is to introduce the reader to the fundamentals of the FD-TD method as applied to practical antennas.

### 2.4.1. Maxwell's Equations in 3D

The Maxwell's equations describe the behavior of electric and magnetic fields. They consist in a set of four partial differential equations:

Faraday's law:

$$\frac{\partial \vec{B}}{\partial t} = -\nabla \times \vec{E} - \vec{M} \quad (0.41)$$

Where :

- $\vec{E}$  the electric field in V/m
- $\vec{B}$  the magnetic flux density Wb/m<sup>2</sup>
- $\vec{M}$  the magnetic current density V/m<sup>2</sup>

The Faraday's law equation describes the phenomenon in which an electric field is created by a changing magnetic field.

Ampere's law:

$$\frac{\partial \vec{D}}{\partial t} = -\nabla \times \vec{H} - \vec{J} \quad (0.42)$$

Where :

- $\vec{H}$  the magnetic field in A/m
- $\vec{D}$  the electric flux density C/m<sup>2</sup>
- $\vec{J}$  the electric current density A/m<sup>2</sup>

The Ampere's law states that magnetic fields can be generated by changing electric fields.

Gauss's Law for the electric field:

$$\nabla \cdot \vec{D} = 0 \quad (0.43)$$

Gauss's Law for the magnetic field:

$$\nabla \cdot \vec{B} = 0 \quad (0.44)$$

This law states that the magnetic field has a divergence equal to zero: magnetic charges come in pairs and the two charges create opposite magnetic field divergences; which cancel each other out.

The Yee Algorithm assumes that the material is linear, isotropic and non dispersive. It implies there is relation between  $\vec{E}$  and  $\vec{D}$  and between  $\vec{H}$  and  $\vec{B}$  :

$$\vec{B} = \mu \vec{H} \quad (0.45)$$

$$\vec{D} = \varepsilon \vec{E} \quad (0.46)$$

Where :  $\mu$  the magnetic permeability in H/m  
 $\varepsilon$  the electric permittivity in F/m

In the medium, it is assumed there are some electric and magnetic losses. We define both equivalent electric and magnetic current taking into consideration these losses:

$$\vec{M} = \rho \vec{H} \quad (0.47) \quad ; \quad \vec{J} = \sigma \vec{E} \quad (0.48)$$

Where :  $\sigma$  the electric conductivity in S/m  
 $\rho$  the magnetic resistivity in  $\Omega/m$

Then, the Ampere's and Faraday's law can be rewritten by combining and substituting the assumptions of eq.0.45 through eq.0.48:

$$\frac{\partial \vec{H}}{\partial t} = -\frac{1}{\mu} \nabla \times \vec{E} - \frac{\rho}{\mu} \vec{H} \quad (0.49)$$

$$\frac{\partial \vec{E}}{\partial t} = -\frac{1}{\varepsilon} \nabla \times \vec{H} - \frac{\sigma}{\varepsilon} \vec{E} \quad (0.50)$$

Finally, these Maxwell's curl equations are developed in the three-dimensional rectangular coordinate (x, y, and z) and we obtain a system of six coupled scalar equations:

$$\frac{\partial H_x}{\partial t} = \frac{1}{\mu} \cdot \left( \frac{\partial E_y}{\partial z} - \frac{\partial E_z}{\partial y} - \rho H_x \right) \quad (0.51)$$

$$\frac{\partial H_y}{\partial t} = \frac{1}{\mu} \cdot \left( \frac{\partial E_z}{\partial x} - \frac{\partial E_x}{\partial z} - \rho H_y \right) \quad (0.52)$$

$$\frac{\partial H_z}{\partial t} = \frac{1}{\mu} \cdot \left( \frac{\partial E_x}{\partial y} - \frac{\partial E_y}{\partial x} - \rho H_z \right) \quad (0.53)$$

$$\frac{\partial E_x}{\partial t} = \frac{1}{\varepsilon} \cdot \left( \frac{\partial H_z}{\partial y} - \frac{\partial H_y}{\partial z} - \sigma E_x \right) \quad (0.54)$$

$$\frac{\partial E_y}{\partial t} = \frac{1}{\varepsilon} \cdot \left( \frac{\partial H_x}{\partial z} - \frac{\partial H_z}{\partial x} - \sigma E_y \right) \quad (0.55)$$

$$\frac{\partial E_z}{\partial t} = \frac{1}{\varepsilon} \cdot \left( \frac{\partial H_y}{\partial x} - \frac{\partial H_x}{\partial y} - \sigma E_z \right) \quad (0.56)$$

These six differential equations constitute the foundation of the Yee algorithm for the electromagnetic waves propagating in three dimensional space. Let's now proceed with the explanation of the FD-TD algorithm introduced by Yee in 1966.

## 2.4.2. The Yee Algorithm

### 2.4.2.1. The principle

In the Yee Algorithm, both Electric and Magnetic fields are solved thanks to a judicious discretization of the space and the time. As illustrated in fig.11,  $\vec{E}$  and  $\vec{H}$  components are centered in such way that each  $\vec{E}$  component is surrounded by four circulating  $\vec{H}$  components [31] and vice versa. The increments in space for rectangular coordinates are represented by  $\Delta x$ ,  $\Delta y$  and  $\Delta z$  and by  $\Delta t$  for the increment in time. The total volume where the fields have to be solved is formed by  $N=N_xN_yN_z$  unit cells each of volume  $\Delta V = \Delta x\Delta y\Delta z$ .

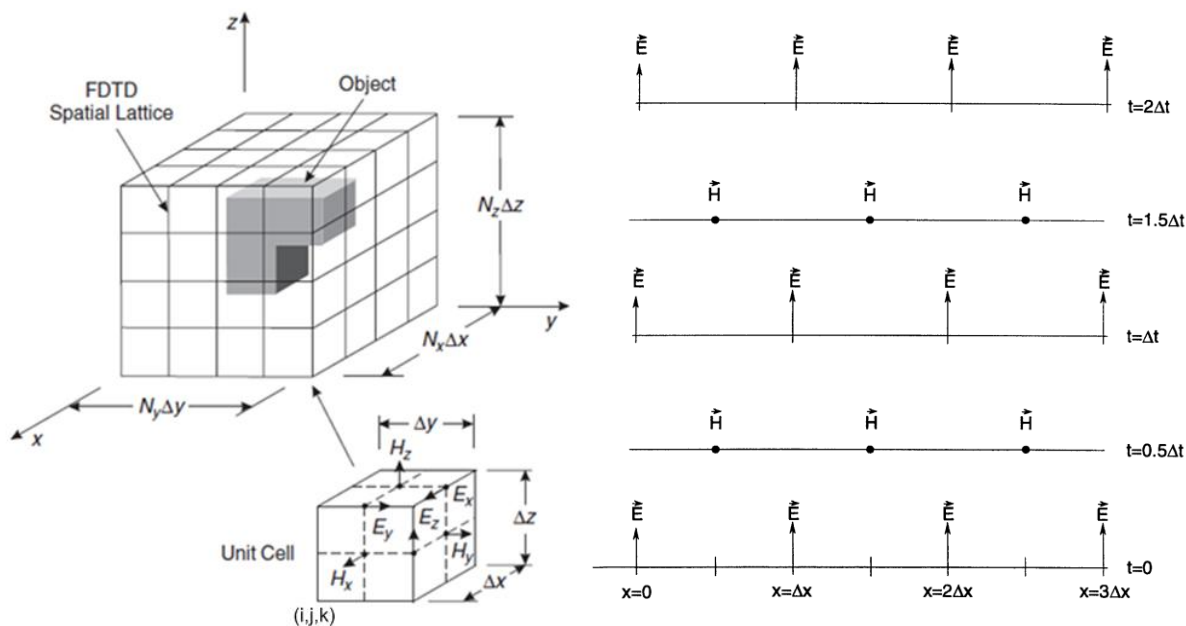


Figure 11 : (a) Schematic drawing showing the computational volume, FD-TD spatial lattice, and unit cell. [8],  
(b) Time Stepping representation [33]

The goal of this specific geometric configuration is to take data to the right and the left of the computed point by only one-half of a spatial increment. With regards to the time, each field component is computed every one-half of the time increment  $\Delta t$ . By these choices, at any space lattice point, the new value of each field vector component depends only on its previous value and the previous values of the other field vector components of at adjacent points. Therefore at any given time step, the computation of a field vector can only proceed one point at a time. All of the  $\vec{E}$  and  $\vec{H}$  fields are computed in the total volume  $N\Delta V$  and stored in the memory until the conclusion of the desired time step,  $N_t \Delta t$ .

This algorithm is known as a “leapfrog time-stepping” and is a “fully explicit” method where the expression is fully explicit, having obtained each of the required terms from previous time steps.

2.4.2.2. Finite-Difference Expressions for Maxwell's Equations in 3D

In the FD-TD algorithm, any H or E fields computed at a discrete point in space and time are denoted as follow:

$$E(i\Delta x, j\Delta y, k\Delta z, n\Delta t) = E_{i,j,k}^n \quad (0.57)$$

Where  $\Delta x$ ,  $\Delta y$  and  $\Delta z$  are respectively the increments in  $x$ ,  $y$  and  $z$  directions and  $i, j, k$  are integers. Likewise,  $\Delta t$  is increment in time and  $n$  an integer.

The space and time derivatives in Maxwell's equations are approximated by centered finite-difference expressions. For example, the partial space derivative of the E field in the  $x$ -direction computed at the time  $t_n = n\Delta t$  is denoted as following:

$$\frac{\partial E}{\partial x}(i\Delta x, j\Delta y, k\Delta z, n\Delta t) = \frac{E_{i+1/2,j,k}^n - E_{i-1/2,j,k}^n}{\Delta x} + O\left[(\Delta x)^2\right] \quad (0.58)$$

For all spatial derivatives, the increment is formed by separating field components from adjacent unit cells  $\pm 1/2 \Delta x$ . By analogy, the temporal derivative of the E field computed at the fixed space point  $(i,j,k)$  is deduced :

$$\frac{\partial E}{\partial t}(i\Delta x, j\Delta y, k\Delta z, n\Delta t) = \frac{E_{i,j,k}^{n+1/2} - E_{i,j,k}^{n-1/2}}{\Delta t} + O\left[(\Delta t)^2\right] \quad (0.59)$$

For the temporal derivatives, it is formed by separating field components from two adjacent time steps  $\pm 1/2 \Delta t$ . With these mathematical tools, each components of the electric field  $\vec{E}$  and the magnetic field  $\vec{H}$  can be approximated in time at one-half of a time increment and in space at one-half of a spatial increment.

By applying these notations to the Maxwell's curl equations in three dimensions given by the equations eq.0.51 till 0.56, two sets of difference equations are formed. They are known as the Finite Difference expressions [31]:

$$H_x \Big|_{i,j,k}^{n+1/2} = \left( \frac{1 - \frac{\rho_{i,j,k}\Delta t}{2\mu_{i,j,k}}}{1 + \frac{\rho_{i,j,k}\Delta t}{2\mu_{i,j,k}}} \right) H_x \Big|_{i,j,k}^{n-1/2} + \left( \frac{\Delta t}{1 + \frac{\rho_{i,j,k}\Delta t}{2\mu_{i,j,k}}} \right) \cdot \left( \frac{E_y \Big|_{i,j,k+1/2}^n - E_y \Big|_{i,j,k-1/2}^n}{\Delta z} - \frac{E_z \Big|_{i,j+1/2,k}^n - E_z \Big|_{i,j-1/2,k}^n}{\Delta y} \right) \quad (0.60)$$

$$H_y \Big|_{i,j,k}^{n+1/2} = \left( \frac{1 - \frac{\rho_{i,j,k}\Delta t}{2\mu_{i,j,k}}}{1 + \frac{\rho_{i,j,k}\Delta t}{2\mu_{i,j,k}}} \right) H_y \Big|_{i,j,k}^{n-1/2} + \left( \frac{\Delta t}{1 + \frac{\rho_{i,j,k}\Delta t}{2\mu_{i,j,k}}} \right) \cdot \left( \frac{E_z \Big|_{i+1/2,j,k}^n - E_z \Big|_{i-1/2,j,k}^n}{\Delta x} - \frac{E_x \Big|_{i,j,k+1/2}^n - E_x \Big|_{i,j,k-1/2}^n}{\Delta z} \right) \quad (0.61)$$

$$H_z \Big|_{i,j,k}^{n+1/2} = \left( \frac{1 - \frac{\rho_{i,j,k}\Delta t}{2\mu_{i,j,k}}}{1 + \frac{\rho_{i,j,k}\Delta t}{2\mu_{i,j,k}}} \right) H_z \Big|_{i,j,k}^{n-1/2} + \left( \frac{\Delta t}{1 + \frac{\rho_{i,j,k}\Delta t}{2\mu_{i,j,k}}} \right) \cdot \left( \frac{E_x \Big|_{i,j+1/2,k}^n - E_x \Big|_{i,j-1/2,k}^n}{\Delta y} - \frac{E_y \Big|_{i+1/2,j,k}^n - E_y \Big|_{i-1/2,j,k}^n}{\Delta x} \right) \quad (0.62)$$

$$E_x \Big|_{i,j,k}^{n+1} = \left( \frac{1 - \frac{\sigma_{i,j,k}\Delta t}{2\varepsilon_{i,j,k}}}{1 + \frac{\sigma_{i,j,k}\Delta t}{2\varepsilon_{i,j,k}}} \right) E_x \Big|_{i,j,k}^n + \left( \frac{\Delta t}{1 + \frac{\sigma_{i,j,k}\Delta t}{2\varepsilon_{i,j,k}}} \right) \cdot \left( \frac{H_z \Big|_{i,j+1/2,k}^{n+1/2} - H_z \Big|_{i,j-1/2,k}^{n+1/2}}{\Delta y} - \frac{H_y \Big|_{i,j,k+1/2}^{n+1/2} - H_y \Big|_{i,j,k-1/2}^{n+1/2}}{\Delta z} \right) \quad (0.63)$$

$$E_y \Big|_{i,j,k}^{n+1} = \left( \frac{1 - \frac{\sigma_{i,j,k} \Delta t}{2\epsilon_{i,j,k}}}{1 + \frac{\sigma_{i,j,k} \Delta t}{2\epsilon_{i,j,k}}} \right) E_y \Big|_{i,j,k}^n + \left( \frac{\frac{\Delta t}{\epsilon_{i,j,k}}}{1 + \frac{\sigma_{i,j,k} \Delta t}{2\epsilon_{i,j,k}}} \right) \cdot \left( \frac{H_x \Big|_{i,j,k+1/2}^{n+1/2} - H_x \Big|_{i,j,k-1/2}^{n+1/2}}{\Delta z} - \frac{H_z \Big|_{i+1/2,j,k}^{n+1/2} - H_z \Big|_{i-1/2,j,k}^{n+1/2}}{\Delta x} \right) \quad (0.64)$$

$$E_z \Big|_{i,j,k}^{n+1} = \left( \frac{1 - \frac{\sigma_{i,j,k} \Delta t}{2\epsilon_{i,j,k}}}{1 + \frac{\sigma_{i,j,k} \Delta t}{2\epsilon_{i,j,k}}} \right) E_z \Big|_{i,j,k}^n + \left( \frac{\frac{\Delta t}{\epsilon_{i,j,k}}}{1 + \frac{\sigma_{i,j,k} \Delta t}{2\epsilon_{i,j,k}}} \right) \cdot \left( \frac{H_y \Big|_{i+1/2,j,k}^{n+1/2} - H_y \Big|_{i-1/2,j,k}^{n+1/2}}{\Delta x} - \frac{H_x \Big|_{i,j+1/2,k}^{n+1/2} - H_x \Big|_{i,j-1/2,k}^{n+1/2}}{\Delta y} \right) \quad (0.65)$$

These two sets of equations allow the computation of each components of the electric field  $\vec{E}$  and the magnetic field  $\vec{H}$  at every increment of time since they depend on their own previous value and those of the other field. The computation processes as following:

- At  $t=0$ , the electric field is known and the magnetic field is known at the earlier time  $t=-\Delta t/2$ .
- The set of the finite difference equations of the magnetic field are then applied to compute the magnetic field at time  $t=\Delta t/2$ .
- Next, the set of the finite difference equations of the electric field are applied to compute the electric field at time  $t=\Delta t$  by using the results of the magnetic field at time  $t=\Delta t/2$  and the previous values of the electric field at time  $t=0$  and so on.

Therefore, by alternatively applying the different set of finite difference equations, the solution advances in time until the electromagnetic field is completely known through all the computational volume  $N \cdot \Delta V$  and at the wanted time  $N_t \Delta t$ .

In order to simplify the implementation of the finite difference equations, some coefficients are defined, enabling the calculation of a constant to be substituted into the expressions . These constants are known as the material dependent coefficients, depending on the electric and the magnetic properties of the medium.

*Electric field coefficient at point (i,j,k)[31] :*

$$C_a \Big|_{i,j,k} = \left( \frac{1 - \frac{\sigma_{i,j,k} \Delta t}{2\epsilon_{i,j,k}}}{1 + \frac{\sigma_{i,j,k} \Delta t}{2\epsilon_{i,j,k}}} \right) \quad (0.66)$$

$$C_b \Big|_{i,j,k} = \left( \frac{\frac{\Delta t}{\epsilon_{i,j,k} \Delta s}}{1 + \frac{\sigma_{i,j,k} \Delta t}{2\epsilon_{i,j,k}}} \right) \quad (0.67)$$

*Electric field coefficient at point (i,j,k)[31] :*

$$D_a \Big|_{i,j,k} = \left( \frac{1 - \frac{\rho_{i,j,k} \Delta t}{2\mu_{i,j,k}}}{1 + \frac{\rho_{i,j,k} \Delta t}{2\mu_{i,j,k}}} \right) \quad (0.68)$$

$$D_b \Big|_{i,j,k} = \left( \frac{\frac{\Delta t}{\mu_{i,j,k} \Delta s}}{1 + \frac{\rho_{i,j,k} \Delta t}{2\mu_{i,j,k}}} \right) \quad (0.69)$$

In eq.(0.66) and (0.69),  $\Delta s$  represents the increments in space such as  $\Delta x=\Delta y=\Delta z=\Delta s$ , implying that the Yee cell is considered as a cube, and therefore the number of computations is reduced.

### 2.4.3. Numerical stability

The success of the Yee algorithm and its solution depends on the choice of the space and time increment, since their sizes determine the accuracy of the approximation of the finite difference equations. Thus, the space and time increments are related, indeed to guarantee convergence and numerical stability of the solution. Therefore, the time increment  $\Delta t$  must satisfy the Courant, Friedrich and Lewy condition, which is in free space [31]:

$$\Delta t \leq \frac{1}{c \sqrt{\frac{1}{(\Delta x)^2} + \frac{1}{(\Delta y)^2} + \frac{1}{(\Delta z)^2}}} \quad (0.70)$$

Since the space increments  $\Delta x$ ,  $\Delta y$ ,  $\Delta z$  are equal for cubical cells, this condition can be reduced to:

$$\Delta t \leq \frac{\Delta s}{c\sqrt{3}} \quad (0.71)$$

With  $\Delta s = \Delta x = \Delta y = \Delta z$ .

If this condition is not fulfilled, the numerical solution will endure an ongoing instability which means the computed values will grow exponentially.

### 2.4.4. Numerical dispersion

The numerical dispersion is an unwanted effect present during the FD-TD computation, highlighting the fact that the wave propagation velocity is related to the frequency. The dispersion occurs when the wave number  $k = 2\pi/\lambda$  of a propagating wave varies with angular frequency  $\omega = 2\pi f$ . In effect, after large propagation distances results a cumulative phase error and delay and then, a distortion of wave shapes. The choice of the space increment in the grid, the wavelength or the direction of propagation might cause this dispersion. In order to limit this effect, it has been investigated and quantified in the three-dimensional case [31]:

$$\left[ \frac{1}{c\Delta t} \sin\left(\frac{\omega\Delta t}{2}\right) \right]^2 = \left[ \frac{1}{\Delta x} \sin\left(\frac{\tilde{k}_x \Delta x}{2}\right) \right]^2 + \left[ \frac{1}{\Delta y} \sin\left(\frac{\tilde{k}_y \Delta y}{2}\right) \right]^2 + \left[ \frac{1}{\Delta z} \sin\left(\frac{\tilde{k}_z \Delta z}{2}\right) \right]^2 \quad (0.72)$$

Where  $\tilde{k}_x, \tilde{k}_y, \tilde{k}_z$  are the numerical wave number components and  $\omega$  is the angular frequency of the numerical sinusoidal wave present traveling in the FD-TD grid. In general,  $\tilde{k}$  differs from  $k$  which is the wave number of the continuous wave. It is difference between these two wave numbers that represents the numerical phase velocity which gives rise to the numerical errors.

The ideal dispersion case for a numerical plane wave in three dimensions in a lossless medium reduces (0.72) to [31]:

$$\frac{\omega^2}{c^2} = k_x^2 + k_y^2 + k_z^2 \quad (0.73)$$

This ideal case is possible for a cubic lattice with uniform cell size if the space and time increments of the grid and also the direction of the wave propagating through the grid, are properly selected. It's verified when the time increment is equal to the bound, established by the numerical stability condition ( $\Delta t = \Delta s/\sqrt{3}$ ) and uniquely for diagonal propagation of the plane wave. Therefore, even if the ideal case exists, it regards only one direction of propagation and cannot be applied to some more general ones. However, the dispersion being related to the space lattice, it can be reduced by relevant choice of space and time increment. The figure below (fig.12) shows how the numerical phase velocity varies with angle of the propagating wave and the resolution of the grid, in the two dimensional case.

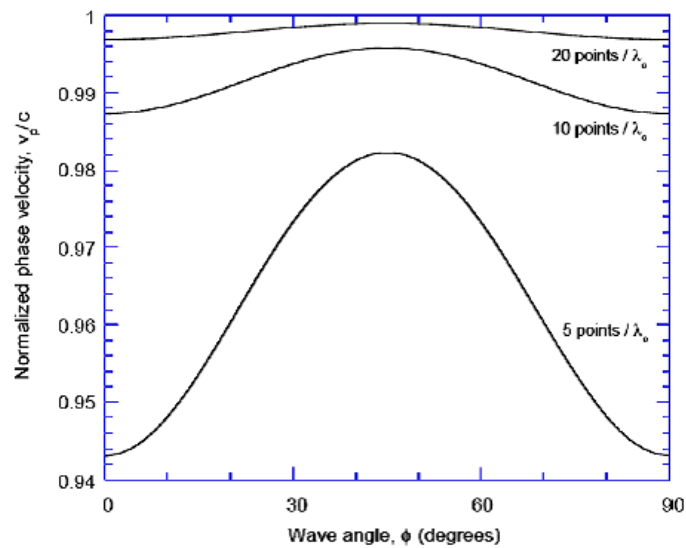


Figure 12 : Variation of the numerical phase velocity with wave propagation angle in a two dimensional FD-TD grid for three grid resolution [31]

Some comments about the variation of the numerical phase velocity can be made:

- The numerical phase velocity  $v_p$  is always smaller than the free space speed of light  $c$ .
- The distortion reduces when the grid resolution is increasing.
- The numerical phase velocity reaches its maximum for wave propagating with a  $45^\circ$  angle and a minimum for wave propagating along the grid axis ( $0^\circ$  and  $90^\circ$ ).

#### 2.4.5. Absorbing Boundary Conditions (ABC).

Most of the electromagnetic field propagations studies arise in an unbounded volume. This assumption is an issue for computational method since any computer is able to store infinite amount of data. Therefore absorbing conditions are set down at the boundaries of the computational domain. The objective for these boundaries is to reproduce the same conditions on the outer perimeter of the domain that would be in an infinite volume. For this, all of the waves propagating within the bounded volume should be absorbed by the boundary and spurious reflections caused by the outward waves suppressed. Several estimated local ABCs have been performed since the existence of FD-TD, but at this time, the Perfectly Matched Layer (PML) settled by Berenger remains the most effective ABC.

##### 2.4.5.1. Berenger Perfectly Matched Layer

To absorb the outgoing waves, different computational methods have been performed. However none of them provide an exact solution. The PML technique settles the computational domain by surrounding it with specific absorbing layers. This new domain is designed to absorb the outgoing electromagnetic waves without any reflection. At any frequency and any direction of propagation, the theoretical reflection factor with this technique is null. In this layer, electric and magnetic field components are splitting into subcomponents and are replaced in the Maxwell's equations with the matching impedance condition satisfied [36]:

$$\frac{\sigma}{\epsilon_0} = \frac{\sigma^*}{\mu_0} \quad (0.74)$$

$\sigma$  and  $\sigma^*$  are respectively, the electric and the magnetic conductivities.

$\mu_0$  and  $\varepsilon_0$  are respectively the permittivity and the permeability in free-space.

With this condition satisfied, it means that the wave impedance in the free-space medium is the same as wave propagating in the lossless vacuum and there is no reflection at the vacuum layer interface. In [36], further demonstrations show that specific set of electric and magnetic conductivities  $\sigma$  and  $\sigma^*$  permit reflectionless transmission of a wave from a PML interface to another one. Fig.13 shows the structure of a two dimensional grid with the PML technique.

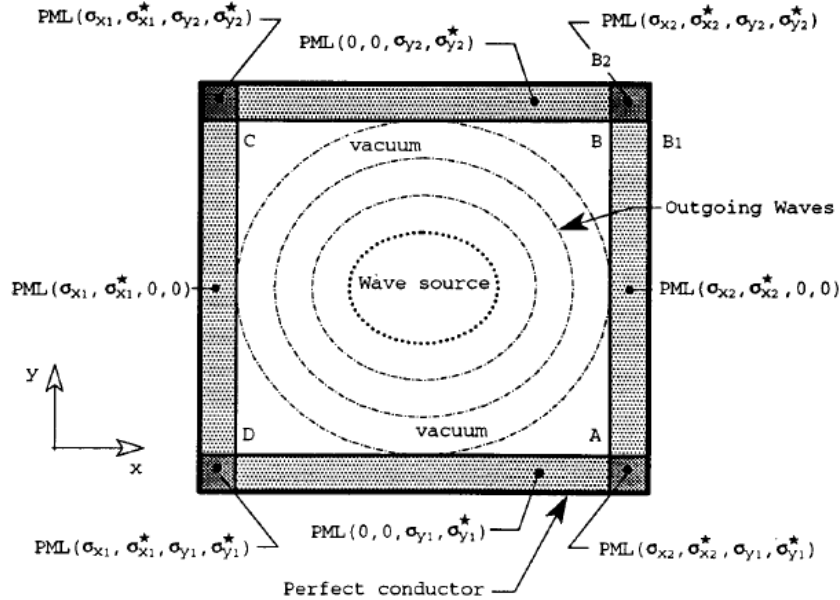


Figure 13 : Two dimensional grid structure [36]

The computational domain is surrounded first by PML and then perfect conductors. Inside the domain, the FD-TD method is applied to solve the Maxwell's equations. At the right and left PML-Interfaces, the reflection factor is null since  $\sigma_x$  and  $\sigma_x^*$  verify the condition (1.31) and  $\sigma_y = \sigma_y^* = 0$ . Likewise, at the lower and upper sides, the reflection factor is null since  $\sigma_y$  and  $\sigma_y^*$  verify the condition (1.31) and  $\sigma_x = \sigma_x^* = 0$ . Therefore, the outgoing waves can propagate through all of these interfaces without suffering reflection. However, at the four corners of the structure, the two PMLs  $(\sigma_x, \sigma_x^*, 0, 0)$  and  $(0, 0, \sigma_y, \sigma_y^*)$  overlap, and so all of the conductivities are present there  $(\sigma_x, \sigma_x^*, \sigma_y, \sigma_y^*)$ . Nevertheless, when a wave propagates through an interface, it is reflected according to the perfect conductor conditions surrounding the domain, and then returns into the vacuum. This implies a reflection factor which is defined as a function of the layer thickness  $\delta$  and the conductivity properties  $\sigma(\rho)$  of the PML, with  $\rho$  represents the distance from the interface and  $\sigma$  could be either  $\sigma_x$  or  $\sigma_y$ . As a result of Berenger's study [36], "in practical computations, the layer has to be a few cells thick with conductivity increasing from zero at the vacuum layer interface to a value  $\sigma_m$  at the outer side of the layer" and then tuning the layers thickness  $\delta$  allows reducing the amount of reflections.

### 2.4.6. FD-TD applied for the Antenna Analysis

The FD-TD is a useful method applied to the antenna analysis since it provides an accurate and direct calculation of the antennas impedance, and its radiation pattern. These two parameters are essential for the antenna design.

This section begins with a description of the FD-TD methodology applied to an antenna, particularly the far-fields computation. Since the performance of an antenna is performed in the frequency domain, the different parameters are then investigated and an overview of the excitation source used in the FD-TD model is discussed.

#### 2.4.6.1. The FD-TD formulation for an antenna

One of the first concerns when designing an antenna is to determine its far field radiation pattern.

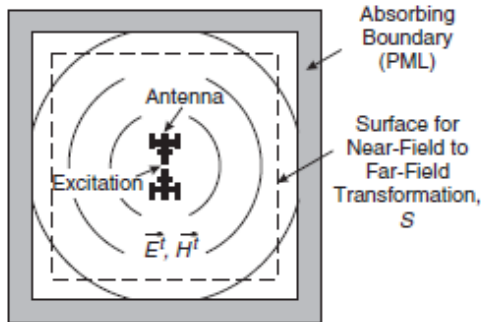


Figure 14 : Antenna configuration in the computational domain [8]

Consider an antenna placed close to the FD-TD domain center as shown in the fig.14. The antenna is excited by a transmission line connected to a source and radiates electromagnetic fields in the entire domain ( $\vec{E}_t$  and  $\vec{H}_t$ ). The computational zone is surrounded by a PML backed by perfect conductors in order to simulate an infinite domain. A surface encloses the antenna and is used to obtain the far field.

Indeed the Near-field to Far-field (NFFF) transformation implies the application of the equivalence theorem where equivalent sources replace the actual sources allowing the knowledge of the equivalent electric and magnetic surface current densities. This concept is illustrated in the fig.15 where the dashed line represents the closed observation surface  $S$ .

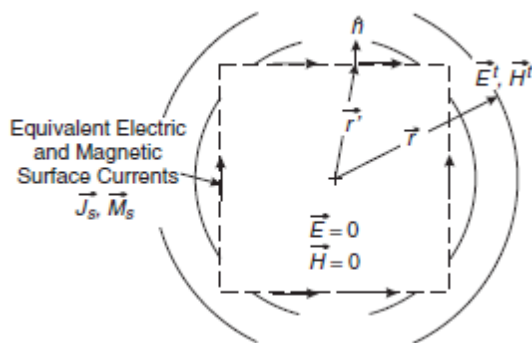


Figure 15 : Detail for the near field to the far field transformation [8]

Since the fields of interest are  $\vec{E}_t$  and  $\vec{H}_t$ , it is assumed that the electric and the magnetic fields inside the surface  $S$  are null ( $\vec{E} = \vec{H} = 0$ ). Then, the current densities flowing tangentially along  $S$  are simplified:

$$\vec{J}_s(r', t) = \hat{n} \times (\vec{H}_t - \vec{H}) \Big|_{\vec{H}=0} = \hat{n} \times \vec{H}_t(r', t) \quad (0.75)$$

$$\vec{M}_s(r', t) = -\hat{n} \times (\vec{E}_t - \vec{E}) \Big|_{\vec{E}=0} = -\hat{n} \times \vec{E}_t(r', t) \quad (0.76)$$

Then, the magnetic and the electric vector potentials, respectively  $\vec{A}$  and  $\vec{F}$  can be expressed regarding to this configuration:

$$\vec{A} = \iint_S \vec{J}_s \frac{\mu e^{-jkR}}{4\pi R} ds' \quad (0.77)$$

$$\vec{F} = \iint_S \vec{M}_s \frac{\epsilon_0 e^{-jkR}}{4\pi R} ds' \quad (0.78)$$

Where  $s'$  is the surface enclosing the electric current density  $\vec{J}_s$  and  $R$  is the distance from any source  $r'$  on  $S$  to the observation point  $r'$ . For the far field computations, the vectors  $R$  and  $r$  are assumed parallel, therefore that the potential vectors  $\vec{A}$  and  $\vec{F}$  can be simplified as follows [8]:

$$\vec{A} \approx \frac{\mu_0 e^{-jkr}}{4\pi r} \vec{N} \quad \text{where} \quad \vec{N} = \iint_S \vec{J}_s e^{jkr' \cos \psi} ds' \quad (0.79)$$

$$\vec{F} \approx \frac{\varepsilon_0 e^{-jkr}}{4\pi r} \vec{L} \quad \text{where} \quad \vec{L} = \iint_S \vec{M}_s e^{jkr' \cos \psi} ds' \quad (0.80)$$

$\psi$  : angle between  $r$  and  $r'$

Once the vector phasors  $\vec{N}$  and  $\vec{L}$  are known, the  $\vec{A}$  and  $\vec{F}$  can be approximated, and then the total E- and H- fields in the far field are obtained by using the following relations [8]:

$$\vec{E}_t = -j\omega\vec{A} - j\frac{1}{\omega\mu_0\varepsilon_0} \nabla(\nabla \cdot \vec{A}) - \frac{1}{\varepsilon_0} \nabla \times \vec{F} \quad (0.81)$$

$$\vec{H}_t = \frac{1}{\mu_0} \nabla \times \vec{A} - j\omega\vec{F} - j\frac{1}{\omega\mu_0\varepsilon_0} \nabla(\nabla \cdot \vec{F}) \quad (0.82)$$

#### 2.4.6.2. Electronic circuit fundamentals

The analysis of the antennas implies most of its parameters should be obtained in the frequency domain. However the FD-TD method is intrinsically a time-domain approach, therefore the Fourier transform is applied to allow the evaluation of the antennas performance.

The configuration of the feed region for an antenna can be depicted by the fig.16. The antenna is excited by a transmission line connected to a feed and radiates electromagnetic fields ( $\vec{E}_{tr}$  and  $\vec{H}_{tr}$ ) in the entire domain. The transmission line has characteristic impedance  $Z_0$  at the reference plane (usually a ground plane) obtained from:

$$Z_0(\omega) = F[V(t)] / F[I(t)] \quad (0.83)$$

where  $F[ ]$  represents the Fourier Transform. Typically, the characteristic impedance is real and is equal to a  $50\Omega$  resistance  $R_0$ . No reflection occurs for a wave ingoing to the source, meaning that the feed is matched to  $R_0$ . The voltage of the antenna excitation  $V_t$  is the sum of its incident reflected voltages, reciprocally  $V_t^+$  and  $V_t^-$ , at the reference plane.

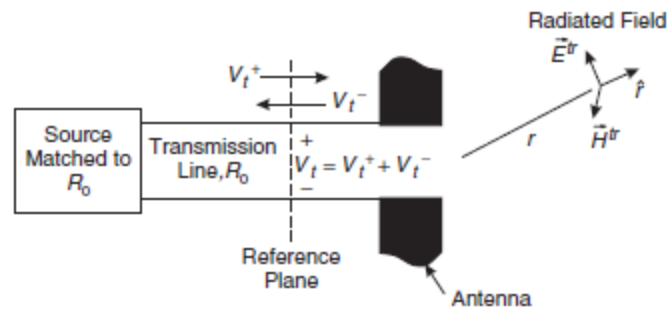


Figure 16: Antenna excitation [8]

Then, the voltage reflection coefficient and the input impedance can be calculated:

$$\Gamma(\omega) = \frac{F[V_t^-(t)]}{F[V_t^+(t)]} \quad (0.84)$$

$$Z_A(\omega) = Z_0(\omega) \left[ \frac{1 + \Gamma(\omega)}{1 - \Gamma(\omega)} \right] \quad (0.85)$$

#### 2.4.6.3. Excitation Source

The excitation source for the antenna analysis is given by the incident voltage in the transmission line and it is a time function,  $f(t)$ . This source is assigned to the electric and magnetic fields in the FD-TD space lattice. A common input signal chosen for the antenna analysis is a narrow pulse such as the Gaussian pulse with finite dc content [31]:

$$f(t) = e^{-\left[ \frac{(t-\tau)}{\tau_{decay}} \right]^2} \quad (0.86)$$

The pulse is centered at time step  $\tau$  and  $\tau_{decay}$  is the characteristic time. However, the dc component contained in this kind of source is never radiated by the antenna. Thus, the simulations of the near field's antenna with the Gaussian pulse might take too much time. To avoid this problem, another common source is defined as a sinusoidal wave of frequency  $f_0$  is modulated by a Gaussian pulse with any dc content:

$$f(t) = e^{-\left[ \frac{(t-\tau)}{\tau_{decay}} \right]^2} \sin(2\pi f_0(t-\tau)) \quad (0.87)$$

The pulse is again at time step  $\tau$  and  $\tau_{decay}$  is the characteristic time. The Fourier spectrum is symmetrically about  $f_0$  which is useful since the performance of an antenna is evaluated over a band of frequencies.

# CHAPTER 3: SIMULATIONS

---

This section presents the results of the simulations of the user interactions and, more particularly, the hand of the user with different types and configurations of handset antennas. Results are obtained using the 3rd generation FD-TD program implemented on the Matlab software.

This chapter begins with a brief sensitivity analysis of different parameters defined by the FD-TD which can alter the accuracy of the simulations results. It allows these parameters to be set for the rest of the simulations and guarantees relevance in the results analysis. Then, an investigation of the basic handset antennas which are the monopole and the PIFA follows. The effects of playing with different parameters such as the ground plane configuration and the position of the feed are presented and different models of hands are introduced. Next, the five PIFAs antennas are described, their performance are analyzed in free space and also with the presence of the hands. Finally, a comparative study of these antennas is made, focusing on their interaction with the hands. The reader will find the details of each simulation in the Appendix part at the end of the report.

## 3.1. Sensitivity analysis

The FD-TD method provides accurate results useful for designing antennas. However, these results can be altered if some parameters are not well defined. The influence of three parameters is investigated in this sensitivity analysis over a reference PIFA antenna.

- Number of time steps: For a fixed excitation pulse, the number of time steps varies by taking the values 5 000, 10 000, 20 000, 50 000 and 100 000.
- The PML thickness: Boundary conditions allow avoiding spurious reflections due to the outward waves. By varying the thickness of the layers, respectively (none, 2, 4, 6, 8, and 10), the reflection factor can be diminished.
- The computational domain boundaries: The domain is set to be at least 10 cells gap to the structure and the boundaries. Then, it will increase by step of ten (20, 30, 40, and 50).

The reference PIFA antenna used for this sensitivity analysis has been designed to resonate at 900MHz. Its configuration can be found in the Appendix (A). The same excitation source is applied to the antenna. This is a sinusoidal modulated by Gaussian pulse centered in time at 4ns and in frequency at 900MHz over a range of 1000MHz. On the graph, the curves are defined by the three parameters (TS/PML/DC). The first one (TS) is the number of time steps, the second one PML represents the number of cells defining the PML, and the third (DC) is the number of cells between the structure of interest and the domain boundaries.

### 3.1.1. Number of time steps

For this parameter, the PML thickness is set at 4 cells and the domain is extending to 20 cells from the structure.

The number of time steps alters the calculation of the impedance as the fig.17 shows. However, after 10000 time steps, it is difficult to distinguish the different return loss measurements. Looking at the table 17 in the Appendix (A), the same remark can be made for the radiation efficiency. For the rest of the sensitivity analysis, the number of time steps is set at 20 000.

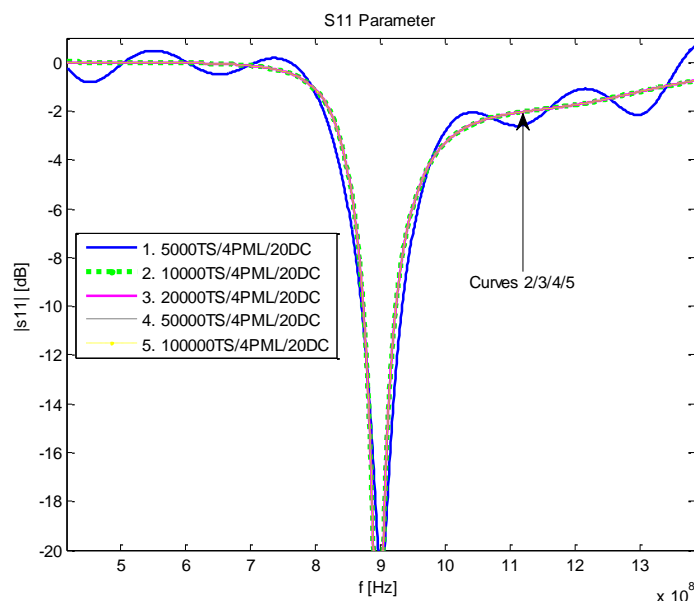


Figure 17: Time steps alteration analysis

### 3.1.2. PML thickness

The simulations are still running with the same PIFA antenna, excitation pulse and domain size but the number of time steps is now fixed at 20 000 and the PML depth is varying from 0 cell to 10 cells by a step of 2. The results of these simulations are shown in the table.18 of the Appendix (A) and also by the comparative graphs of the return loss. The influence of the PML thickness is significant according to the results. In fact, when no PML thickness is applied, the different performance parameters return some absurd values since the outgoing waves are not absorbed and therefore it causes reflection of the waves occurring at the vacuum-layer interface. As soon as the PML thickness is greater than 6 cells, the results seem to stabilize and provide a better accuracy in the antenna performance. Therefore, from now on, 8 depth cells will be used in the PML.

### 3.1.3. The Computational domain size

Finally, the domain size is investigated by increasing its boundaries from 10 to 50 cells. It appears that this parameter barely altered the performance of the antenna. Any distinction can be made between the different curves representing the return losses on the fig.64 in the Appendix (A). Thus, the gap between the structure in the computational domain and its boundaries is set to 20 cells.

### 3.1.4. Conclusion

This Sensitivity analysis provides a reasonable idea of the tendency of different parameters to impact upon the antenna performance. Therefore, they need to be specified when using the FD-TD method;

PML thickness (cells)	Number of time steps	Structure/Domain boundaries (cells)
8	20 000	20

Table 1 : Parameters of the FDTD

However these values cannot be taken as unalterable since the analysis has been lead only for one specific structure and excitation pulse.

## 3.2. Basic Handset Antennas

This section is focused on basic handset antennas which are the monopole and the PIFA. The purpose is to become more familiar on how an antenna is working and the influence of its different components on the parameters. Finally, the different models of the hand are introduced for both PIFA and monopole antennas and their influences are compared using the mismatch and the absorption losses.

As a result of the sensitivity analysis, all of simulations in this section are settled as follows:

$f_c$ [MHz]	$f_s$ [MHz]	$\tau$ [s]	PML thickness [cells]	Number of time steps	Cell size [m]	Structure/Domain boundaries [cells]
900	1000	4e-9	8	20 000	0,001	20

Table 2 : The FD-TD parameters used in the simulations

In this section, both the monopole and the PIFA are designed to resonate at a theoretical frequency of 900MHz, but all of the parameters are acquired at their own resonant frequency which differs from 900MHz.

### 3.1.5. The Monopole

To begin a monopole antenna has been designed in order to play on different parameters and understand the behaviour of the antenna. A monopole antenna is formed by replacing one half of the dipole antenna with a large ground plane. The configuration of the monopole is shown in the Appendix (B) along with the details of the simulations. First, the effect of the feed position is investigated, and then the influence of the ground plane on the antenna performance is presented. Finally, different models of hand are introduced in the computational domain.

#### 3.1.5.1. The effect of the feed position

The feed is moved from the corner of the ground plane's upper edge to the centre. The table.20 and the figure.66 in the appendix (B) give the results of these simulations.

The resonance frequency is the smallest when the resonating distance over the ground plane is the largest, i.e. when the feed is put at the upper corner of the ground plane. At the same time, with the same configuration, the matching of the antenna is the best one and its quality factor is the greatest.

#### 3.1.5.2. The effect of the ground plane

An infinite, planar and perfectly conducting ground plane provides the ideal configuration for the monopole antenna. Therefore, dealing with electrically small antennas as the handset antenna, implies a finite ground plane.

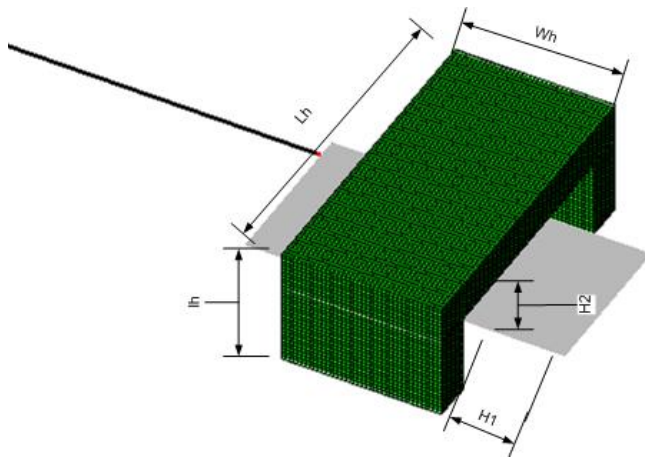
The effect of the ground plane size variation on the performance of the monopole is now investigated. The ratio between the length and the height is decreased, and the results are presented in the table. 21 in the Appendix B and the figure.67 .By decreasing this ratio, the resonant frequency moves closer to the theoretical resonant frequency and its mismatch loss is reduced.

#### 3.1.5.3. Hand influence

In order to comprehend the effect of the hand on the antenna performance, a hand is added to the simulation. First, the presence of a simple brick hand is investigated and then the six different hands provided by Mauro Pelosi from Aalborg University are introduced.

➤ The brick hand:

The design of this hand is simplistic, made with rectangular brick as the fig.18 below shows:



$Lh$ : the length of the hand fixed at 80mm  
 $lh$ : the height of the hand fixed at 30mm  
 $Wh$ : the width of the hand fixed at 40mm  
 $H1$ : the distance the bottom of the ground plane and the hand  
 $H2$ : the gap between the ground plane and the palm of the hand.

Figure 18: Monopole antenna surrounded by a basic brick design

This hand has been modeled for simulations at 900MHz. According to the reference (), the values of its relative permittivity  $\epsilon_r$  and its electrical conductivity  $\sigma$  have been defined as:

$$\epsilon_r = 36,2 \quad \sigma = 0,79S.m^{-1}$$

The results are presented in the table.23 in the Appendix (B):

The presence of the brick hand alters the resonance frequency of the monopole from approximately 10 to 20MHz in less. It affects also but the radiation efficiency of the monopole antenna even if the antenna still radiates 91% of its input power.

By increasing  $H1$  and  $H2$ , the resonant frequency is also increased, and the mismatch loss reduced. When the hand is the closest to the feed ( $H1=80$ ), the radiation efficiency is the lowest at 91%.

➤ The hand models:

The different models of hand can be found in the Appendix (C). They can be classified in two groups: the Soft Grip and the Firm Grip. Then, for each kind of grips, the index is localized at three different positions: right, middle and left. These six models are introduced in the computational domain with the electrical properties defined for simulations at 900MHz. From hands 1 to 3, they are set at the same position in the grid (and reciprocally for the hands 4 to 6). The simulations are run with the same monopole (see table.24 and figure.69 in the Appendix B).

The results show that in the monopole case the firm grip provides a better radiation efficiency since 81% of the input power is radiated whereas, for the soft grip, 74% is radiated. However, the mismatch loss is reduced by 2 with the soft grip hands, going from 0,48 dB for the 0,23dB.

The position of the index doesn't alter the radiation efficiency and barely affects the mismatch loss in the soft grip case where it is the best with the hand 6(soft grip / left). It can be explained since the index placed on the left is the furthest from the feed.

### 3.1.6. The PIFA

#### 3.2.1.1. Introduction of a short circuit element

Introducing a parallel inductance, such as a short circuit, is permitting the antenna to match the characteristic impedance, when connected closely to the feed point. This is verified thanks to the mismatch loss value that is equal to 4,9 without any short circuit versus 0,33 once the short wire is setup.

Moreover, when the short circuit is well placed, ideally where the electric field of the  $TM_{100}$  mode is null, the resonant frequency is soaring. This allows designers to reduce the PIFA dimensions, and consequently to imagine new antenna shapes that would fit into smaller devices. The different remarks given below are making some references to the results exposed in appendix B section B.3

#### 3.2.1.2. Influence of the gap between the ground plane and the plate

Decreasing the gap  $H$ , increases the resonance frequency and the bandwidth at resonance. This fact can easily be explained by the formula applied for the PIFA dimension.

$$f_R = \frac{c}{4 \times (L_1 + L_2 + H - W)}$$

As  $L_1$ ,  $L_2$  and  $W$  are fixed, decreasing  $H$ , increases the resonance frequency.

In addition, we remark that the return loss  $S_{11}$  becomes lower with the reduction of the gap since it goes from -44 dB for a 10mm gap to -24,7 dB for a 2mm gap even though it is not that meaningful as the mismatch loss is 0 for every gap but the 2mm which is at 0,01 dB.

To finish, the bandwidth is increasing when the patch and the ground plane are getting closer each other. The 8mm gap PIFA will be used in the next comparisons as a reference. (cf. table26 in appendix B)

#### 3.2.1.3. Length and width configuration of the Plate

On the one hand, keeping the same overall dimensions of the plate does not affect the resonance frequency, no matter if the width is longer than the length or “vice versa”. On the other hand mismatch loss is rising with the growth of the  $(L_1 / L_2)$  ratio whereas; the bandwidth is going down linearly. (cf. table27 in appendix B)

#### 3.2.1.4. Ground Plane dimensions

The width of the ground plane is kept fixed for this experiment to cover the whole part of the patch at each simulation. When the length is made smaller, the resonant frequency is increasing. In a similar way, the  $Q$  factor is rising up to attain 91,7. Consequently the bandwidth is very low since, apart from the reference antenna ( $N^{\circ}4$ ), none of them has a bandwidth superior to 30 MHz. (cf. table34 in appendix B)

#### 3.2.1.5. Short circuit width effects

Varying the size of the cut circuit element allows the size of the resonating plate to be reduced since the resonant frequency is surging. In addition, it has to be noticed that the matching loss is reaching a non-acceptable level one the width becoming bigger than 4mm. Indeed, once this length exceeded, the  $S_{11}$  becomes lower than 6 dB which is considered as the low bound. However, this factor is influencing the bandwidth in the right way. (cf. table28 in appendix B)

#### 3.2.1.6. Feed size effects

In a slower way than that of the short size, the feed size is inching up the resonance frequency as well. Nevertheless, the  $S_{11}$  remains to an acceptable level since it never goes higher than -9,6dB. Besides, the bandwidth is slightly modified following the different cases, but is never varying of 35MHz between the two extremities. The simulation with the triangle shaped feed source gave some pretty similar results as the source with the same base size of 4 mm. The shape is therefore not so much important in this case to excite the antenna. (cf. table29 in appendix B)

#### 3.2.1.7. Short position

Moving the short away from the feeding source shows that both the bandwidth and frequency resonance are modified. The most far is the short away from the source, and the higher is the resonant frequency. From the  $S_{11}$  side, no rule can be determined since it goes up from 2mm to 5 mm, whereas it falls from 5mm to 10mm, and increases again at 40mm. This depends on the values of the electric field value at the short position. (cf. table30 in appendix B)

#### 3.2.1.8. Feed position

The feed has been moved together with the short wire to prevent distortion of the results according to the previously observed results corresponding to the influence of the distance Feed-Short. These simulations illustrate the fact that the corners of the plate are the most appropriate to place the feed as these are the positions with the lowest mismatch loss. However, when connected to the middle of the patch, the PIFA exhibits the highest resonant frequency with an acceptable level of loss, and most of all, the best bandwidth that is almost doubled up compare to the original reference. (cf. table31 in appendix B)

#### 3.2.1.9. Introduction of a variable capacitor

The introduction of the capacitor in the PIFA configuration is tuning the antenna of about plus 100MHz, and the mismatch loss is passing from 0 to 2,57 which is a real problem as it implies a  $S_{11}$  above the -6dB .

Once the capacitor is installed on the antenna, changing the value of it does not really change any of our parameters, but the bandwidth that is slightly decreasing of 2 MHz.

However, using a fixed value capacitor of 1nF and moving it over the patch gives some interesting results. Firstly, the frequency resonance is rising with the distance to the short cut element and reaches 1435MHz. The bandwidth is moving up, as well, and is reaching a peak with the antenna N°35 at 811MHz. However, the mismatch loss becomes, here again, higher than 1,26dB which corresponds to the -6dB limit that poses a real problem here. (cf. table32 in appendix B)

#### 3.2.1.10. Hand effect

Owing to their “grip style” described in Appendix C, two hand categories can be set among those six different hands.

First category from hand 1 to 3, which corresponds to antenna numbers 41 to 43 represents the hands handling firmly the handset. The second category formed by hand 4 to 6, which are the antennas 44 to 46, corresponds to the hands handling softly the handset.

To begin, one can say that the resonant frequency of this PIFA is not influenced so much by the different hands as the maximum difference between the lowest resonating frequency and the highest one is of 10MHz. Nevertheless, all of these frequencies are, at least tuned of 86 MHz down compared to the free space one. This illustrates one of the main influences of the hand phantom on the antenna parameter. (cf. table 35 in appendix B)

Secondly, the radiation efficiency is quite the same in one group, but it is relevant to notice that the average radiation efficiency for the soft grip is slightly better than that of the firm one (0,24 dB gap at the closest values) . This can be explained by the fact that the electromagnetic fields have more room to irradiate beyond the hand when the palm is not stuck to the device. In addition, the last hands in both firm and soft groups give the best result in terms of radiation efficiency (with 36% and 40% respectively). This relies on the position of the index finger and demonstrates that it can act as notably as the hand palm position.

To finish, the  $S_{11}$  at the resonant frequency permits to quantify the worsening of the handled antennas, compared to the free space model. Antennas 41 and 42 show the worst mismatch loss, while 45 and 46 gives the best ones. These results are actually in accordance with the fact that the soft grip style hands with the third index position are the less disturbing models. All of these results can be noticed in the figure 71 in the Appendix B for a more visual comprehension.

### 3.2.2. Comparison PIFA/Monopole

In this comparison, it is important to remember that hands 1 to 3 correspond to the “firm grip style”, and 4 to 6 correspond to the “soft grip style”. Moreover, in these “two groups”, the more the hand index number increases, the more to the left the index finger of the hand is located. The explanations given below can be observed in the figure. 19.

First of all, the most obvious point to note, is that the global performances are definitely better for the monopole than for the PIFA. Both curves for the mismatch loss and the radiation efficiency of the monopole are located above the PIFA’s ones. Second of all, the mismatch loss and the absorption loss follow the same tendency, having better behaviors with the soft grip than with the firm one. This can be explained, taking into consideration the vicinity of the hands for both types of antennas. Considering the PIFA, it is understandable that there will be a lot more of resonating surface covered by the hand than that of the monopole that is located above the user hand. For that reason, the PIFA is detuned in a greater way, and thus, its overall performances are lowered more than the monopole ones.

However, it is worth to note that the radiation efficiency of the monopole is the only parameter showing worse results for the soft grip than the firm one. This is due to the fact that, holding the handset this way is placing the hand in a more radiated zone by the antenna. Besides, it is noticeable that the PIFA performances are modified by both the grip style and the finger position, whereas, only the grip style is influencing significantly the performances of the monopole antenna. This suggests that the finger position is not directly influencing the electromagnetic fields of the monopole contrary to the PIFA case.

Finally, in free space, the absorption loss is null for the two antenna types, since, there is no external object to disturb the power radiated all around. Nonetheless, the mismatch loss is equal to 0,33dB for the monopole, contrary to 0 dB for the PIFA. This result confirms that, originally, the PIFA is better matched than the monopole.

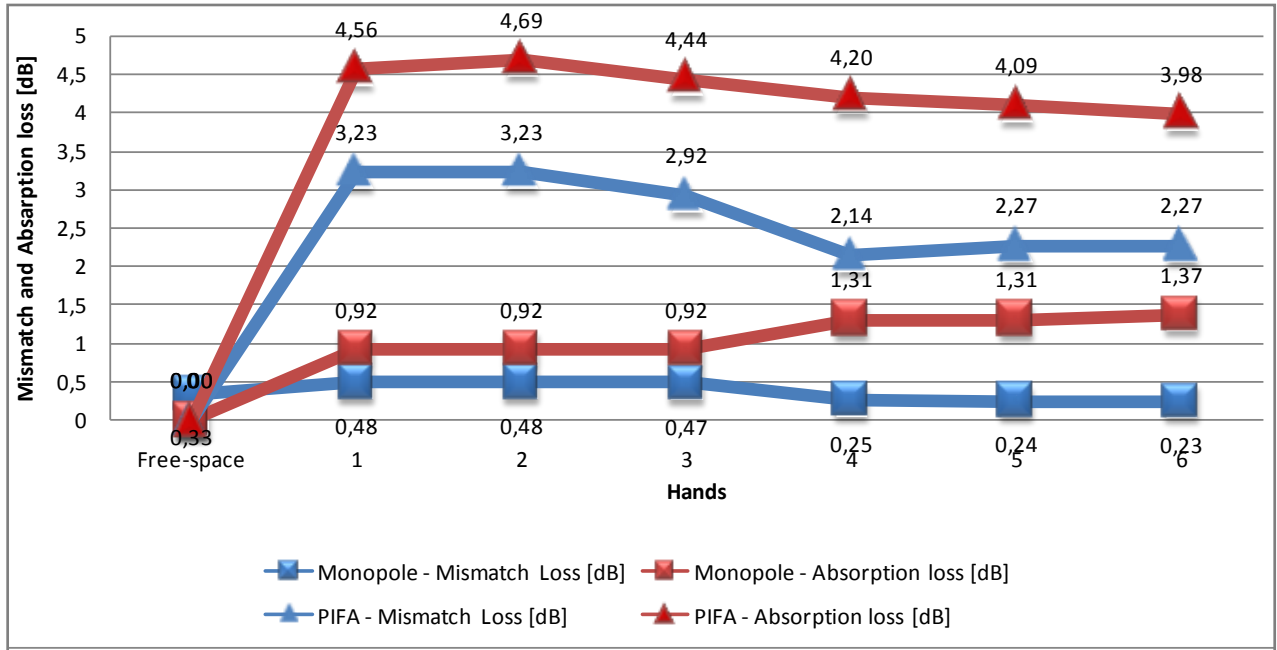


Figure 19: Losses comparison according to the six hand models

### 3.3. Hand influence on mobile phone antenna

In this section, five types of handset antennas are used to investigate the effect of hand phantom on mobile phone antenna performance. These five PIFA antenna models are designed for the GSM 900 and 1800. Some of them cover also the UMTS frequencies range (1920-2170MHz). The details of the frequency bands used in wireless personal communications are shown by the figure.72 in the appendix D. Each antenna is first described in free space and with the different models of hands (see Appendix C). They can be classified in two groups: the Firm Grip (hands 1, 2 and 3) and the Soft Grip (hands 4, 5 and 6). Then, for each kind of grips, the index is localized at three different positions: right (hands 1 and 4), middle (hands 2 and 5) and left (hands 3 and 6). For these simulations the antenna is situated at the top of the handset. Then, in order to investigate the impact of the position of the antenna within the handset, the same simulations are run but with the antennas placed on the bottom of the PEC ground plane. Finally, the impact of the presence of the phantom hand is analyzed and compared for the five PIFAs.

All of the simulations are running with the same program (3<sup>rd</sup> generation FD-TD) and with these following parameters:

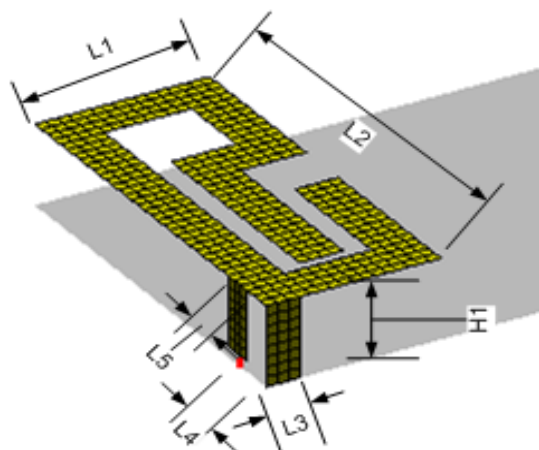
$f_c$ [MHz]	$f_s$ [MHz]	$\tau$ [s]	PML thickness [cells]	Number of time steps	Cell size [m]	Structure/Domain boundaries [cells]
1500	2000	8e-9	8	100 000	0,001	20

Table 3 : The FD-TD parameters used in the simulations

### 3.3.1. PIFA1 Profile

The first designed PIFA is a dual band antenna operating over the GSM 850-900 and the frequency range.

#### 3.3.1.1. Design Description



- L1, L2: Length and width of the Pifa plate
- L3: Width of the short circuit
- L4: Distance between the source and the corner
- L5: Width of the source
- H1: Height between ground plane and the patch
- H2: Height of the bended part

Figure 20: PIFA1 design

The original conception of this antenna can be found in [32]

This first antenna can be qualified as a PIFA bi-band since it is designed to resonate in both GSM 900 and GSM1800. It is composed by a main patch radiator at a height of 8mm from the ground plane of dimensions: 40mm x 100mm. A feed source is positioned at the ground plane and linked to the patch by a 2mm large conductor, and a short plate of 3mm is placed 6mm away from the feed.

Pifa Bi-band	Parameters							Results				
	L1	L2	L3	L4	L5	H1	H2	$f_r$ [MHz]	S11 [db]	Q	Bw [MHz]	Mismatch Loss [dB]
<b>PIFA 1_900</b>	16	40	2	6	3	8	-	911	-19,3	5,5	165	0,05
<b>PIFA1_1800</b>	16	40	2	6	3	8	-	1891	-15,5	12,9	147	0,12

Table 4: PIFA1 performance in free space

#### 3.3.1.2. Performance in free space

The first resonating frequency is found at 911MHz. At this frequency, the reflection coefficient equals to -19,3 which gives a mismatch loss of 0,05 dB. To finish, its bandwidth is of 147MHz. The second resonating frequency is 1891MHz, where the  $S_{11}$  value is -15,5 that provides a mismatch loss of 0, 12 dB. According to the Q, the bandwidth is of 147 MHz.

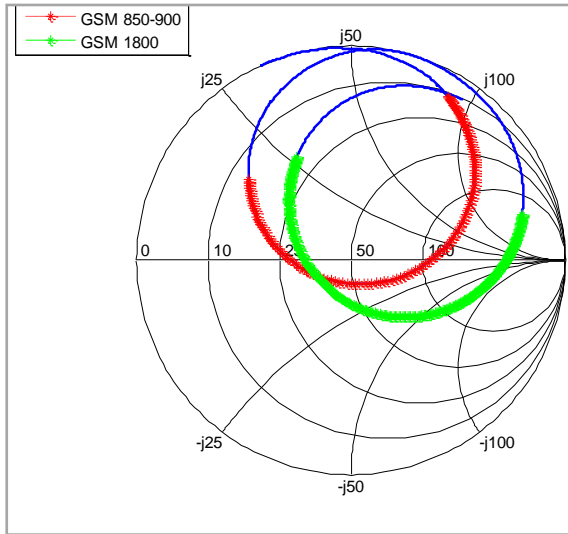


Figure 21: PIFA1 Smith chart

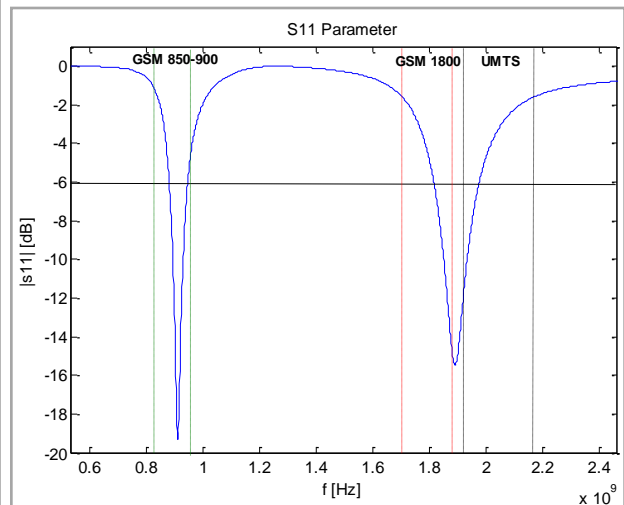


Figure 22: Return Loss plot of the PIFA1

3.3.1.3. Hands Influence on the antenna performances

➤ PIFA1 performance in talk position

First, this graph shows (fig.23) that variations are more significant for the 900 MHz than the 1900MHz one. Results are globally better for the soft grip hands, with a significant improvement of the Absorption Loss at 1900MHz. The worst results are found for the absorption loss is with the first hand at 900MHz. A last thing to notice is that the mismatch loss at 1900MHz is not significantly moving following the grip style, even though, the position finger has a little influence.

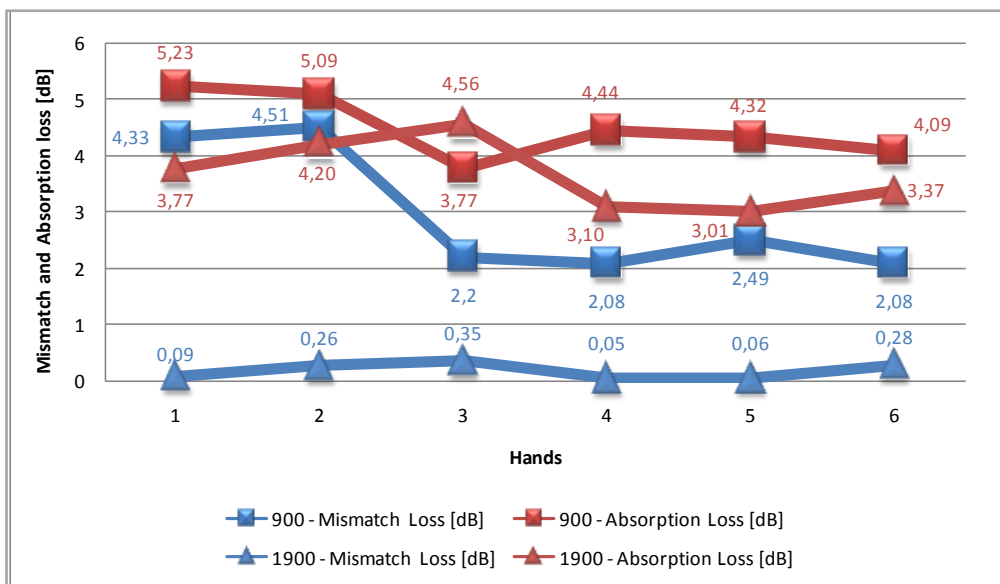


Figure 23: PIFA1 Mismatch and Absorption Loss with Hand Models for both frequencies

➤ Top/bottom comparison at 900MHz and 1900MHz

- 900MHz : Thanks to this figure (fig.24), it is noticeable that the losses at 900MHz are greater when the antenna is located at the top for both the firm and soft hands grip group. The only case where the top antenna is slightly better, is for the third hand in mismatch loss, and the most significant gap between the top and the bottom results concern the mismatch loss.

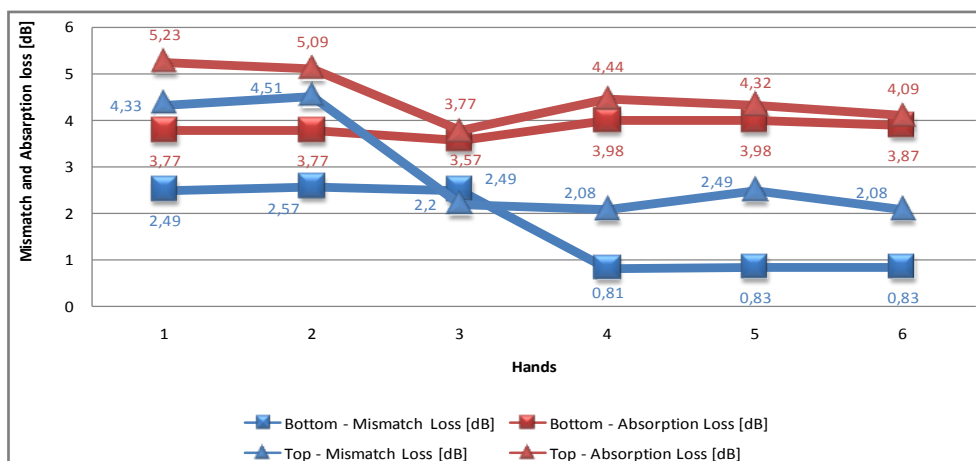


Figure 24: PIFA1 Top/Bottom Mismatch and Absorption loss comparison at 900MHz

- 1900MHz: According to this graph, mismatch losses, are pretty similar whether the antenna is at the top or at the bottom, with a small advantage for the bottom in firm grip, and for the top in soft grip. The difference for the absorption loss is more obvious for the firm hands with some worst results for the top antenna, especially at the third hand. Nevertheless, for the soft hand grip, here again, the results are not so different between the two locations, and it is interesting to see that the best results is found with the sixth hand at the top.

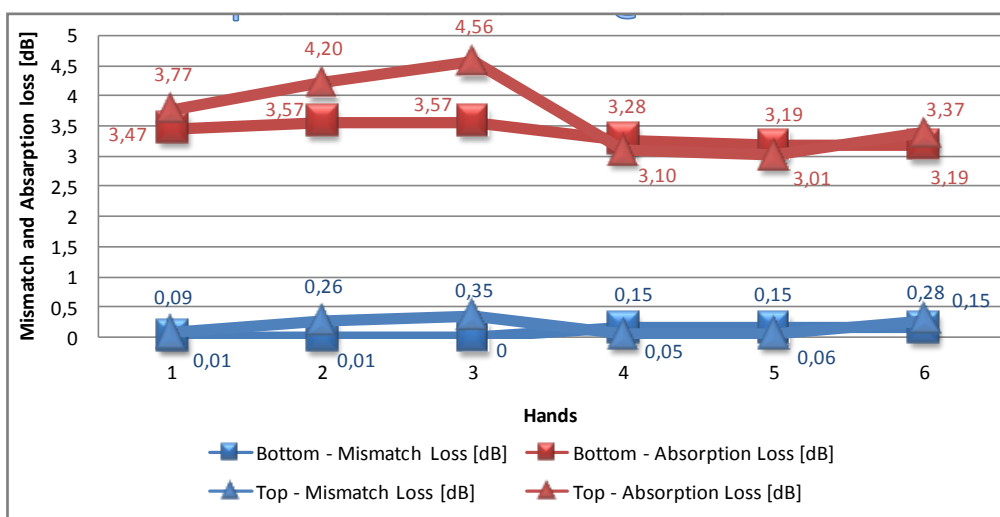


Figure 25: PIFA1 Top/Bottom Mismatch and Absorption loss comparison at 1900MHz

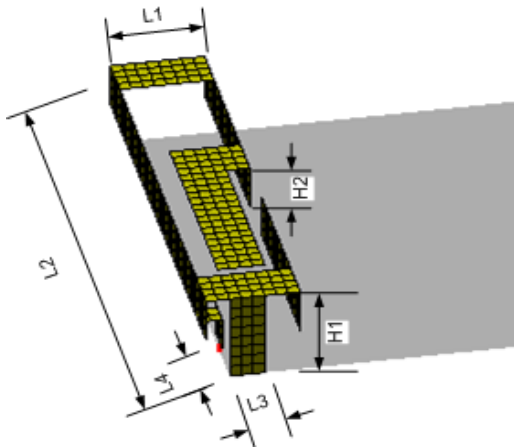
To summarize, this antenna is more disturbed by hands at the low frequencies, especially the absorption loss. Moreover, the bottom placed antenna presents some overall better results at 900MHz. A last thing that is worth to point out is that when handled firmly, the antenna at 1900MHz

reacts in a better way when positioned at the bottom, contrary to the soft grip, where the antenna presents some better results at the top.

### 3.3.2. PIFA2 Profile

#### 3.3.2.1. Design Description

This PIFA has been designed based on the previous model (PIFA 1). The modification that has been performed is to bend the extremities. Otherwise, all the other dimensions are the same as PIFA 1. The idea here is to analyze the behavior of the antenna when a smaller surface is directly covered by the human tissues.



- L1, L2: Length and width of the plate
- L3: Width of the short circuit
- L4: Distance between the source and the corner
- L5: Width of the source
- H1: Height between ground plane and the patch
- H2: Height of the bended part

Figure 26: PIFA2 design

Below is the dimensions and performances table.

Pifa Bi-band	Parameters							Results				
	L1	L2	L3	L4	L5	H1	H2	$f_r$ [MHz]	S <sub>11</sub> [dB]	Q	Bw [MHz]	Mismatch Loss [dB]
PIFA2_900	8	40	3	4	2	8	4	953	-27,4	2,2	430	0,01
PIFA2_1800	8	40	3	4	2	8	4	2026	-10,5	15,7	129	0,41

Table 5: PIFA2 performance in free space

#### 3.3.2.2. Performance in free space

The performances presented here are different from the previous model since the geometry of the antenna is not the same anymore. The first resonating frequency is 953 MHz, which is 40 MHz more than the first resonating frequency of PIFA 1. Likewise, the second resonating frequency has increased, to reach 2026 MHz, which corresponds to a rise of 135MHz. Besides, a big change here is the detuning of the second resonating frequency in the UMTS band. The two resultants S<sub>11</sub> at these frequencies are equal to -27,4 dB and -10,5 dB respectively. This corresponds to a mismatch loss of 0,01 dB for the 953MHz frequency and of 0,41 dB for the 2026 MHz frequency.

Finally, it is clear that the bandwidth of the first frequency resonance has moved up to 430 MHz contrasting with the 165 MHz for the PIFA 1, whereas, it slightly decreased at the second resonant frequency with 129 MHz compared to 147 MHz. A comparison of the reflection coefficient curves is displayed on fig.27.

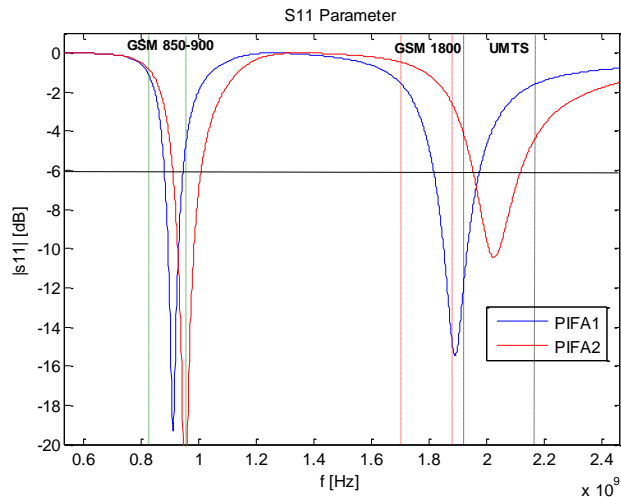


Figure 27: Return Loss comparison plot between PIFA1 and PIFA2

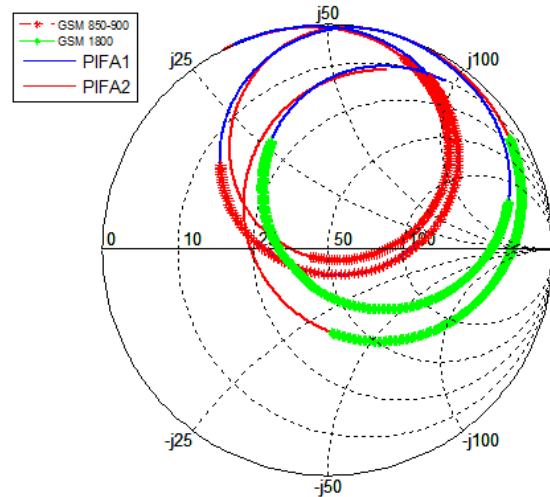


Figure 28: PIFA2 vs. PIFA1 Smith chart

### 3.3.2.3. Hands Influence on the antenna performances

#### ➤ PIFA2 performance in talk position

Here again, the mismatch loss for the high frequency (2000 MHz) is the lowest parameter, that implies that the high frequencies are less susceptible to the environment than the smaller ones.

In addition, the mismatch loss for the 900MHz band presents the most significant changes between the firm and soft style. On the other side, the absorption loss varies in an opposite way to each other, and following the grip style. It is noticeable that the biggest losses are found for the second hand not only for the mismatch loss, but for the absorption one as well.

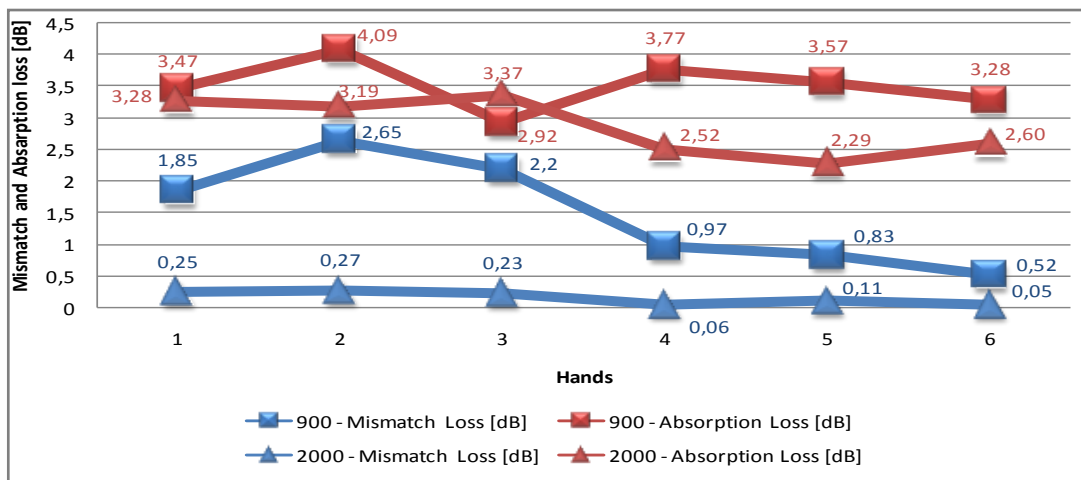


Figure 29: PIFA2 Mismatch and Absorption Loss with Hand Models for both frequencies

#### ➤ Top/bottom comparison at 900MHz and 2000MHz

- 900MHz: This chart that evaluates the difference between the top and bottom position of the antenna at 900MHz, illustrates that they behave in a similar style. The only perceptible differences are that the absorption loss at the bottom is stable at a higher value than that of the top one. The mismatch loss at the top, is a bit upper for second hand, but is behaving very closely to the bottom results for the other ones.

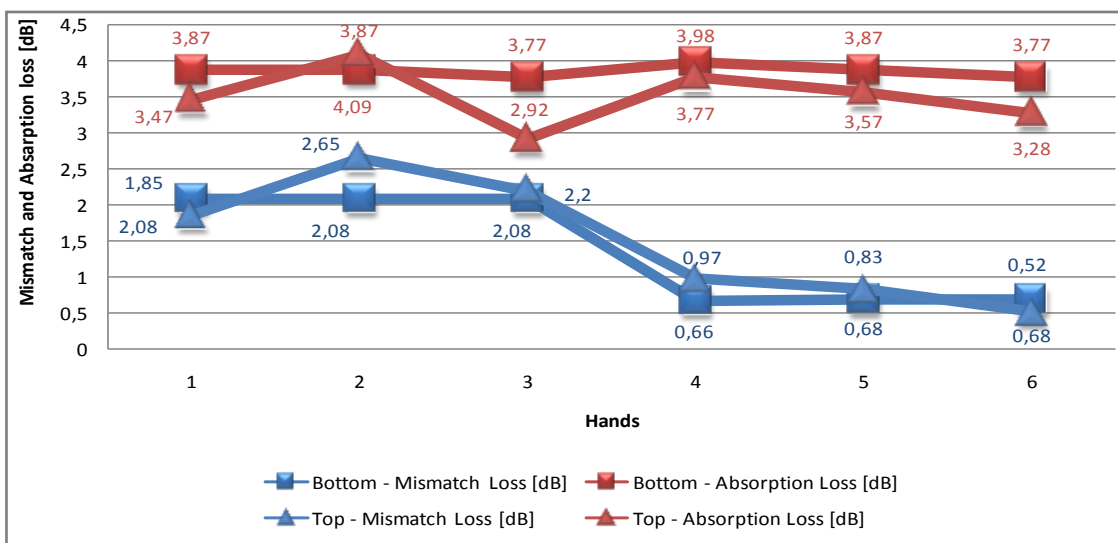


Figure 30: PIFA2 Top/Bottom Mismatch and Absorption loss comparison at 900MHz

- 2000MHz: The tendency observed at 900 MHz is even more accentuated here. As it can be seen, the two antennas, at the bottom or at the top express some very similar results. The absorption loss is moving in parallel with the two antennas handled with the soft grip, and is really close with the firm one. Concerning the mismatch loss now, the position of the finger does not change the results that are remaining stable, whereas the grip style inverses the advantage between the top and the bottom one. The top antenna is actually better for the firm grip, whereas this bottom one for the soft grip. Though, results for the mismatch loss are never far away for each case.

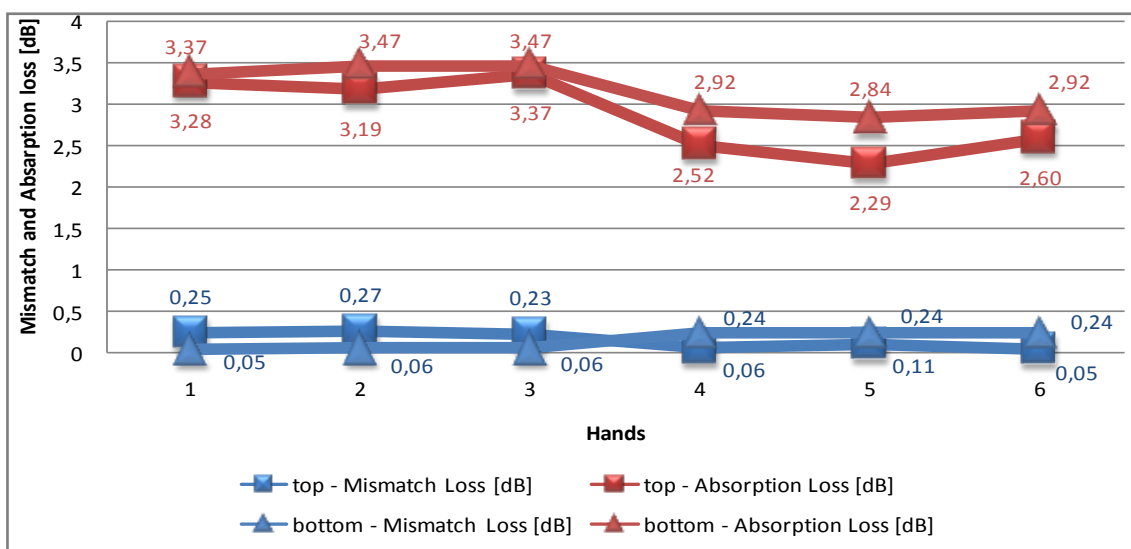


Figure 31: PIFA2 Top/Bottom Mismatch and Absorption loss comparison at 2000MHz

### 3.3.3. PIFA3 Profile

#### 3.3.3.1. Design description

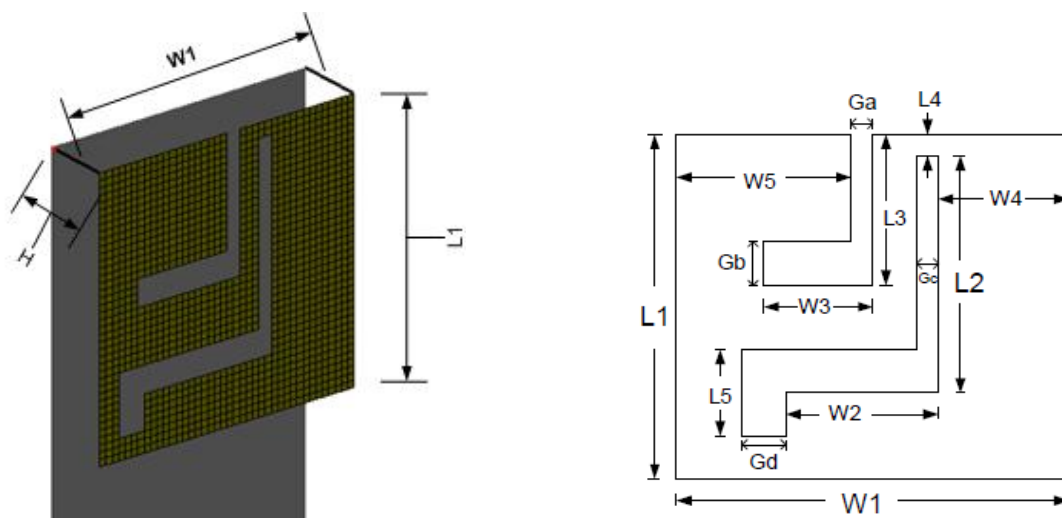


Figure 32: PIFA3 design

L1: Length of the plate ; W1: Width of the plate ; H: Height between ground plane and the plate

Parameters														
Pifa Bi-band	L1	L2	L3	L4	L5	W1	W2	W3	W4	W5	Ga	Gb	Gc	Gd
PIFA3	0	23	20	2	9	40	21	16	13	20	2	4	2	4

Table 6: Pifa3 parameters

The design of this PIFA is inspired from [33]. As it can be observed, two slots to provide different radiating frequencies are directly inserted over the plate. In addition, the feeding source and the shorting elements are localized at the top edge of the patch, precisely, at the two opposite corners. The two slots that can be described as “the L slot” for the smallest one and the “S slot” for the longest, are of a same width vertically ( $G_a=G_c=2\text{mm}$ ), and horizontally ( $G_b=G_d=4\text{mm}$ ). The overall dimensions of the plate are: 40 x 40 mm.

#### 3.3.3.2. Performance in free space

Results					
Pifa Bi_band	$f_r$ [MHz]	$S_{11}$ [db]	Q	Bw [MHz]	Mismatch loss [dB]
PIFA3_900	948	-21,3	6,7	143	0,03
PIFA3_1800	1934	-24,4	12,5	154	0,02

Table 7: PIFA3 performance in free space

The original performances of the antenna in free space are: a first resonating frequency at 948MHz with a  $S_{11}$  at -21,3 dB, and a bandwidth of 143MHz. A second resonating frequency is observed at 1934 MHz with a  $S_{11}$  of -24,4 dB, and a bandwidth of 154 MHz. Both these frequencies give a very good mismatch loss, not exceeding 0,03 dB. The  $S_{11}$  chart is presented below:

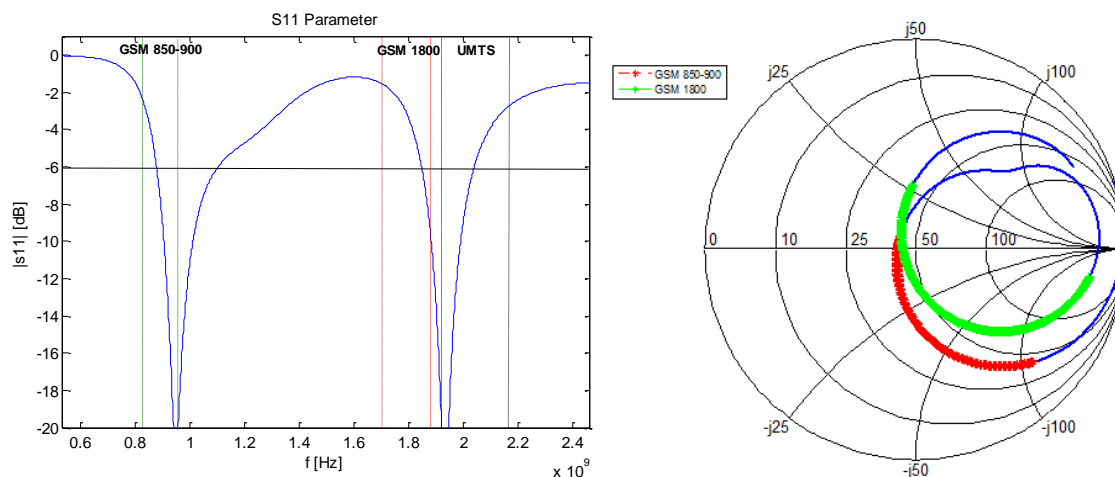


Figure 33: Return Loss and Smith Chart plot of the PIFA3

### 3.3.3.3. Hands Influence on the antenna performances

#### ➤ PIFA3 performance in talk position

This graph is interesting to study for several reasons. Firstly, the peak noticed at the second hand for the mismatch loss at 1900 MHz is quite surprising. A deeper study of the near field when the antenna is transmitting is actually demonstrating that the highest electromagnetic point is exactly matching with the index finger position. A schema representing the EM fields in the near field is exposed in figure.36 a little further in this section. Otherwise, the absorption loss at 900 MHz is constantly decreasing with the hand index and there is a notable improvement for the absorption loss at 1900MHz as well as 900 MHz. Same conclusion can be formulated for the mismatch loss but the difference is less effective.

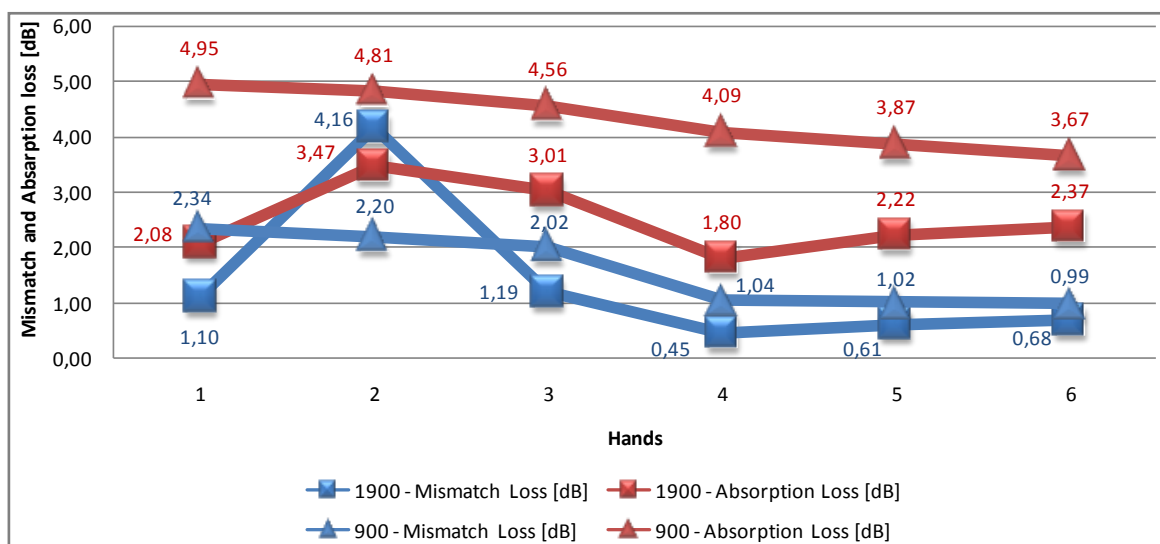


Figure 34: PIFA3 Mismatch and Absorption Loss for both frequencies

#### ➤ Top/bottom comparison at 900MHz and 1900MHz

- 900MHz: The influence of the localization of the antenna is acting in this case importantly. In fact, the top located antenna is exhibiting some worse performances than the bottom one, especially when the handset is handled. On the other hand with the soft grip style, tendencies are inversed, and top placed antenna is improving

its performance, contrary to the bottom placed one even if the bottom antenna is still at least as good as the top one.

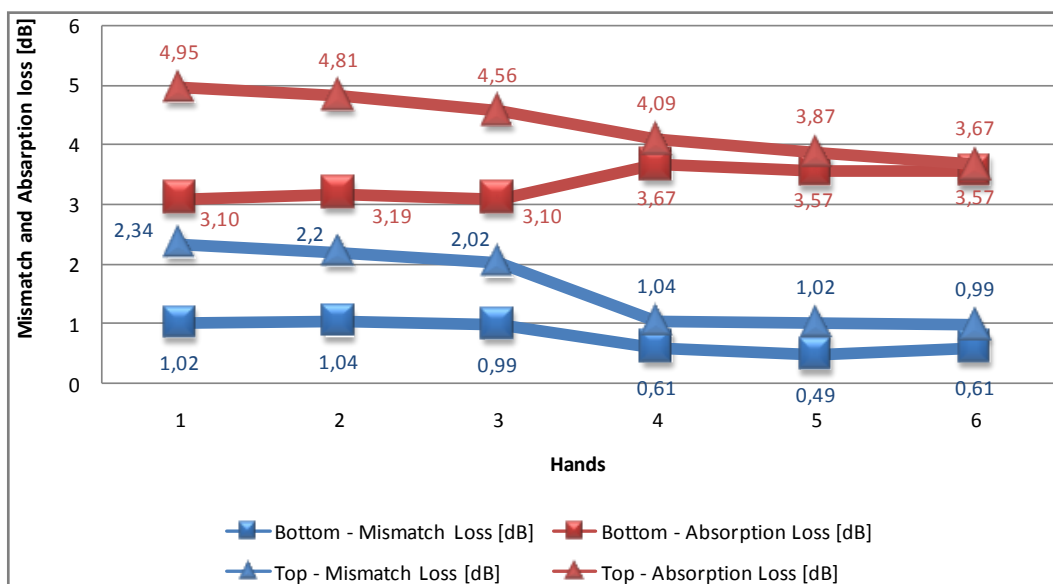


Figure 35: PIFA3 Top/Bottom Mismatch and Absorption loss comparison at 900MHz

- 1900MHz: At 1900 MHz, with the firm style, the top antenna is actually giving some better results, except for the second hand. But first and third hands have a very lower mismatch and absorption loss than the bottom one. The most apparent changes with the soft grip handling are the enhancement of the mismatch loss for the bottom antenna that is even better than the top one. Best results are examined at the fourth hand, with the top antenna, that illustrates that the top antenna is the most promising for this configuration. As we can see on the fig.36, the second hand is placing the index at the very same place where the biggest amount of field is radiated. This observation, gives a logic explanation to the peak observed for the second hand when working at 1900MHz.

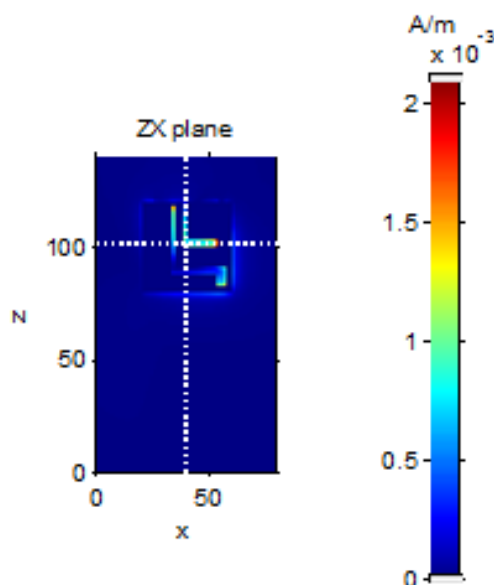


Figure 36: PIFA3 Near Field radiation in the ZX plan at 1900MHz

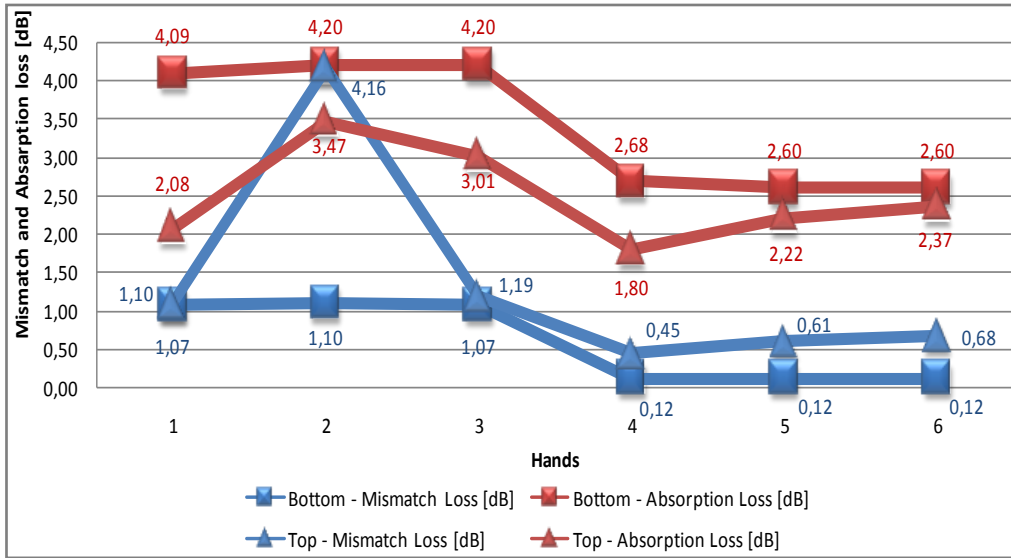
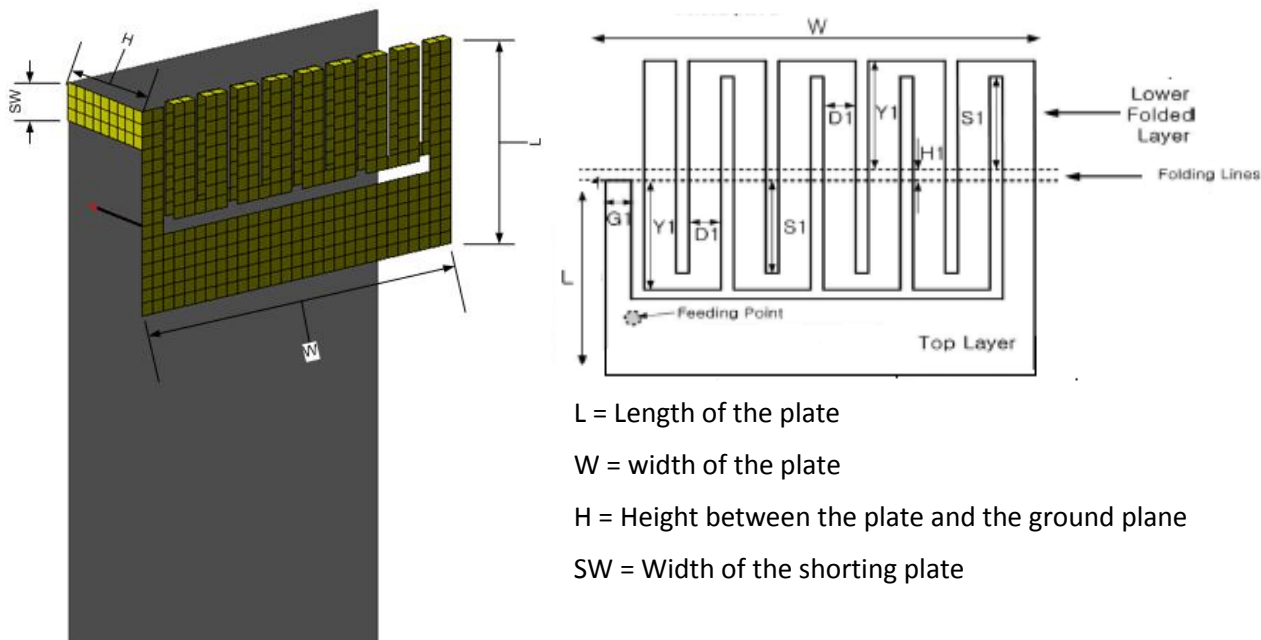


Figure 37: PIFA3 Top/Bottom Mismatch and Absorption loss comparison at 1900MHz

### 3.3.4. PIFA4 Profile

#### 3.3.4.1. Design description



The design of this antenna has been customized for the purpose of this thesis, but the first conception approach can be found in [34]. This PATCH is constituted by two main parts that are the top layer, and the lower resonating part. The different elements are the feed source with a wire connecting it to the PATCH, the short circuit element, the ground plane of size : 29 x 100 mm and, of course, the PATCH composed by a meandered, and a plain section. Dimension details are given in the table.8:

Parameters									
Pifa Bi-band		W	G1	H	H1	D1	S1	SW	Y1
PIFA4	6	29	2	9	1	2	8	3	9

Table 8: PIFA4 Parameters

#### 3.3.4.2. Performance in free space

Results					
Pifa Bi-band	$f_R$ [MHz]	S11 [db]	Q	Bw [MHz]	Mismatch loss [dB]
Pifa4_900_freespace	958	-24,6	6,5	147	0,02
Pifa4_1800_freespace	1800	-14,3	14	129	0,16

Table 9: PIFA4 performance in free space

As readable in the above table, the two radiating frequencies are 958MHz and 1800MHz. The corresponding  $S_{11}$  is equal to -24,6 dB and -14,3 dB respectively. In accordance with these values, the mismatch loss calculated equals to 0,02 dB for the low frequency and 0,16 dB for the high one. To finish, the bandwidth at 958MHz is of 147 MHz, and at 1800 MHz of 129 MHz.

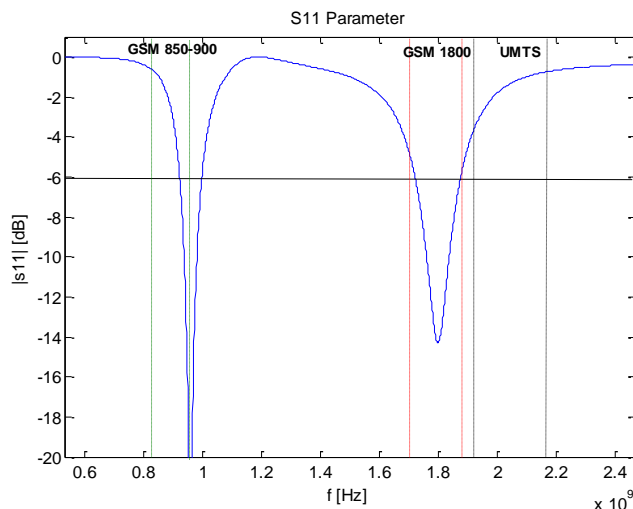


Figure 38: Return Loss plot of the PIFA4

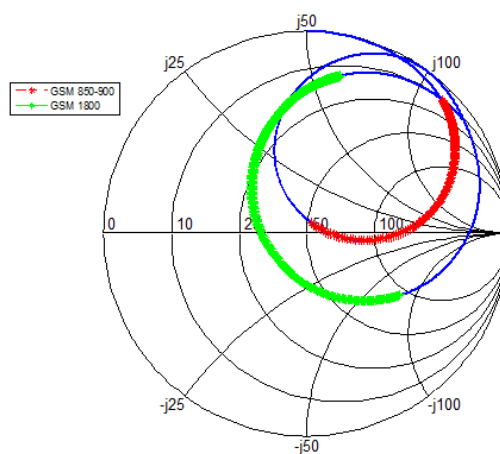


Figure 39: Smith chart of the PIFA4

### 3.3.4.3. Hands Influence on the antenna performances

#### ➤ PIFA4 performance in talk position

To begin, the mismatch loss is the most willing to change in function of the hand, in particular for the 900MHz antenna. Second hand is giving the worst result here again for the absorption and mismatch loss at 900MHz, as well as the absorption loss at 900 MHz. As described previously, the explanation comes from the position of the index finger at a crucial radiating point of the PIFA. Best results tendency is found for the soft grip style hands. The hand six is presenting some improved results with the two kinds of losses at both frequencies. It has to be noticed, that, once again, parameters varying in the most notable way concern the low frequency.

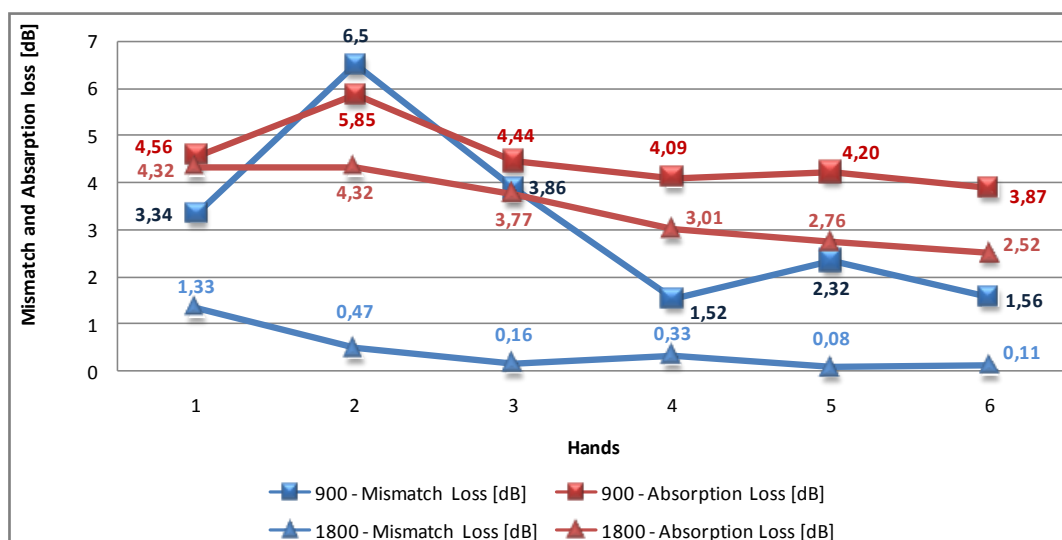


Figure 40: PIFA4 Mismatch and Absorption Loss for both frequencies

#### ➤ Top/bottom comparison at 900MHz and 1800MHz

- 900MHz: Firstly, the results concerning the soft hands are particularly similar for top and the bottom PIFAs. Neither the absorption loss nor the mismatch loss is notably affected by the finger position with these hands models. Secondly, there are some noteworthy changes among the different firm grip hands. Likewise the two previous antennas, the second position of the index finger is fading the law resonance

frequency in a significant manner. However, the third hand is giving a very good mismatch loss for the bottom and top antennas, although, the bottom one is definitely smaller than the top one.

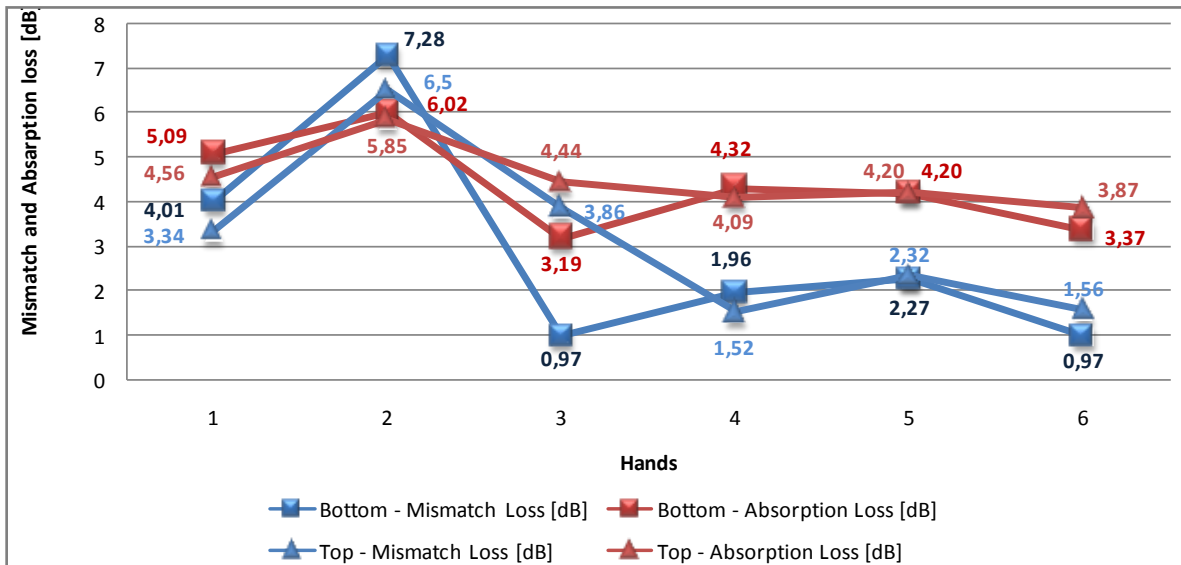


Figure 41: PIFA4 Top/Bottom Mismatch and Absorption loss comparison at 900MHz

- 1800MHz: This chart is demonstrating how the mismatch loss is reacting in a similar style for both the bottom and the top, for any of the tested hands. The worst results are acquired for the first hand, and the best one at the sixth one, according to both antennas location. For the absorption loss, it can be noticed that the performances increase with the hand index number. This signifies that not only the index finger location is an active parameter, but the firm grip is shifting the results as well.

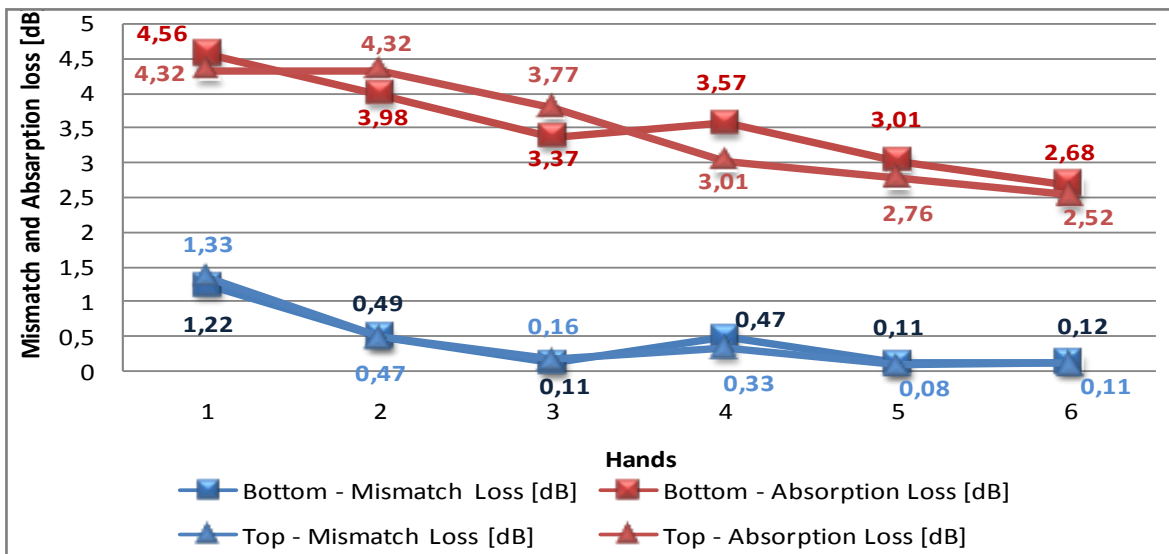


Figure 42: PIFA4 Top/Bottom Mismatch and Absorption loss comparison at 1800MHz

Consequently, the absorption loss is found to be the lowest at the sixth hand, and highest at the first one as well. Depending whether the antenna is handling firmly or softly, the bottom or the top antennas have better behaviors one after another respectively.

### 3.3.5. FICA Profile

#### 3.3.5.1. Design description

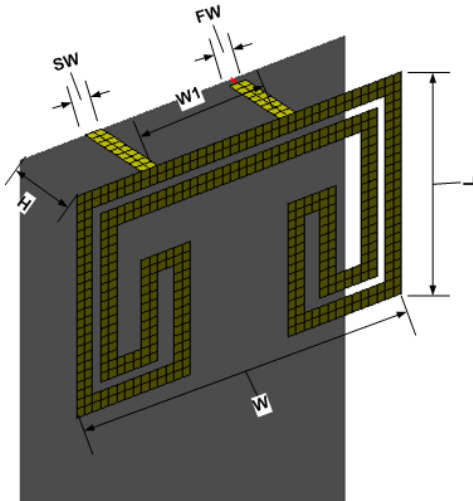


Figure 43: FICA design

		Parameters [mm]				
Pifa Bi-band		W	W1	H	SW	FW
FICA	0	26	16	9	2	2

Table 10 :FICA parameters

The Folded Inverted Conformal Antenna (FICA) is an internal antenna designed for multiband cell phones. According to [35], its particularity comes from its unusual “U-shaped elongated flat conductor featuring a closed meandered slot”. This specific shape is interesting to study for the influence of hand-hold position problem since the slot in the design assumes a smaller impact with the hand. The FICA used in the simulations is shown in the figure.44 and the parameters of the antenna dimensions are listed in the table.10. The antenna is mounted on a ground plane with size 40x100mm.

#### 3.3.5.2. Performance in free space

The FICA antenna operates at GSM900 and GSM 1800. The third band at 1500MHz is not investigated here. The figure.45 indicates these three resonances. The details of the antenna performance are presented in the table.11. In the Smith chart (see figure.46), the tree loops representing the three bands are depicted and for the GSM 1800 the matching of the antenna seems perfect as the loop passed at the middle of the Chart.

		Results				
Pifa Bi-band		$f_R$ [MHz]	S11 [dB]	Q	Bw [MHz]	Mismatch loss [dB]
FICA_900_freespace		932	-20,4	11,7	80	0,04
FICA_1800_freespace		1802	-34,3	10,6	170	0

Table 11 : FICA performance in free space

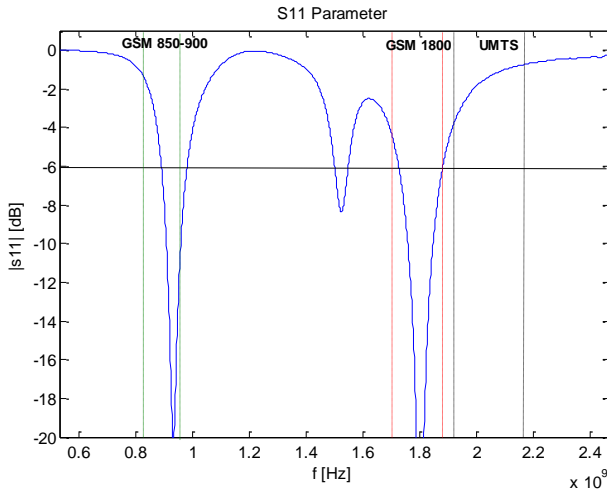


Figure 44: Return Loss plot of the FICA

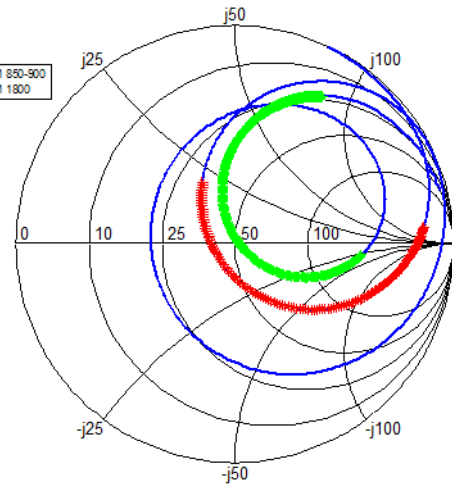


Figure 45: Smith chart of the FICA

### 3.3.5.3. Hands Influence on the antenna performances

#### ➤ FICA performance in talk position

The six hand models are now introduced and their influences on the FICA antenna are investigated. The details of each simulations are reported in the table () in the Appendix (letter). The below figure.47 shows the mismatch and the absorption loss for the six hand models at both 900MHz and 1800MHz.

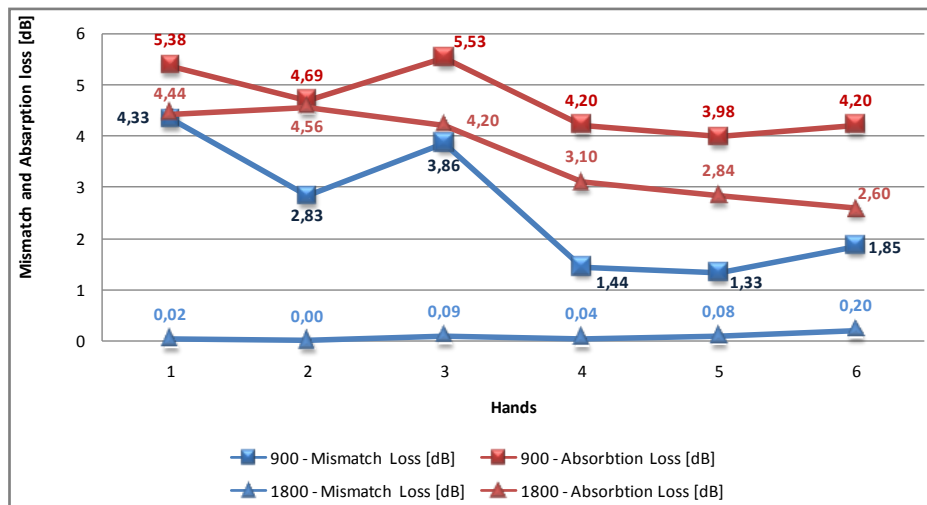


Figure 46: FICA Mismatch and Absorption Loss for both frequencies

The reading of this graph brings different comparisons and conclusions:

- The Mismatch loss is higher than the Absorption loss;
- The 900MHz band is more affected by the hand presence than the 1800MHz one since the highest Mismatch and Absorption loss are both found for the 900MHz frequency.
- The mismatch and the Absorption loss are reduced when using the soft Grip at both frequencies (except for the mismatch loss at 1800MHz which is not significantly affected by the firm grip).
- As expected the FICA antenna is less affected by the hands with index placed on the middle of the ground plane (hand 2 and hand 6). Indeed, this position corresponds to the slot in the antenna design.

➤ Top/bottom comparison at 900MHz and 1800MHz

A comparison between the top and the bottom position of the FICA on the Ground plane is provided in this section. This comparison is made at 900MHz and 1800MHz and presented reciprocally by the fig.49 and fig.50 :

- 900MHz: As the fig.49 shows, the lowest mismatch and the absorption losses for the six hands are found when the FICA is placed on the bottom. Moreover when the plate is placed on the bottom, only the grip style alters the amount of loss of the antenna. In fact, the mismatch and the absorption losses remain constant even if the position of the index is changed.

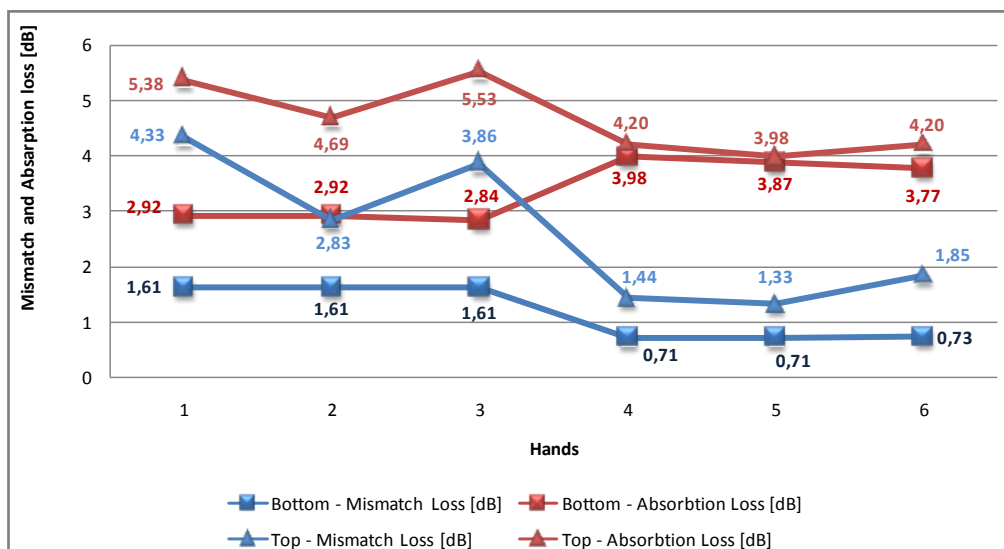


Figure 47: FICA Top/Bottom Mismatch and Absorption loss comparison at 900MHz

- 1800MHz: For the six hands, the lowest mismatch and the absorption losses are still found when the FICA is placed on the bottom. For both positions (top and bottom), the mismatch loss remains constant with the six hands. It is approximately null which means that the matching of the antenna is still acceptable.

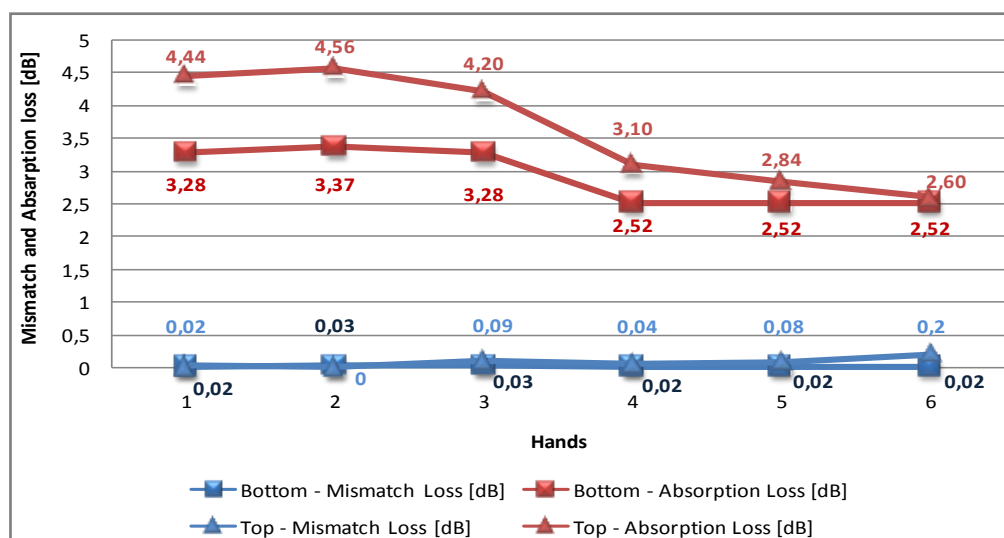


Figure 48: FICA Top/Bottom Mismatch and Absorption loss comparison at 1800MHz

### 3.4. Hand influence Benchmark on five dual-band antennas

#### 3.4.1. Introduction

This last section compares the five antennas previously described and particularly the impact of the different hand models on the efficiency. The PIFAs designs and their performance in free space are reminded. Then, the simulation procedure is described when the hand is introduced in the immediate vicinity of the antennas. Finally, the analysis of the results is provided using a statistical approach based on the mismatch and absorption loss. The grip style, the position of the index, and the antenna configuration are more specifically investigated.

#### 3.4.2. The different antenna models

The five antenna models used in the hand interaction tests have been described in the previous section and are reminded by table.12. All of them are PIFAS dual- or tri- band. However only the frequency ranges 824-960MHz and 1710-2170MHz are investigated.

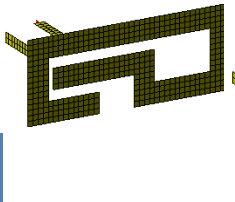
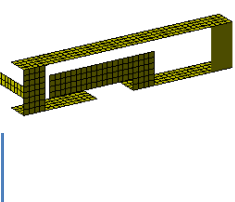
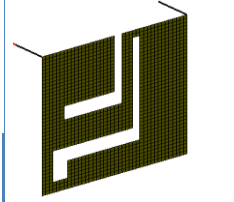
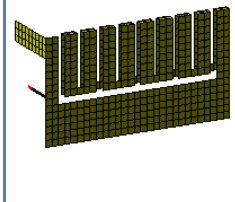
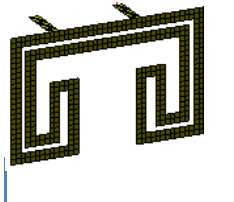
	PIFA1	PIFA2	PIFA3	PIFA4	FICA
Design					

Table 12 : PIFAs designs

Each antenna has a specific design but they are all mounted on a perfectly electric conductor ground plane of  $100 \times 40 \text{ mm}^2$ , except for the PIFA3 which has a  $100 \times 29 \text{ mm}^2$  ground plane with no thickness. Moreover, the antennas don't occupy the same volume since the spacing between the upper plate and the ground plane is not the same for each antenna. Fig.51 shows the return loss measurement of all five designs. On the one hand, they are all covering the GSM 900 band; on the other hand, their higher resonant frequency can differ significantly from one to another. From now on, the higher frequency range will be referred as the 1900MHz band.

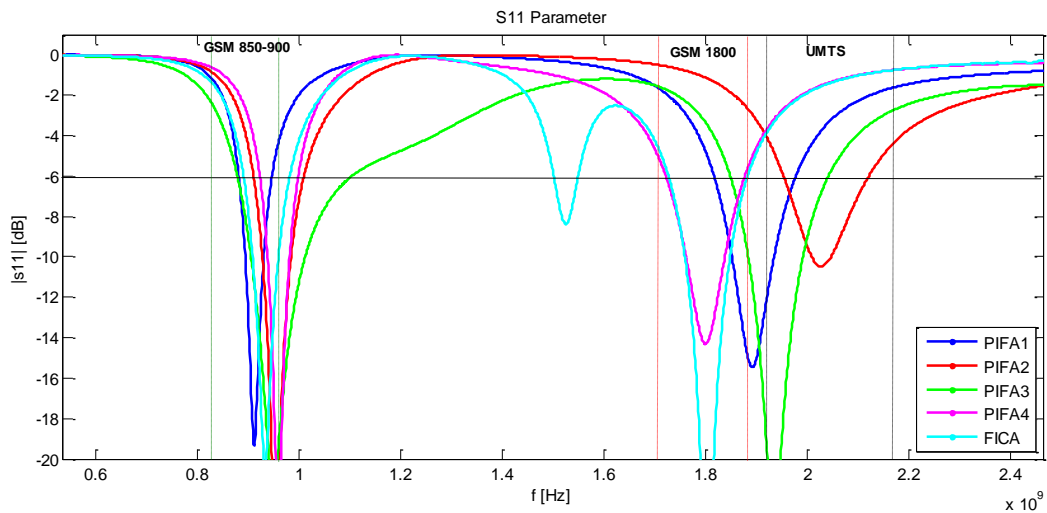


Figure 49: Overall Return Loss Illustration for the Five Antennas

The performance of the antennas working in free space are shown in the below table. More details about their specific performance when they interact with the hand can be found in the previous section. The radiation efficiency is not presented here since in the free space the input power of each antenna is equal to its radiated power which corresponds to a radiation efficiency of 1.

		Frequency /900MHz					Frequency/ 1900MHz				
Variables	Antenna model	PIFA1	PIFA2	PIFA3	PIFA4	FICA	PIFA1	PIFA2	PIFA3	PIFA4	FICA
	GP [mm <sup>2</sup> ]	100x40	100x40	100x40	100x40	100x29	100x40	100x40	100x40	100x40	100x29
	Plate [mm <sup>2</sup> ]	16x40	8x40	40x40	16x29	26x40	16x40	8x40	40x40	16x29	26x40
	H [mm]	8	8	10	9	9	8	8	10	9	9
Results	f <sub>R</sub> [MHz]	911	953	948	958	932	1891	2026	1934	1800	1802
	S <sub>11</sub> @ f <sub>R</sub> [dB]	-19,3	-27,4	-21,3	-24,6	-20,4	-15,5	-10,5	-24,4	-14,3	-34,3
	Q	5,5	2,2	6,7	6,5	11,7	12,9	15,7	12,5	14	10,6
	Bw[MHz]	165	430	143	147	80	147	129	154	129	170
	ML[dB]	0,05	0,01	0,03	0,02	0,04	0,12	0,41	0,02	0,16	0,00

Table 13 : PIFAs Performance in free space

From the table, the antenna providing more bandwidth in the 900MHz band is the PIFA2 since the folded sides of the antenna are close to the ground plane. The FICA is the antenna which operates on a wider range at 1800MHz but it is also the one with the narrower band at 900MHz.

### 3.4.3. Simulations and measurements in talk position

#### 3.4.3.1. Simulations setup

The simulations are run on the five antennas, mounted at the top and at the bottom of the ground plane. The six different hand models are introduced for these two distinct configurations. The purpose is to investigate the influence of the hand when the antenna is moving on the ground plane. All of the simulations are run for both 900MHz and 1900MHz bands. Based on their higher resonant frequency, the PIFA1 and PIFA3 are run at 1900MHz, the PIFA2 at 2000MHz. Finally the PIFA4 and the FICA simulations are performed for a frequency of 1800MHz. For the hand models used in the simulations, specific values of permittivity and conductivity are used depending on the frequencies of interest. Based on ref [28] these values are presented in the table below:

	PIFA 1		PIFA 2		PIFA 3		PIFA 4		FICA	
f <sub>SIMU</sub> (MHz)	900	1900	900	2000	900	1900	900	1800	900	1800
Permittivity ε'	36,2	32,4	36,2	32,1	36,2	32,4	36,2	32,6	36,2	32,6
σ (S.m-1)	0,79	1,32	0,79	1,37	0,79	1,32	0,79	1,26	0,79	1,26

Table 14: Electric properties of the hand models

In order to estimate the impact of the hand on these five antenna designs, a comparative study is driven focused on the mean value of the absorption and the mismatch losses.

#### 3.4.3.2. Results and Comparative study

The comparative study takes into account all of the simulation results with the different configurations of antennas. Specific parameters are investigated in order to observe a global tendency of the antenna performance. This comparative analysis is divided as following:

- 1) The six hands: The mean value of the absorption and mismatch loss of each antenna is represented and analyzed for the six hand models.
- 2) Firm/Soft: This comparison is based on the grip style of the hand which alters significantly the antenna performance.

- 3) Position of the index: The position of the index might affect the impedance matching and the radiation of the antenna depending on its design.
- 4) Top/bottom: This section compares the performance of the antenna when this one is mounted on the top and on the bottom of the ground plane.
- 5) 900MHz/1900MHz: The influence of the frequency is finally investigated.

The figures in this study are reduced for a practical purpose but the original scaled ones can be found in the Appendix (E). The colors in the graphs represent either the hand models (Legend n°1) or the mismatch and absorption loss (Legend n°2).

Legend n°1	■ hand 1	■ hand 2	■ hand 3
	■ hand 4	■ hand 5	■ hand 6
Legend n°2	■ Average Mismatch Loss [dB]		■ Average Absorption Loss [dB]

Table 15: Graph Legends

1) The six hand models comparison

This first performance analysis is based on the absorption loss and the mismatch loss in the presence of the hands models. It is represented by the fig.52.

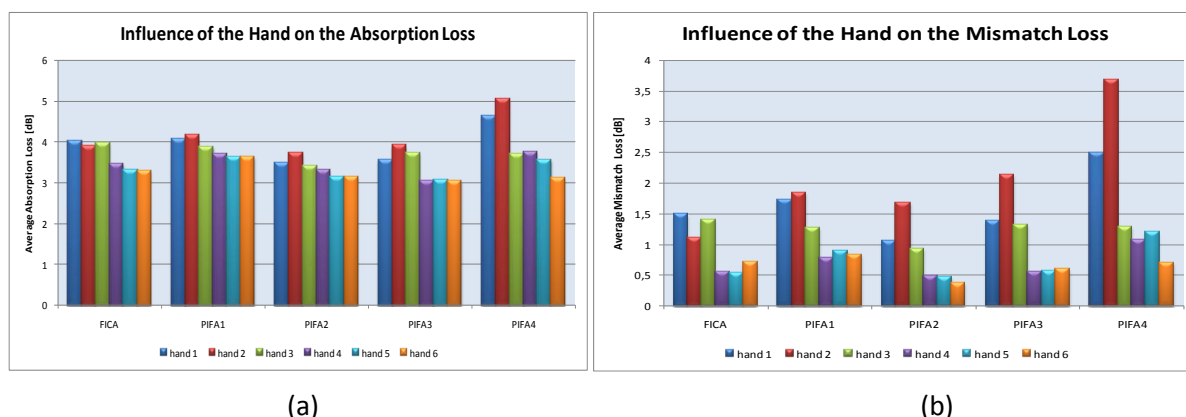


Figure 50: Mismatch(a) and Absorption(b) Losses Comparison Between the hand models

- The Absorption loss: As the graph of the fig.52 shows, the highest absorption losses are found for the PIFA4 with the hands 1 and 2. In fact, these hand models belong to the firm grip style which means that the gap between the palm and the handset is minor. Moreover, among the antennas designs, the PIFA4 is the only one where the feed is not positioned on the top of the plate but in the middle of the left edge. The size of the PIFA4 plate (16x29mm<sup>2</sup>) presents also a unusual feature since it is the smallest one among the other antennas. Therefore the power is more concentrated and then, the hand strongly affects its absorption loss. Except for the FICA, the hand2 provides the largest amount of absorption loss. On the contrary, the hands providing the lowest absorption losses are clearly the hands with a soft grip (hands 4 to 6), more particularly the hand6 is lightly better than the other.
- The Mismatch loss: The highest mismatch losses are also found for the PIFA4 with hands 1 and 2. Except for the FICA, the radiation of the antennas is more affected by the presence of the hand2. As the absorption loss, the hands 4, 5 and 6 presents the lowest mismatch losses. Finally, in a general manner, the mismatch loss for one antenna with one hand presents a smaller value than the absorption loss in the same configuration.

2) Firm/Soft Comparison

The influence of the grip style is now investigated. The Mean mismatch and absorption loss for both soft and firm grip are represented by the fig.53. These values are calculated by classifying the results with hand 1, 2 and 3 as the firm grip and 4, 5 and 6 as the soft one.

For each antenna, the firm grip affects both the mismatch and the absorption loss more than the soft grip. Moreover, the PIFA4 with the firm grip is the antenna which presents the highest mismatch and absorption loss for soft grip. The mean value of the mismatch loss in the firm grip is reduced to half in the soft grip whereas the absorption loss is slightly decreased.

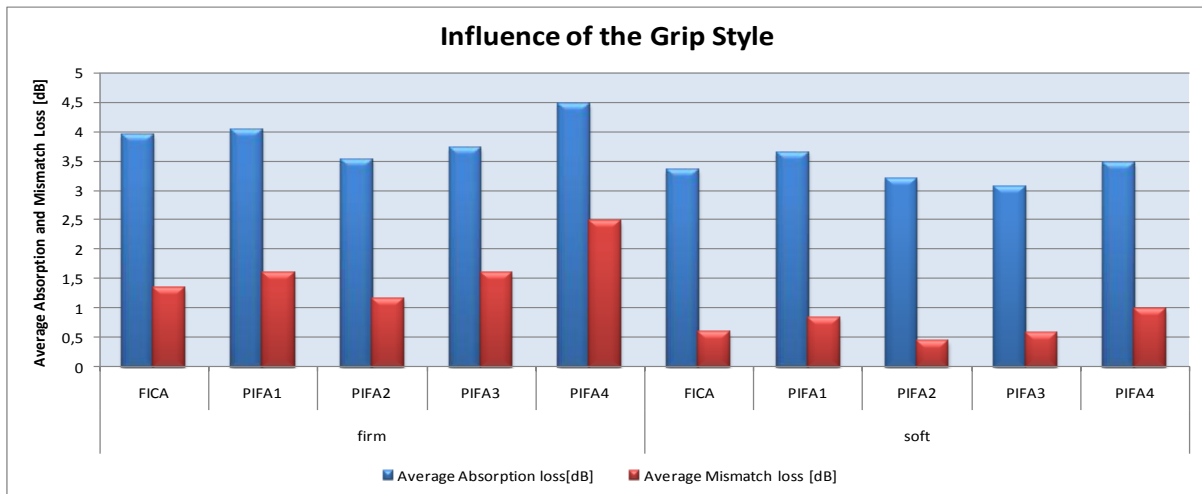


Figure 51: Antennas Analysis based on the grip Styl

3) Index position comparison:

For the index position analysis the hands have been classified into three groups: left, middle and right. Reciprocally, the hand 1 and 4 belongs to the first group, the hand 2 and 5 to the second group and 3 and 6 to the last one. As the influence of the index is minor when the antenna is moved to the bottom of the ground plane, these simulations haven't been taken into consideration in the calculation of the mismatch and absorption loss. The fig.54 represents the influence of the index on the antenna performance when this one is at the top of the ground plane.

- Absorption loss: As the figure shows, the absorption loss slightly differs between the different index positions, except for the PIFA4 where the right and middle positions of the index provides higher loss than the left position. The explanation is given in the first comparison about the hands.
- Mismatch loss: The mean value of the mismatch loss presents more variation than the absorption loss, except for the PIFA2 where both absorption and mismatch loss don't vary with finger position. As well as the absorption loss, is the highest values for mismatch loss are reached by the PIFA4 with the middle and right position.

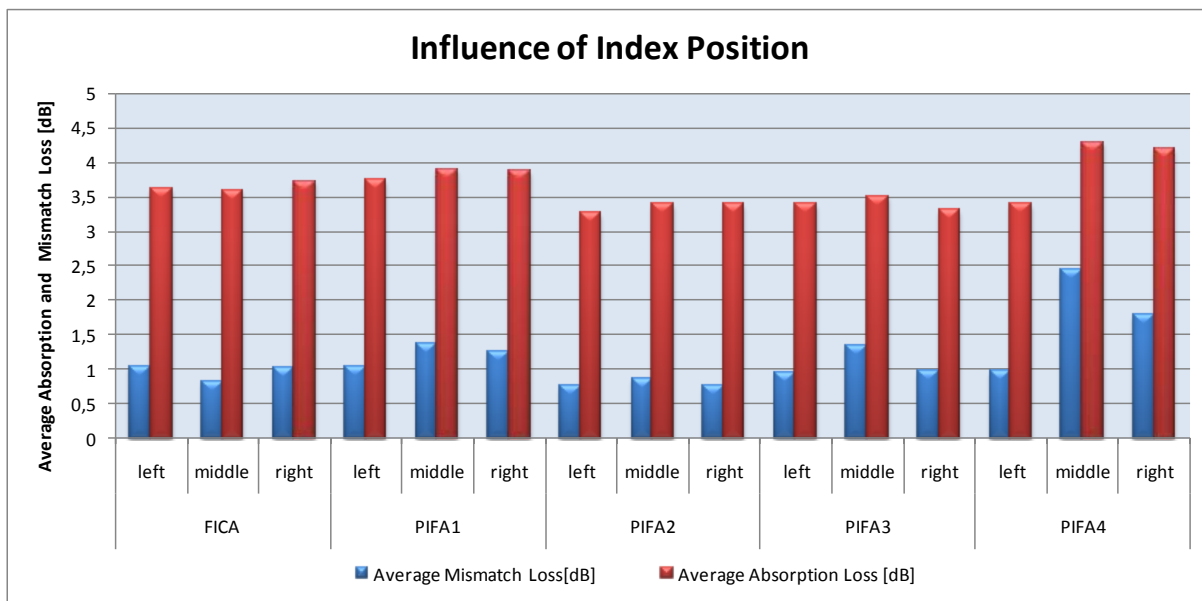


Figure 52: Antennas Analysis Based on the Index Position

4) Hands influence study according to the frequency range

This last losses analysis is built from the results found at both resonating frequency of each antenna. Graphical results can be seen on the fig.55. These two frequencies will be referred as the “low frequency”, for the 900MHz one, and as the “High frequency” for the 1800 MHz, 1900MHz and 2000MHz ones.

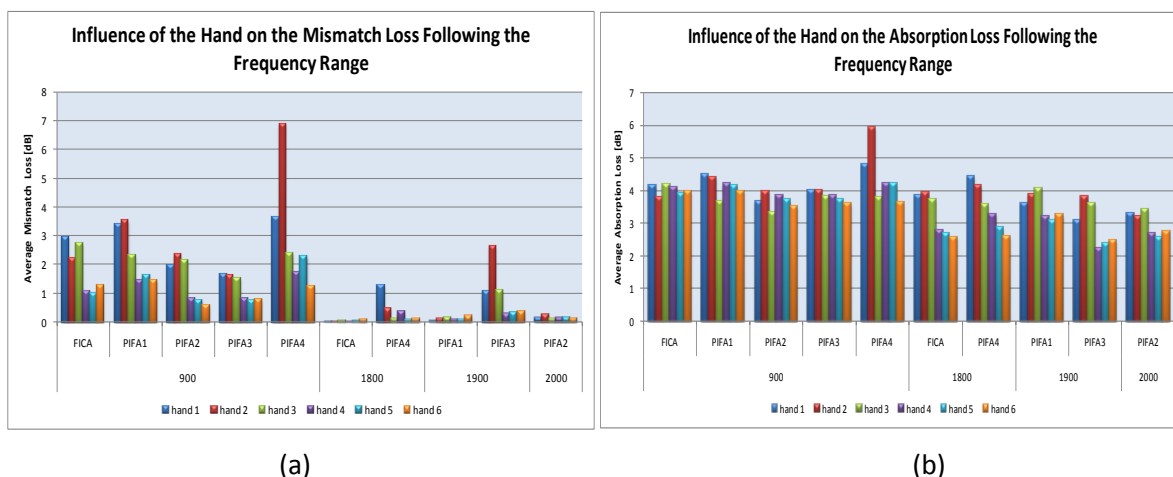


Figure 53: Mismatch(a) and Absorption(b) Losses Analysis According to the Frequency Range

- The Absorption Loss: First thing to notice is that the PIFA4 exhibits the highest absorption loss for the lowest frequency, with a particularly elevated value for the hand2. As aforementioned, the feed position and the smaller plate size may explain these special values. Still for the low frequency, results are not displaying a real difference between the firm hands group and the soft one or the different index positions, except for the hand3. This last remark illustrates that, when the finger is placed around the shorting element, the absorption loss presents a better reaction. On the contrary, the high frequency displays a notable difference between the firm hands group and the soft ones. For every antenna, the hands 4, 5 and 6 are presenting a smaller absorption loss than the other ones that are similar to the results at the low frequency. Therefore, handling the

handset with the soft style is increasing the radiation efficiency, which is logical since the radiated power is less faded by the hand tissues.

- The Mismatch Loss: Once again, the PIFA4 in the low frequency is giving the worst results, especially with the second hand. Hence, reasons given before are influencing both types of losses. In addition, it is noticeable that the mismatch loss is pointing to the fact that at the high frequencies, the results are much better than that of the low frequency. The FICA, PIFA1 and PIFA2 especially have a very low mismatch loss for every hand. It has to be remembered that, the higher is the resonating frequency, and the shorter is the resonating path on the antenna patch. These three specific PIFAs do have their high frequency patch well positioned when hand-handled. Finally, in a similar way to the absorption loss, the mismatch loss has a better behavior for the soft hands group than the hands handling firmly the mobile.

5) Antenna position (top or bottom localization) influence following the six hands

The results presented in this section are describing the absorption and mismatch loss when the patch is placed at the top or at the bottom of the antenna ground plane.

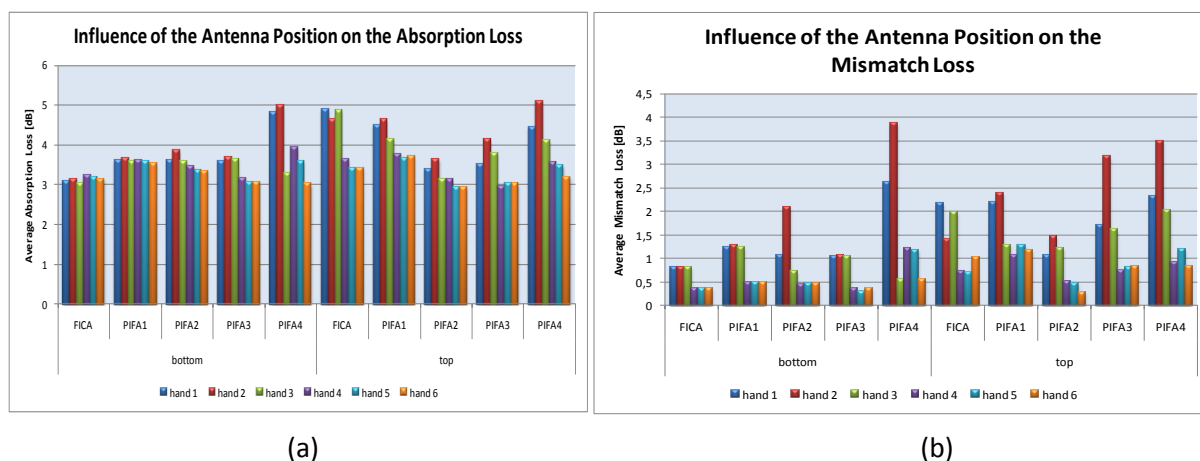


Figure 54: Mismatch(a) and Absorption(b) Losses Analysis according to the Antenna Position

- The Absorption Loss: Firstly, it is apparent that the bottom results are better than the top ones concerning the three first hands. In other terms, the firm hand style should be adopted when the antenna is located at the bottom of the handset.

Secondly, The FICA, is giving the best results when placed at the bottom, but the worst results when at the top. Likewise previous analysis, the PIFA4 is produces worst results for the three first hands at the bottom as well as the top position. Its small size and the concentrated fields of this antenna are definitely not an advantage when surrounded by a large element like a human hand. Otherwise, no general tendency can be revealed from the soft hand style as they are varying according to each different antenna.

Finally, one can notice that the fluctuations between absorption losses when antenna is located at the bottom are the smallest among the different hands. This is easily explained by the fact that moving the index finger situated at the upper part of the design does not affect significantly the radiations located at the lower part of the design.

-The Mismatch Loss. Bottom and top position have this time a strong influence on the results between the firm and the soft grip hands for both top and bottom positioned antenna. PIFA4 is showing again the worst results especially for the first and the second hands, and the PIFA4 is the worst antenna for firm handled antennas when placed at the top, and is ranked at the middle when position at the middle. Concerning the bottom especially, the firm grip hands group, results are

showing constancy, which is explained here again with the lack of influence for the finger when the antenna is positioned at the bottom.

### 3.4.4. Benchmark conclusion

In this comparative study, five dual-band PIFAs with dissimilar shape have been compared using the FD-TD method. The impact of six hand models on these antennas has been investigated. It has been shown that the absorption loss and the mismatch loss are strongly affected by the presence of the hand. The absorption loss seems to be the main issue since it has always reached higher value than the mismatch loss. As the graph (a) suggests, based on the results, the hand2 (firm grip with the index placed on the middle) is the hand model which has provided the highest amount of mismatch and absorption loss. On the contrary, the hand6 (soft grip with the index placed on the left) presents the lowest amount of loss. Moreover, it has been observed that the position of the index is also influencing the antenna performance. In most of the case, the influence of the index position is related to the design antenna. For example, the PIFA3, when working in the high frequency, reaches a peak of loss with the hand2 (firm grip the index placed on the middle) due to the presence of the S-slot in middle of its plate.

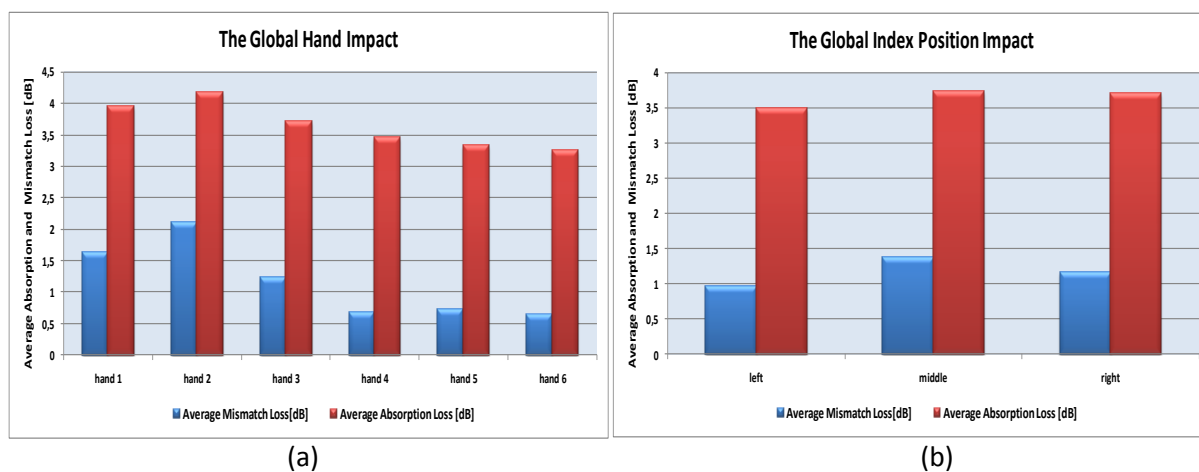


Figure 55: (a) Hand position (from one to six) and (b) Index Position (Left, Middle and Right) impact on mismatch and absorption loss merged

In this comparative study, a distinction between two kinds of grip has been made: The firm grip and the soft grip. The firm grip corresponds to the one with the shortest gap between the hand palm and the handset and therefore it has been observed that a larger amount of both mismatch and absorption loss is generated with this kind of grip. However, the mismatch loss is more affected than the absorption loss (see figure()) since it is reduced by 60% with the soft grip whereas the absorption loss is only attenuated by 15%.

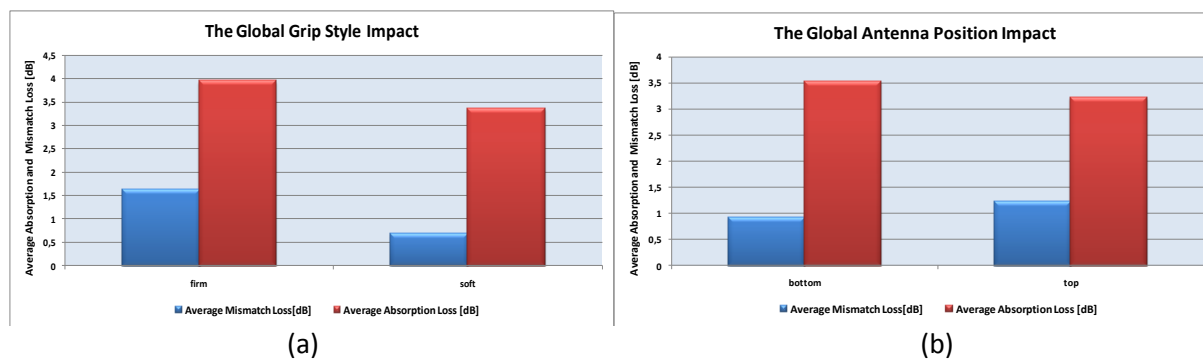


Figure 56 : (a) Grip style (firm and soft) and (b) Antenna Position (Bottom and Top) impact on mismatch and absorption loss merged

The antenna’s position was also investigated since it has been moved from the top to the bottom of the ground plane. In the bottom position, the antenna is more influenced by the palm of the hand than the finger. The total mean value for the mismatch and absorption loss is calculated in both configurations and represented by the figure (). The lowest losses are found in the “bottom” case since the index influence is reduced. This means that the presence of the finger in this study has more impact on the antenna performance than the palm of the hand.

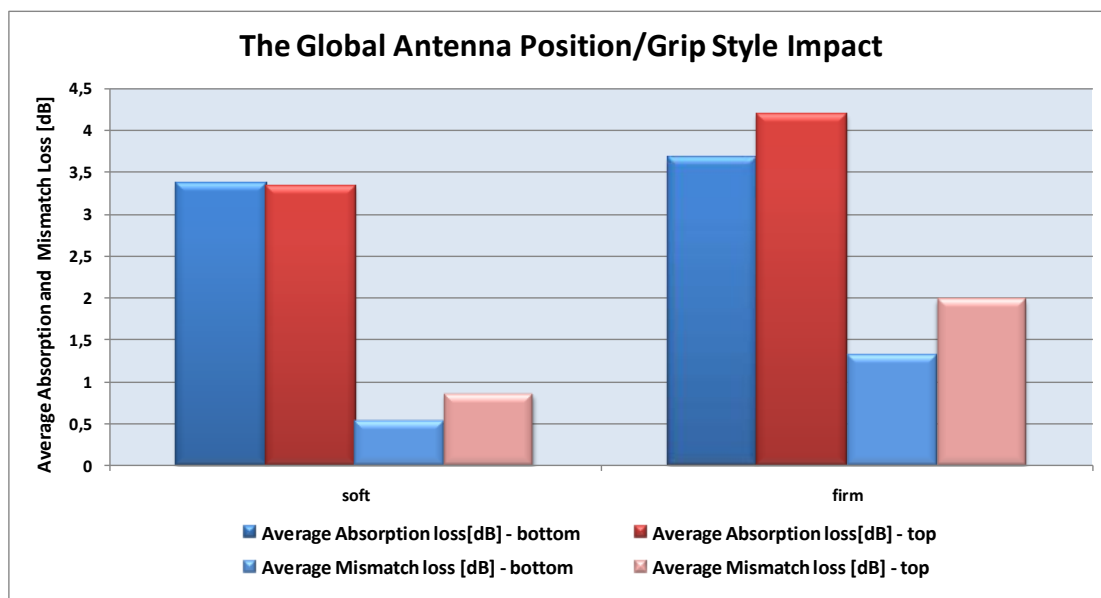


Figure 57 : The global antenna position and grip style impact

Looking deeper with the two different grips (see figure()), it can be noticed that the firm grip affect more strongly the performance of the antenna when its placed at the top than at the bottom where the soft grip generates similar Absorption loss and a bit higher mismatch loss at the top position.

A quick remark can be made on the impact of the hand when the antenna is working at different frequency.

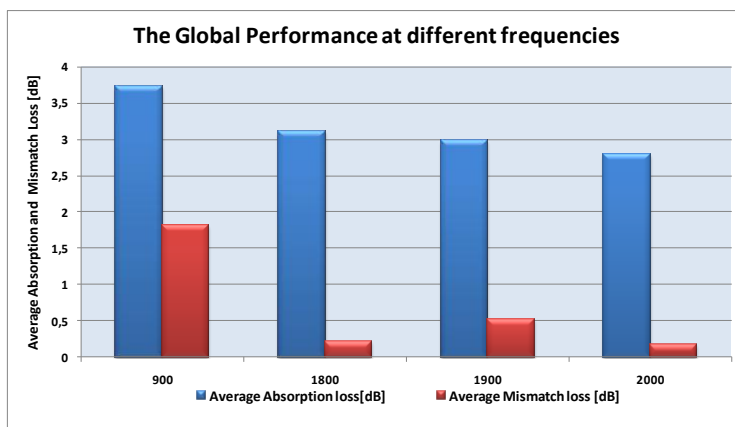


Figure 58 : The global performance at different frequencies

In fact, both mismatch and absorption losses are significantly decreased in the highest frequency bands, where detuning and loss are less influenced by the hand. However, the mismatch loss is much more affected by the frequency than the absorption loss; in the 1900MHz band, the mismatch is from 3 (at 1900MHz) to 9 (2000MHz) times lower than in the 900MHz band and on the other hand, whereas the absorption is only decreased by 20% .

Finally, this comparative study predicts the highest mismatch loss is reaches by the PIFA4 at both bottom and top position as the figure () shows. When positioning at the bottom, the PIFA4 also generates the highest absorption loss. Whereas at the top position, the largest amount of Absorption loss is given by the FICA antenna. The strong influence of the hand on the PIFA4 is due to the unusual reduced size of its plate ( $16 \times 29 \text{ mm}^2$ ) and ground plane ( $29 \times 100 \text{ mm}^2$ ). At the bottom position, both mismatch and absorption losses are the lowest with the FICA. However when placed at the top the FICA is not the most efficient since it presents its radiation is the most affected by the hand. Placed the top position the PIFA2 presents the best performance since its loss and detuning are lass influenced by the hand. This may be explained its bended plate on both sides which reduces the surface of impact with the hand and the index.

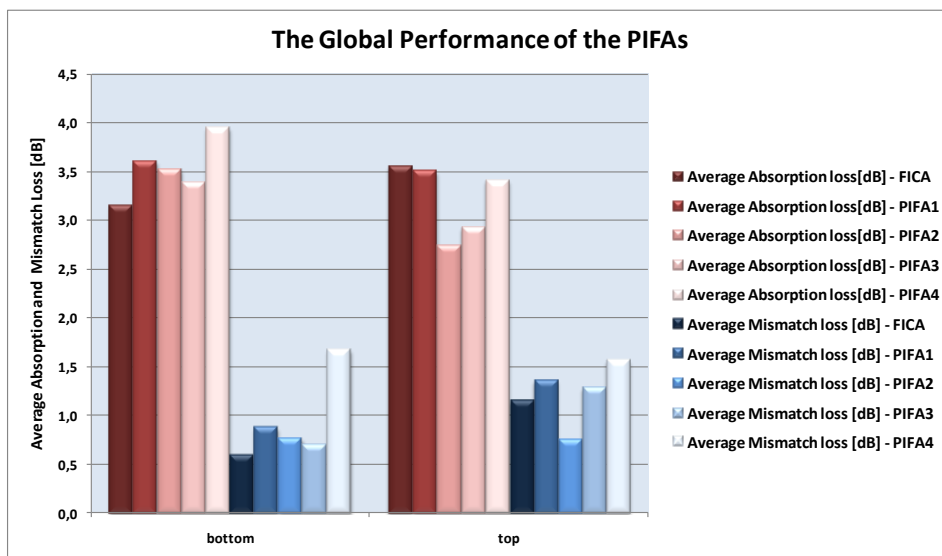


Figure 59 : The global performance of the PIFAs

The purpose of this study was to investigate the hand influence on different antenna in different configuration, more than trying to find the most efficient antenna. It has been shown that the impact of the hand on the antenna performance is directly related to its design.

# CHAPTER 4: CONCLUSION

---

## 4.1. General Conclusion

In the aim of providing the most relevant thesis, an obligatory step by step development had to be followed. Firstly, the simulation approach gave the possibility to apply the theoretical knowledge learnt during the eighth semester. Indeed, the simulator provided by the Aalborg University to realize this project is a direct application of the Finite Domain-Time Difference algorithm. Thanks to this tool and all the features included in there, all the elements were gathered to start and work on a simulation study.

The first main step was to reach an acceptable background level about electromagnetism and more specifically, about the mobile antennas radiations. To do so, literatures researches, combined with the first simulations performed on the simulator, gave good raw material to go ahead. In agreement with the supervisors' advices, deeper investigations on the Planar Inverted Folded Antenna (PIFA) were conducted during the first few weeks.

In addition, this new approach, taking in account the hand user effects on the radiated signal by a handset antenna was a great opportunity to investigate a field that has barely been opened. Since only a few papers taking care of the hand influence have been published yet, any directions were possible to go through. However, it must be remembered that some surveys are actually led by the Center for Person Kommunikation (CPK) at Aalborg University. Therefore, new consistent basis can be found giving an idea of what to begin with. Among those ones, the grip study [7] published in 2008 was one of the best supports to start the investigation.

Once basic antennas such as the monopole or the "simple" PIFA were analyzed, changing their different parameters, the idea was to go further toward the PIFA design. As one of the most promising and widespread antenna, it seemed coherent to go by this way. Therefore, a specific analyze concerning five characteristic PIFAs has been performed with the intention to point out the principal relevant parameters when working against a human hand. The aforementioned conclusions of the previous chapter have shown that hand influences on antennas are mainly linked to the PIFA design itself. Moreover, focusing on the two specific losses that fade antennas signal, the results illustrate that the absorption loss is globally larger than the mismatch loss. Besides, as expected, the hand position against the mobile phone is playing a major role in the results acquired. Surprisingly, the index finger can, in some cases being the biggest cause of interferences with the radiated signal. Obviously, when the index finger is directly positioned above a high radiating point, major losses are occurring.

What's more, this thesis was strictly focused on mobile telecommunications part. Nevertheless, it has be remembered, that handset devices are nowadays working not only with a specific hardware components, but also, with an embedded software part. The combination of both sections could be the key of success, particularly considering the lasts works that are carried out on the cognitive radio.

To put it in a nutshell, more than the results themselves, the use of such a scientific approach to explore next generation telecommunications has revealed some rewarding conclusions. However it must be remembered that results have to be taken from a higher standpoint so as to deal with objectiveness.

## 4.2. Future Work

Owing to a limited timeframe, the analyses of the other antenna parameters like the radiation patterns, or the bandwidth have not been performed in an efficient way. In addition, a real case study giving the possibility to check the results simulated would be a very interesting approach to validate or not, our theoretical results.

Another good way to go would be to perform more design changes simulations of the hereby studied antennas. As we saw, the PIFA design has a major role in the final antennas' performances. A larger study based on several parameters changes as it has been done for the "simple" PIFA would be interesting to perform for each of these "advanced" PIFAs. Last but not least, as the thesis revealed that external antennas were less sensitive to the human tissues proximity there is the potential for further investigation of a new type of external antennas that would keep the mobile robust, light, well proportioned and good looking, which would show a great appeal toward the market demand.

## REFERENCES

---

- [1]. *Effects on portable antennas of the presence of a person*. **J. Toftgard, S. N. Hornsleth, and J. B. Andersen**. 1993.
- [2]. *A study of the handset antenna and human body interaction*. **Stuchly, M. Okoniewski and M. A.** 1996.
- [3]. *Reliable Prediction of Mobile Phone Performance under Real Usage Conditions using the FDTD Method*. **P. Futter, N. Chavannes, R. Tay, M. Meilil, A. Klingenboeck, K. Pokovicl, N. Kuster**. 2005.
- [4]. *The Performance of GSM 900 antennas in the presence of people and phantoms*. **Boyle, K.R.** 2003.
- [5]. "Analysis of Mobile Phone, Antenna Impedance Variations With user Proximity". **K.R. Boyle, Yuan Yun, L.P Lightart**. 2007.
- [6]. "Internal Compact Dual-Band Printed Loop Antenna for Mobile Phone Application". **Y.-W. Chi, K.-L. Wing**. 2007.
- [7]. *A Grip Study for Talk and Data Modes in Mobile Phones*. **Mauro Pelosi, Ondrej Franek, Mikeal B. Knudsen, Morten Christensen, Gert F. Pedersen**. 2008.
- [8]. *Modern Antenna Handbook*. **Balanis, Constantine A.** 2008.
- [9]. *Two Methods for the Measurement of Antenna*. **EDWARD H. NEWMAN, ETER BOHLEY, AND C. H. WALTER**. 1975.
- [10]. *Impedance, Bandwidth, and Q of Antennas*. **Best, Arthur D. Yaghjian and Steven R.** 2005.
- [11]. **F. Gustrau, D. Manteuffel**. "EM Modeling of Antennas and RF Components for Wireless Communication Systems". 2006.
- [12]. *Multiband Integrated Antennas for 4G*. **Sanchez-Hernandez, David A.** 2008.
- [13]. *Antennas, from Theory to Practice*. **Yi Huang, Kevin Boyle**. 2008.
- [14]. **Authority**, "Sweden's Radiation Protection. *Mobiltelefoner och stralning*. 2003.
- [15]. **Kazuhiro Hirasawa, Misao Haneishi**. "Analysis, Design, and Measurement of Small and Low-Profile Antennas". 1992.
- [16]. *Physical Limitations of Omni-Directional Antennas*. **Chu, L. J.** 1948.
- [17]. *A Re-Examination of the Fundamental Limits on the Radiation Q of Electrically Small Antennas*. **McLean, James S.** 1996.

- [18]. *Review of Narrowband Impedance-Matching Limitations*. **Lopez, Alfred R.** 2004.
- [19]. *Handset communication antennas, including human interactions, in Wireless Networks: From the Physical Layer to Communication, Computing, Sensing and Control*. **Li, Y. Rahmat-Samii and Z.** 2006.
- [20]. *A research program on the human impact of wireless telecommunications and other electromagnetic-field-emitting systems*. **Lin, J. C.** 2004.
- [21]. *Antennas and Propagation for Body-Centric Wireless Communications*. **Peter S. Hall, Yang Hao.** 2006.
- [22]. *Antennas for Portable Devices*. **Chen, Zhi Ning.** 2007.
- [23]. *EM interaction of handset antennas and a human in personal communications*. **Rahmat-Samii, M. A. Jensen and Y.** 1995.
- [24]. *Short- or Open Circuited Dipole Parallel to Perfect Reflector Plane Embedded in Substrate and Acting at Resonance*. **Dubost, G.** 1981.
- [25]. *Increasing the Beamwidth of a Microstrip Radiating Element*. **Klein, G. Sanford and L.** 1979.
- [26]. *Considerations for the evaluation of human exposure to electromagnetic fields (EMFs) from mobile telecommunication equipment (MTE) in the frequency range from 30 MHz–6 GHz*. **CENELEC, European Specification ES 59005.** 1998.
- [27]. *Human exposure to radio frequency fields from hand-held and body-mounted wireless communication devices – Human models, instrumentation, and procedures*. **622209-1, IEC international standard.** 2004.
- [28]. *Tissue equivalent material for hand phantoms*. **Gabriel, C.** 2007.
- [29]. *Antenna Proximity Effects for talk and Data Modes in Mobile Phones*. **Mauro Pelosi, Ondrej Franek, Mikael B. Knudsen, Gert F. Pedersen, Jorgen B. Andersen.** 2008.
- [30]. *Design of a Compact Tri-Band PIFA Based on Independent Control of the Resonant Frequencies*. **Dong-yeon Kim, Jae W. Lee, IEEE, Choon Sik Cho, Taek K. Lee.**
- [31]. *Computational Electrodynamics –The Finite-Difference Time-Domain Method*. **Allen Taflove.** 1995
- [32]. *Multiband Antenna for GSM and 3G Mobile System*. **ABDURAHMAN M M OWAG.** 2006
- [33]. *Wideband Antenna Radiators*. **University of Liverpool.** 2005
- [34]. *Design of a Compact Tri-Band PIFA Based on Independent Control of the Resonant Frequencies*, **Dong-yeon Kim, Jae W. Lee, IEEE, Choon Sik Cho, Taek K. Lee**
- [35]. *The Folded Inverted Conformal Antenna (FICA) for Multi-band Cellular Phone*. **Carlo Di Nallo and Antonio Faraone.** 2005
- [36]. *A Perfectly Matched Layer for the Absorption of Electromagnetic Waves*. **Jean-Pierre Berenger.** 1993

# APPENDICES A: SENSITIVITY ANALYSIS

For the sensitivity analysis, the simulations have been run with the same PIFA antenna in order to allow the comparisons between the different results. The configuration of this antenna can be found in this appendix along with the details of each simulation. Some comparative graphs show the influence of the different tested parameters.

## A.1. The reference Antenna

Here is the configuration of this antenna plane, a plate, a feed, and a short circuit.

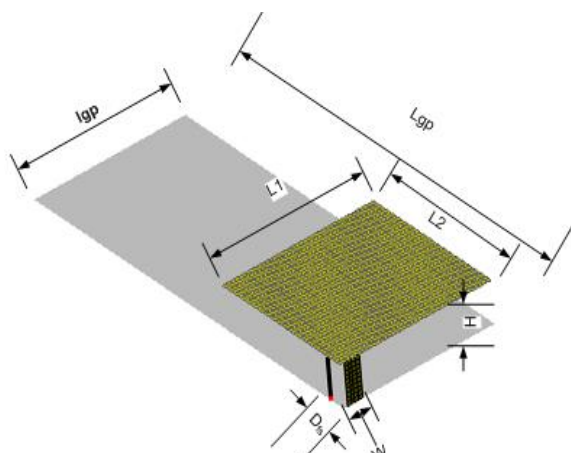


Figure 60: Basic PIFA Design

$l_{gp}$ : the length of the ground plane

$L_{gp}$ : the height of the ground plane

$L2$ : length of the pifa

$H$ : height gap between the ground plane and the plate.

$D_{FS}$ : Distance short-feed

$W$ : the width of the short circuit.

Parameters [mm]						
PIFA	H	$D_{FS}$	W	L1	L2	L1/L2
1	8	5	1	40	33	1,21

Table 16: Reference Pifa parameters

This antenna has been designed to resonate at 900MHz according to the formula:

$$f_R = \frac{c}{4 \times (L1 + L2 + H - W)}$$

$c$ : speed light =  $3 \times 10^8$  m/s

$f_R$ : resonance frequency = 900MHz

## A.2. The Results

The results of the sensitivity analysis are collected in table and represented in graphs. This section is divided in three parts; one for each parameter investigated.

1) Number of time steps:

variable	Results				
Nb Time Step	$f_R$ [MHz]	S11 [db]	$\eta$	Q	Bw [MHz]
5000	902	-20,9	0,90	1,5	614
10 000	897	-44,5	1,08	5,3	170
20 000	897	-42,9	1,08	5,4	165
50 000	897	-42,9	1,08	5,4	165
100 000	897	-42,9	1,08	5,4	165

Table 17 : Results for the number of time steps

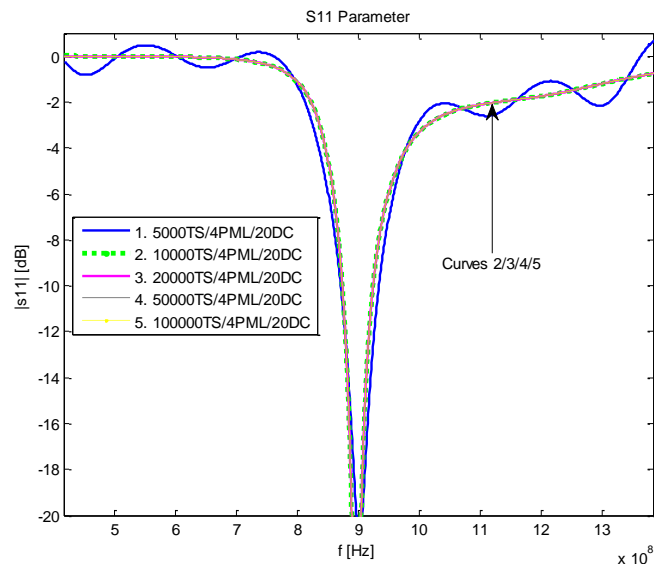


Figure 61: Time Steps Number Influence on the Return Loss

2) PML Thickness :

variable	Results				
	$f_R$ [MHz]	S11 [db]	$\eta$	Q	Bw [MHz]
0	1775	-36,2	2217	241,1	7
2	879	-15,8	1,7	14,7	60
4	897	-42,9	1,08	5,4	165
6	897	-24,4	0,98	3,5	256
8	897	-27,5	1,01	4,2	216
10	897	-26,7	1,00	4,0	226

Table 18: PML thickness Results

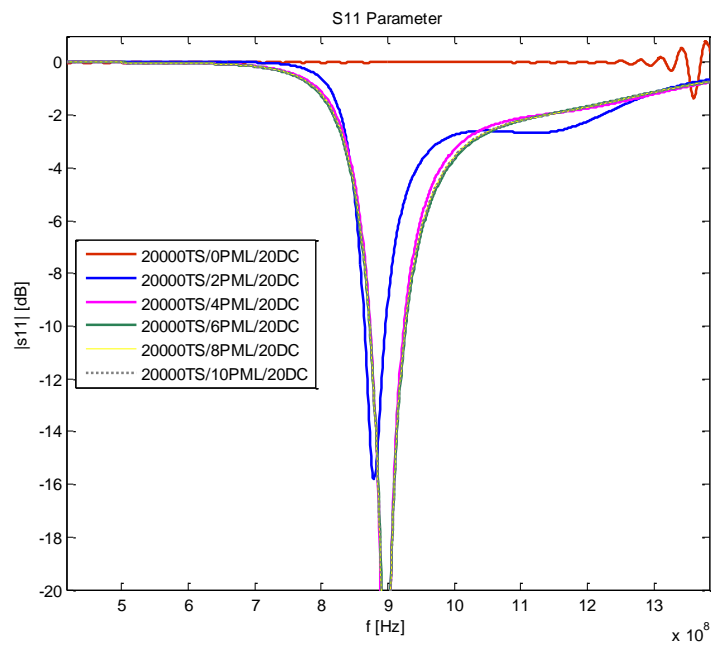


Figure 62: PML Thickness Influence on the Return Loss

3) Computational domain size

variable	Results				
DC (Cells)	$f_R$ [MHz]	S11 [db]	$\eta$	Q	Bw [MHz]
10	897	-27,6	1,01	4,1	217
20	897	-27,5	1,01	4,2	216
30	897	-27,4	1,01	4,1	216
40	897	-27,1	1,01	4,1	217
50	897	-26,9	1,01	4,1	217
10	897	-27,6	1,01	4,1	217

Table 19: Domain size results

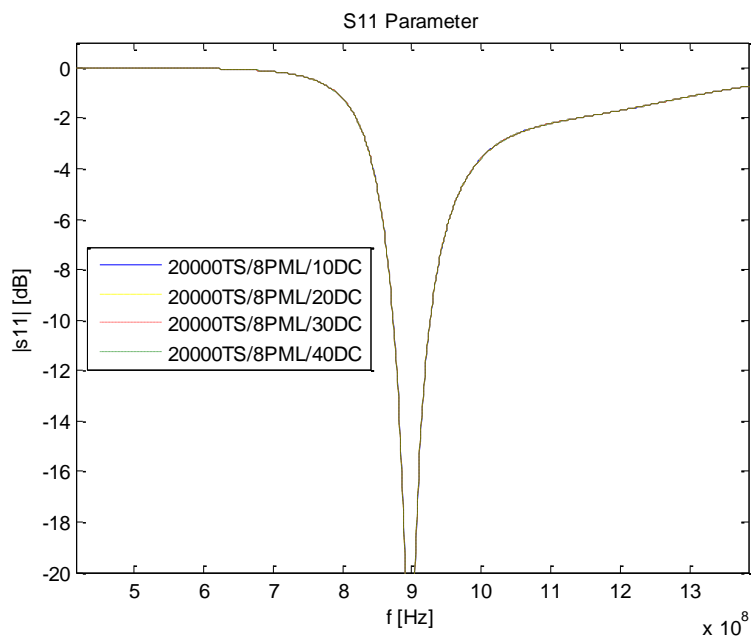


Figure 63: Computational Domain Size Influence on the Return Loss

# APPENDICES B: BASIC HANDSET ANTENNA

In this Appendix, the configuration of the monopole and the PIFA antennas and also the details of each simulation are presented. This section is divided in two; first the simulations with the monopole and then with the PIFA. Some comparative graphs show the influence of the different tested parameters.

## B.1. The Monopole

### 1. Design of a monopole

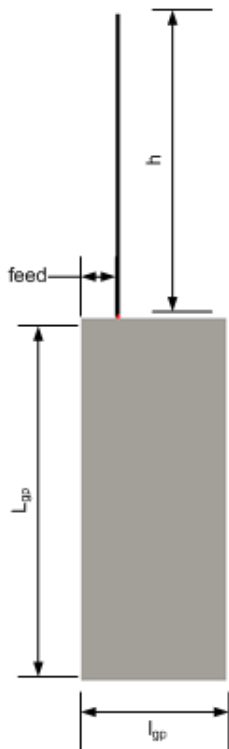
The formula applied to calculate the height of the monopole is the one below:

$h$ : height of the monopole in meters

$c$ : speed light =  $3 \cdot 10^8$  m/s

$f$ : resonance frequency = 900MHz

$$h = \frac{c}{4 \times f}$$



Therefore, a monopole resonating at 900MHz should have a height equal to 8,33cm.

$$l = \frac{3 \times 10^8}{4 \times 900 \times 10^6} = \frac{1}{12} = 0,083m$$

The design of the monopole is very simple. It is formed by a ground plane without thickness, a feed and a wire.

$l_{gp}$ : the length of the ground plane in [mm]

$L_{gp}$ : the height of the ground plane in [mm]

$h$ : the height of the monopole in [mm]

feed: Distance corner-feed in [mm]

For the simulations the following parameters are returned and investigated:

$f_R$ : The resonance frequency in Hz

$S_{11}$ : The reflection coefficient in dB

$\eta$ : The radiation efficiency (dimensionless)

$Q$ : The Quality factor at resonance (dimensionless)

$Bw$ : The bandwidth at resonance in Hz

$ML$ : The Mismatch Loss

Figure 64: Basic Monopole Design

## B.2. Simulations

We are playing on two parameters: the position of the feed and the ground plane size.

- Effects of the feed position:

Monopole	Parameters			variable	Results					
	$L_{gp}$ [mm]	$l_{gp}$ [mm]	$L_{gp}/l_{gp}$	feed [mm]	$f_R$ [MHz]	S11 [db]	$\eta$	Q	Bw [MHz]	ML [db]
1	100	40	2,5	0	780	-11,4	1,01	3,4	227	0,33
2	100	40	2,5	5	788	-10,9	1,01	3,2	242	0,37
3	100	40	2,5	10	793	-10,6	1,01	3,1	252	0,40
4	100	40	2,5	15	797	-10,4	1,01	3,0	260	0,42
5	100	40	2,5	20	798	-10,2	1,01	3,0	263	0,44

Table 20 : Feed position effects on the monopole

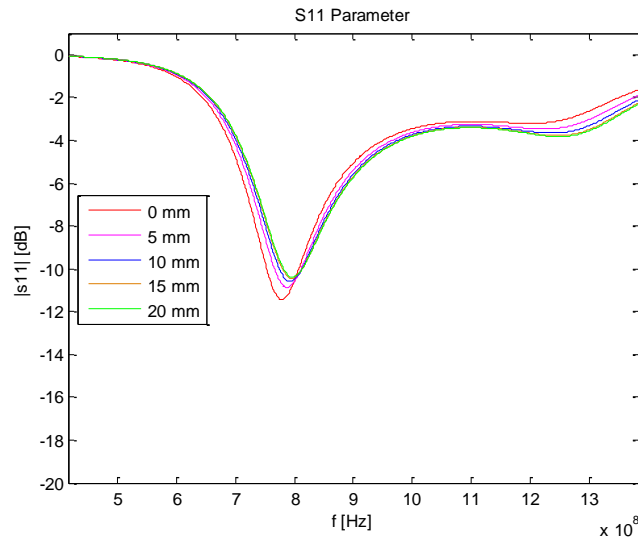


Figure 65: Feed Size Influence

- Effects of the Ground plane size:

Monopole	Parameters			variable	Results					
	$L_{gp}$ [mm]	$l_{gp}$ [mm]	feed [mm]	$L_{gp}/l_{gp}$	$f_R$ [MHz]	S11 [db]	$\eta$	Q	Bw [MHz]	ML [db]
6	130	10	0	13	693	-8,8	1,01	4,1	171	0,61
7	120	20	0	6	726	-8,9	1,01	3,4	212	0,60
8	110	30	0	3,67	755	-9,8	1,01	3,3	230	0,48
9	100	40	0	2,5	780	-11,4	1,01	3,4	227	0,33
10	90	50	0	1,8	795	-13,8	1,01	3,9	205	0,18
11	80	60	0	1,33	804	-17,0	1,01	4,4	182	0,09
12	70	70	0	1	807	-20,4	1,01	4,9	164	0,04

Table 21: Effects of the ground plane size on the monopole

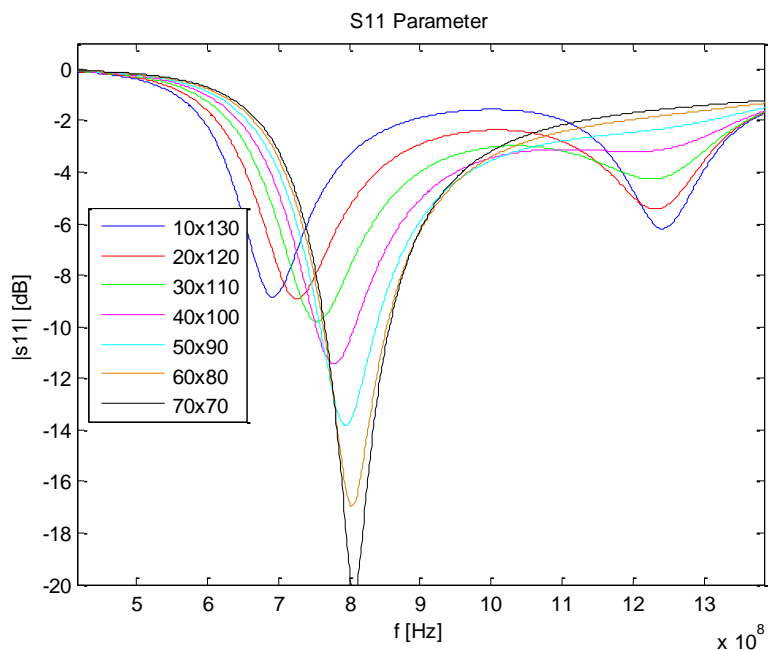


Figure 66: Ground Plane Size Influence

- Effects of the brick hand:

The following results are with the monopole in a free space without the hand influence:

Monopole	Parameters				Results				
	$L_{gp}$ [mm]	$l_{gp}$ [mm]	$L_{gp}/l_{gp}$	feed [mm]	$f_R$ [MHz]	S11 [db]	$\eta$	Q	Bw [MHz]
10	90	50	1,8	0	795	-13,8	1,01	3,9	205

Table 22: Performance of the monopole in free space

For the simulation, two parameters are evaluated: H1 and H2

Monopole	Parameters		Results					
	H1 [mm]	H2 [mm]	$f_R$ [MHz]	S11 [db]	$\eta$	Q	Bw [MHz]	ML [db]
12	0	10	773	-12,3	0,98	3,5	220	0,26
13	0	20	781	-13,0	0,99	3,7	214	0,22
14	0	30	786	-13,4	1,00	3,7	211	0,20
15	0	40	787	-13,7	1,00	3,8	206	0,19
16	10	10	776	-13,0	0,98	3,7	211	0,22
17	20	10	779	-13,6	0,98	3,8	205	0,19
18	30	10	783	-13,9	0,98	3,8	205	0,18
19	40	10	785	-14,0	0,98	3,8	206	0,18
20	80	10	788	-14,3	0,91	3,5	224	0,16

Table 23 : Brick hand effects on the monopole

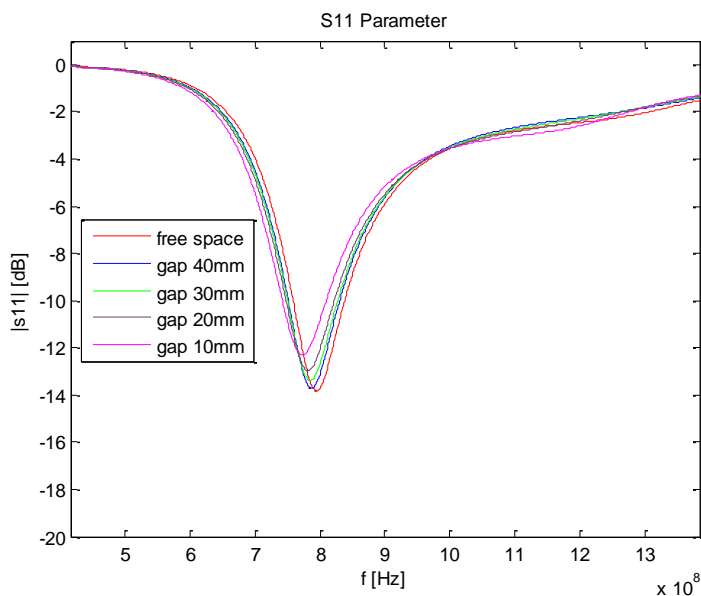


Figure 67: Feed Source Position Influence

- Effects of the Hand models :

Monopole	Parameters			variable	Results						
	$L_{gp}$ [mm]	$I_{gp}$ [mm]	feed [mm]	hand	$f_R$ [MHz]	S11 [db]	$\eta$	Q	Bw [MHz]	S11 @ $f_0$	ML [db]
1	100	40	0	Free-space	780	-11,4	1,01	3,4	227	-	0,33
2	100	40	0	1	801	-10,1	0,81	3,6	220	-9,8	0,48
3	100	40	0	2	801	-10,7	0,81	3,7	219	-9,8	0,48
4	100	40	0	3	801	-10,8	0,81	3,7	215	-9,9	0,47
5	100	40	0	4	783	-12,6	0,74	4,1	181	-12,6	0,25
4	100	40	0	5	783	-12,7	0,74	4,1	189	-12,7	0,24
5	100	40	0	6	783	-12,8	0,73	4,1	191	-12,8	0,23

Table 24: Effects of the hand models on the monopole

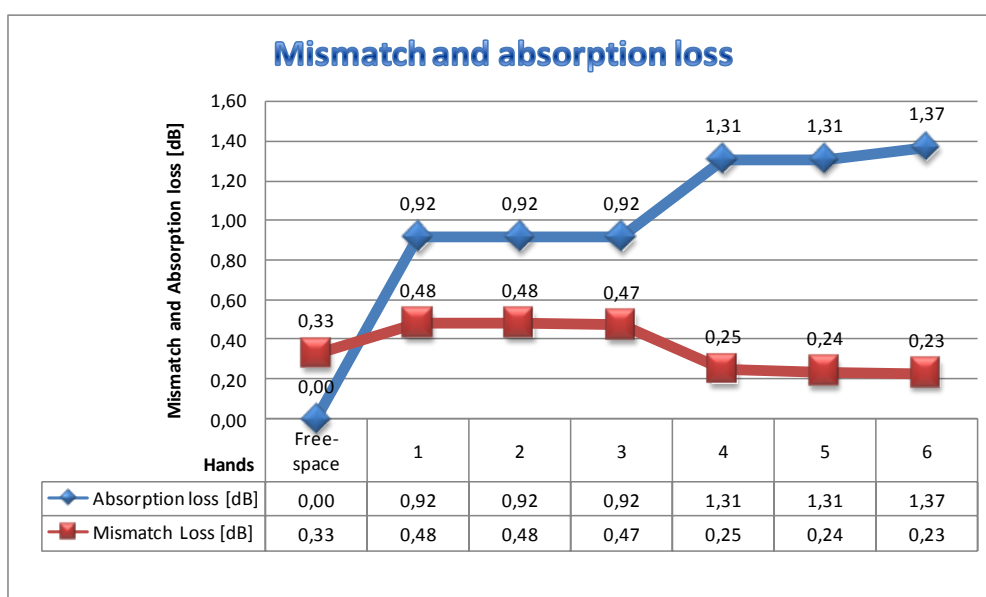


Figure 68: Mismatch and Absorption Loss Results

### B.3. The PIFA

Now, some simulations are run on the PIFA antenna. The design of the PIFA is first described and the results of different parameters investigated are presented.

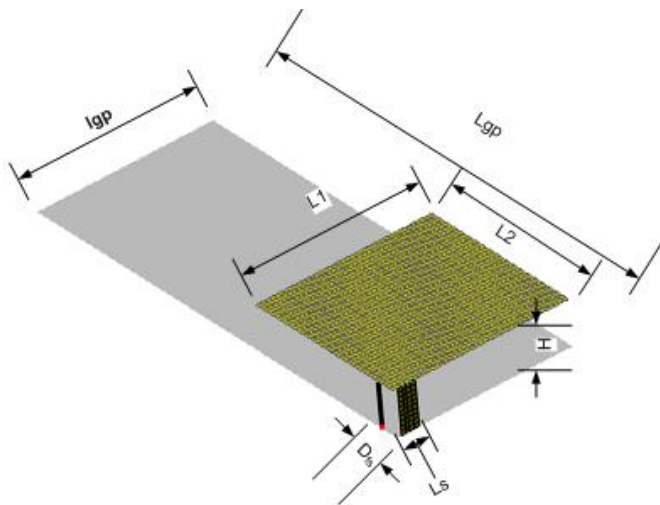
#### 1. Design of a PIFA

The formula applied to calculate the height of the monopole is the one below:

$$f_R = \frac{c}{4 \times (L1 + L2 + H - L_s)}$$

c: speed light = 3e9 m/s  
fr: resonance frequency = 900MHz

The design of the Pifa is formed by a ground plane, a plate, a feed, and a short circuit.



- $l_{gp}$ : the length of the ground plane
- $L_{gp}$ : the height of the ground plane
- $L2$ : length of the pifa
- $H$ : height gap between the ground plane and the plate.
- $D_{FS}$ : Distance short-feed
- $L_s$ : the width of the short circuit.

Figure 69: Basic PIFA Design

#### 2. Simulations

The size of the cell size is still 1mm. The antenna input impedance is calculated over a frequency range of 1000 MHz centered on 900MHz, where 10 samples per MHz are computed, with a total of 20 000 time steps. The table below summarizes the simulations on the PIFA antenna. To have a better comprehension of the different PIFA's parameters, a study has been led. In accordance to it, a brief numerical study has been done for each varying parameters.

- Effects of the short:

In order to analyze the effect of the short in the performance of the PIFA antenna, a first simulation is running without short (PIFA 1) and the same one is running afterwards with a wire short inserted at 5mm away from the feed.

PIFA	Parameters				variable		Results					
	$L_{gp}$	$l_{gp}$	L1	L2	H	$D_{FS}$	$L_s$	$f_R$ [MHz]	S11 [db]	Q	Bw [MHz]	Mismatch loss @ $f_r$
1	100	40	40	38	5	-	-	1158	-1,7	247,6	5	4,9
2	100	40	40	38	5	5	1	900	-11,4	94,2	10	0,33

Table 25 : Short effects on the PIFA

- Effects of the gap between the ground plane and the plate:

PIFA	Parameters					variable	Results				
	L1	L2	L1/L2	D <sub>FS</sub>	Ls	H	f <sub>R</sub> [MHz]	S11 [db]	Q	Bw [MHz]	Mismatch Loss @ f <sub>r</sub>
3	40	33	1,21	5	1	10	868	-44	7,5	115	0
4	40	33	1,21	5	1	8	892	-40,9	5,4	164	0
5	40	33	1,21	5	1	6	925	-33,8	2,7	344	0
6	40	33	1,21	5	1	4	963	-29,7	1,9	497	0
7	40	33	1,21	5	1	2	1010	-27,7	11	92	0,01

Table 26: Gap ground plane/Plate effects on the PIFA

- PIFA Configuration :

PIFA	Parameters			variables			Results				
	H	D <sub>FS</sub>	Ls	L1	L2	L1/L2	f <sub>R</sub> [MHz]	S11 [db]	Q	Bw [MHz]	Mismatch Loss @ f <sub>r</sub>
4	8	5	1	40	33	1,21	892	-40,9	5,4	164	0
8	8	5	1	38	35	1,09	889	-29,1	6,7	133	0,01
9	8	5	1	36	37	0,97	888	-22,9	7,9	112	0,02
10	8	5	1	34	39	0,87	988	-19,9	9	100	0,04
11	8	5	1	32	41	0,78	887	-18,1	9,9	90	0,07

Table 27 : Plate Configuration effects on the PIFA

- Short size:

PIFA	Parameters					variable		Results				
	L1	L2	L1/L2	H	D <sub>FS</sub>	L <sub>s</sub>	L <sub>s</sub> /L <sub>1</sub>	f <sub>R</sub> [MHz]	S11 [db]	Q	Bw [MHz]	Mismatch Loss @ f <sub>r</sub>
4	40	33	1,21	8	5	1	≈0	892	-40,9	5,4	164	0
12	40	33	1,21	8	5	2	0,05	951	-6,1	4,6	205	1,22
13	40	33	1,21	8	5	4	0,1	993	-3	3,6	278	3,02
14	40	33	1,21	8	5	8	0,2	1335	-1,5	1,1	1210	5,35
15	40	33	1,21	8	5	16	0,4	1542	-1,3	2,7	580	5,87
16	40	33	1,21	8	5	35	0,875	1827	-1,2	2,7	684	6,17

Table 28 : Short size effects on the PIFA

- Feed Size

PIFA	Parameters					variable		Results				
	L1	L2	L1/L2	H	D <sub>FS</sub>	L <sub>F</sub>	L <sub>F</sub> /L <sub>1</sub>	f <sub>R</sub> [MHz]	S11 [db]	Q	Bw [MHz]	Mismatch Loss @ f <sub>r</sub>
4	40	33	1,21	8	5	1	≈0	892	-40,9	5,4	164	0
17	40	33	1,21	8	5	2	0,05	900	-18,9	6,4	141	0,06
18	40	33	1,21	8	5	4	0,1	909	-15,4	6,7	135	0,13
19	40	33	1,21	8	5	8	0,2	930	-13,6	6,5	143	0,19
20	40	33	1,21	8	5	33	0,825	978	-9,6	5,8	170	0,5
21	40	33	1,21	8	5	triangular	0,1	895	-14,6	6	150	0,15

Table 29: Feed size Effects on the PIFA

- Short Position

PIFA	Parameters				variable	Results				
	L1	L2	L1/L2	H	$D_{FS}$ [mm]	$f_R$ [MHz]	S11 [db]	Q	Bw [MHz]	Mismatch Loss @ $f_r$
22	40	33	1,21	8	2	835	-34,4	2,6	318	0
4	40	33	1,21	8	5	892	-40,9	5,4	164	0
23	40	33	1,21	8	10	947	-14,6	4	236	0,15
24	40	33	1,21	8	20	1043	-9,3	2,4	427	0,54
25	40	33	1,21	8	40	1061	-17,9	2,4	445	0,07

Table 30: Short Position effects on the PIFA

- Feed Position

PIFA	Parameters					variable	Results				
	L1	L2	L1/L2	H	$D_{FS}$	$D_{origin}$ [mm]	$f_R$ [MHz]	S11 [db]	Q	Bw [MHz]	Mismatch Loss @ $f_r$
4	40	33	1,21	8	5	0	892	-40,9	5,4	164	0
26	40	33	1,21	8	5	-5	875	-7,8	12,7	69	0,79
27	40	33	1,21	8	5	5	875	-7,9	12,6	70	0,77
28	40	33	1,21	8	5	20	994	-21,5	3,1	321	0,03
29	40	33	1,21	8	5	Middle of the plate	1403	-18,1	2	719	0,07

Table 31: Feed Position effects on the PIFA

- Capacitor Value

PIFA	Parameters					variable		Results				
	L1	L2	L1/L2	H	$D_{FS}$	$D_{Short-Capacitor}$ [mm]	C [nF]	$f_R$ [MHz]	S11 [db]	Q	Bw [MHz]	Mismatch Loss @ $f_r$
4	40	33	1,21	8	5	-	-	892	-40,9	5,4	164	0
30	40	33	1,21	8	5	5	0,8	994	-3,5	3,4	289	2,57
31	40	33	1,21	8	5	5	1	994	-3,5	3,4	289	2,57
32	40	33	1,21	8	5	5	1,2	994	-3,5	3,5	287	2,57
33	40	33	1,21	8	5	5	1,5	995	-3,5	3,3	297	2,57

Table 32: Capacitor value effects on the PIFA

- Capacitor Position

PIFA	Parameters					variable		Results				
	L1	L2	L1/L2	H	$D_{FS}$	$D_{Short-Capacitor}$ [mm]	C [nF]	$f_R$ [MHz]	S11 [db]	Q	Bw [MHz]	Mismatch Loss @ $f_r$
4	40	33	1,21	8	5	-	-	892	-40,9	5,4	164	0
34	40	33	1,21	8	5	5	1	994	-3,5	3,4	289	2,57
35	40	33	1,21	8	5	10	1	1314	-2,4	1,6	811	3,72
36	40	33	1,21	8	5	15	1	1388	-2,8	2,6	526	3,23
37	40	33	1,21	8	5	35	1	1435	-4,2	2,7	531	2,08

Table 33: Capacitor position effects on the PIFA

- Ground Plane Dimension

PIFA	Parameters					variables			Results				
	H	D <sub>FS</sub>	L <sub>s</sub>	L1	L2	I	L	I/L	f <sub>R</sub> [MHz]	S11 [db]	Q	Bw [MHz]	Mismatch Loss @ f <sub>r</sub>
4	8	5	1	40	33	40	100	1,21	892	-40,9	5,4	164	0
38	8	5	1	40	33	40	70	1,09	940	-5,5	34,7	27	1,44
39	8	5	1	40	33	40	50	0,97	977	-2,6	71,4	14	3,46
40	8	5	1	40	33	40	33	0,87	1048	-2,1	91,7	11	4,16

Table 34: Ground Plane Dimension effects on the PIFA

- Hand effects

PIFA	Parameters					variables	Results						
	H	D <sub>FS</sub>	L <sub>s</sub>	L1	L2	hand	f <sub>R</sub> [MHz]	S11	η	Q	Bw	S11	ML
8	8	5	1	40	33	Free-	892	-40,9	1,0	5,4	164	-40,9	0,00
12	8	5	1	40	33	1	798	-10,7	0,35	2,5	319	-2,8	3,23
13	8	5	1	40	33	2	796	-10,3	0,34	2,6	305	-2,8	3,23
14	8	5	1	40	33	3	805	-11,0	0,36	2,3	350	-3,1	2,92
15	8	5	1	40	33	4	806	-7,0	0,38	2,6	315	-4,1	2,14
16	8	5	1	40	33	5	803	-6,7	0,39	2,5	319	-3,9	2,27
17	8	5	1	40	33	6	800	-6,2	0,40	2,5	325	-3,9	2,27

Table 35: Hand effects on the PIFA

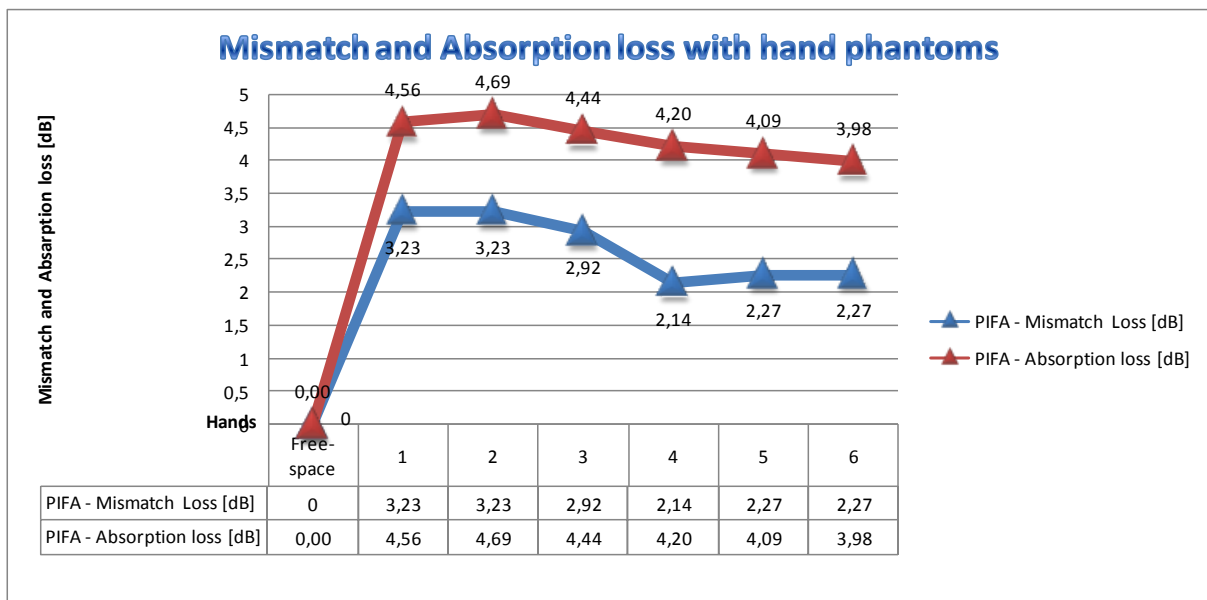


Figure 70: Mismatch and Absorption Loss with Hand Models

# APPENDIX C: THE HAND MODELS

Here are the six models of the hands. They can be classified in two groups: the Soft Grip and the Firm Grip. Then, for each kind of grips, the index is localized at three different positions: right, middle and left.

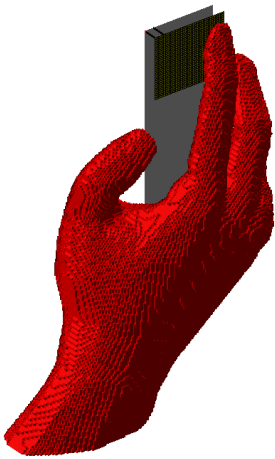
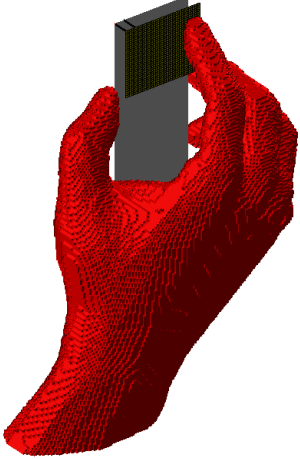
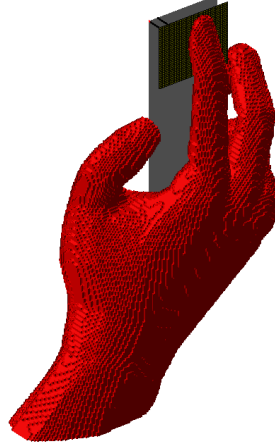
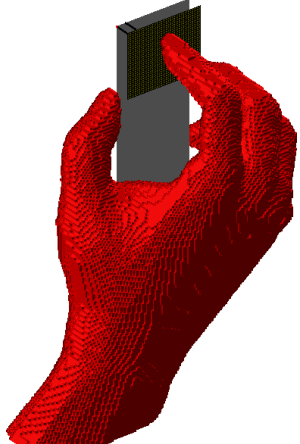
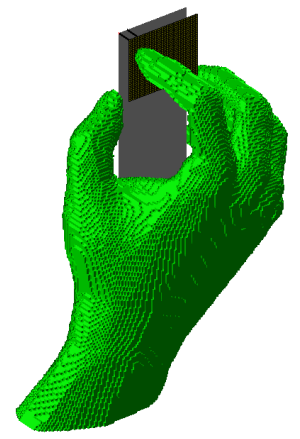
	Firm Grip HAND 1	Soft Grip HAND 4
Index to the right		
	HAND 2	HAND 5
Index to the middle		
	HAND 3	HAND 6
Index to the left		

Table 36: Hand models

# APPENDIX D: HAND INFLUENCE ON FIVE PIFAs

This section presents the details of all simulations for the five pifa's . For each of them, the results at the top position are presented and then the ones at the bottom.

## D.1. PIFA1



Pifa Bi-band	Results						
	$f_R$ [MHz]	S11 [db]	$\eta$	Q	Bw [MHz]	S11 @ $f_0$	Mismatch loss [dB]
PIFA1_hand1_900	807	-12,7	0,3	4,8	165,9	-2	4,33
PIFA1_hand1_1900	1870	-25,6	0,42	9,8	190	-16,9	0,09
PIFA1_hand2_900	809	-12,5	0,31	3,6	221,8	-1,9	4,51
PIFA1_hand2_1900	1852	-24,7	0,38	9,6	194	-12,3	0,26
PIFA1_hand3_900	850	-17,9	0,42	2,9	292,6	-4	2,20
PIFA1_hand3_1900	1841	-23,2	0,35	5,8	319	-11,1	0,35
PIFA1_hand4_900	830	-7,5	0,36	3,6	230,1	-4,2	2,08
PIFA1_hand4_1900	1873	-28,6	0,49	6,7	279	-19,6	0,05
PIFA1_hand5_900	816	-7,1	0,37	3,8	214	-3,6	2,49
PIFA1_hand5_1900	1874	-23,6	0,50	9,6	196	-18,3	0,06
PIFA1_hand6_900	825	-6,7	0,39	3,3	249,4	-4,2	2,08
PIFA1_hand6_1900	1845	-30,4	0,46	8,1	229	-12,0	0,28

Table 37: PIFA1 performance at the top

Pifa Bi-band	Results						
	$f_R$ [MHz]	S11 [db]	$\eta$	Q	Bw [MHz]	S11 @ $f_0$	Mismatch loss
PIFA1_bottom_hand1_900	847	-19,9	0,42	2,6	332	-3,6	2,49
PIFA1_bottom_hand1_1900	1884	-50,6	0,45	8,1	232	-27,3	0,01
PIFA1_bottom_hand2_900	847	-19,9	0,42	2,3	375	-3,5	2,57
PIFA1_bottom_hand2_1900	1885	-46,3	0,44	8,3	227	-28,3	0,01
PIFA1_bottom_hand3_900	849	-21,3	0,44	2,0	429	-3,6	2,49
PIFA1_bottom_hand3_1900	1887	-40,6	0,44	8,4	225	-30,9	0,00
PIFA1_bottom_hand4_900	879	-9,4	0,40	3,1	284	-7,7	0,81
PIFA1_bottom_hand4_1900	1919	-22,5	0,47	9,1	210	-14,8	0,15
PIFA1_bottom_hand5_900	879	-9,2	0,40	3,0	289	-7,6	0,83
PIFA1_bottom_hand5_1900	1919	-22,7	0,48	9,0	213	-14,7	0,15
PIFA1_bottom_hand6_900	878	-9,2	0,41	3,0	293	-7,6	0,83
PIFA1_bottom_hand6_1900	1919	-22,6	0,48	9,1	212	-14,7	0,15

Table 38: PIFA1 Performance at the bottom

## D.2. PIFA2

Pifa Bi-band	Results						
	$f_R$ [MHz]	S11 [db]	$\eta$	Q	Bw [MHz]	S11 @ $f_0$	Mismatch loss [dB]
PIFA2_hand1_900	874	-15,6	0,45	5,5	157,4	-4,6	1,85
PIFA2_hand1_2000	2005	-13,7	0,47	13,0	154	-12,5	0,25
PIFA2_hand2_900	865	-19,0	0,39	2,2	392	-3,4	2,65
PIFA2_hand2_2000	2010	-12,8	0,48	13,3	151	-12,2	0,27
PIFA2_hand3_900	904	-23,6	0,51	0,6	1622,6	-4	2,20
PIFA2_hand3_2000	1999	-14,8	0,46	11,4	175	-12,9	0,23
PIFA2_hand4_900	891	-9,0	0,42	2,4	372,1	-7	0,97
PIFA2_hand4_2000	2020	-18,7	0,56	9,0	226	-18,5	0,06
PIFA2_hand5_900	903	-8,8	0,44	2,2	415,9	-7,6	0,83
PIFA2_hand5_2000	2022	-16,1	0,59	9,9	205	-16,1	0,11
PIFA2_hand6_900	955	-9,5	0,47	1,8	534,1	-9,5	0,52
PIFA2_hand6_2000	2016	-19,9	0,55	8,4	241	-19,2	0,05

Table 39: PIFA2 performance at the top

Pifa Bi-band	Results						
	$f_R$ [MHz]	S11 [db]	$\eta$	Q	Bw [MHz]	S11 @ $f_0$	Mismatch loss
PIFA2_bottom_hand1_900	874	-17,5	0,41	2,4	371	-4,2	2,08
PIFA2_bottom_hand1_2000	2011	-22,6	0,46	9,0	224	-19,7	0,05
PIFA2_bottom_hand2_900	873	-17,6	0,41	2,4	366	-4,2	2,08
PIFA2_bottom_hand2_2000	2011	-21,1	0,45	9,4	214	-18,8	0,06
PIFA2_bottom_hand3_900	875	-18,6	0,42	2,1	421	-4,2	2,08
PIFA2_bottom_hand3_2000	2012	-20,3	0,45	9,7	207	-18,5	0,06
PIFA2_bottom_hand4_900	928	-8,7	0,40	1,8	520	-8,5	0,66
PIFA2_bottom_hand4_2000	2047	-13,7	0,51	11,1	185	-12,7	0,24
PIFA2_bottom_hand5_900	933	-8,5	0,41	1,6	568	-8,4	0,68
PIFA2_bottom_hand5_2000	2047	-13,6	0,52	11,1	185	-12,7	0,24
PIFA2_bottom_hand6_900	930	-8,6	0,42	1,7	552	-8,4	0,68
PIFA2_bottom_hand6_2000	2046	-13,6	0,51	11,2	183	-12,7	0,24

Table 40: PIFA1 performance at the bottom

**D.3. PIFA3**

Pifa Bi-band	Results						
	$f_R$ [MHz]	S11 [db]	$\eta$	Q	Bw [MHz]	S11 @ $f_0$	Mismatch loss
PIFA3_hand1_900	807	-19,0	0,32	5,5	145	-3,8	2,34
PIFA3_hand1_1900	1831	-19,8	0,62	7,6	240	-6,5	1,10
PIFA3_hand2_900	809	-25,7	0,33	5,6	145	-4,0	2,20
PIFA3_hand2_1900	1672	-22,4	0,45	11,6	142	-2,1	4,16
PIFA3_hand3_900	814	-38,8	0,35	5,8	141	-4,3	2,02
PIFA3_hand3_1900	1801	-13,6	0,50	6,1	304	-6,2	1,19
PIFA3_hand4_900	830	-12,1	0,39	3,7	222	-6,7	1,04
PIFA3_hand4_1900	1871	-25,3	0,66	9,1	205	-10,1	0,45
PIFA3_hand5_900	824	-13,4	0,41	3,9	210	-6,8	1,02
PIFA3_hand5_1900	1861	-40,4	0,60	10,0	186	-8,8	0,61
PIFA3_hand6_900	819	-13,4	0,43	3,7	223	-6,9	0,99
PIFA3_hand6_1900	1856	-10,5	0,58	4,0	459	-8,4	0,68

Table 41: PIFA1 performance at the top

Pifa Bi-band	Results						
	$f_R$ [MHz]	S11 [db]	$\eta$	Q	Bw [MHz]	S11 @ $f_0$	Mismatch loss
PIFA3_Bottom_hand1_900	863	-27,5	0,49	7	124	-6,8	1,02
PIFA3_Bottom_hand1_1900	1819	-12	0,39	5,1	355	-6,6	1,07
PIFA3_Bottom_hand2_900	862	-27,3	0,48	7	123	-6,7	1,04
PIFA3_Bottom_hand2_1900	1817	-12	0,38	5	354	-6,5	1,10
PIFA3_Bottom_hand3_900	864	-25,8	0,49	7,2	121	-6,9	0,99
PIFA3_Bottom_hand3_1900	1818	-12	0,38	5,2	351	-6,6	1,07
PIFA3_Bottom_hand4_900	862	-15,2	0,43	4	214	-8,8	0,61
PIFA3_Bottom_hand4_1900	1933	-15,5	0,54	5,8	333	-15,5	0,12
PIFA3_Bottom_hand5_900	861	-14,8	0,44	4	218	-9,75	0,49
PIFA3_Bottom_hand5_1900	1927	-15,7	0,55	5,8	331	-15,7	0,12
PIFA3_Bottom_hand6_900	862	-15	0,44	4	218	-8,8	0,61
PIFA3_Bottom_hand6_1900	1927	-15,4	0,55	5,7	335	-15,7	0,12

Table 42: PIFA1 performance at the bottom

**D.4. PIFA4**

Pifa Bi-band	Results						
	$f_R$ [MHz]	S11 [db]	$\eta$	Q	Bw [MHz]	S11 @ $f_0$	Mismatch loss
Pifa4_900_freespace	958	-24,6	1,0	6,5	147	-	0,02
Pifa4_1800_freespace	1800	-14,3	1,0	14	129	-	0,16
Pifa4_hand1_900	859	-15,5	0,35	1,1	813	-2,7	3,34
Pifa4_hand1_1800	1707	-10,2	0,37	2,5	676,4	-5,8	1,33
Pifa4_hand2_900	804	-11,6	0,26	1,3	612	-1,1	6,5
Pifa4_hand2_1800	1745	-23,7	0,37	7,2	241	-9,9	0,47
Pifa4_hand3_900	864	-16	0,36	1,4	618	-2,3	3,86
Pifa4_hand3_1800	1780	-17	0,42	12,5	143	-14,4	0,16
Pifa4_hand4_900	892	-7,7	0,39	1,2	715	-5,3	1,52
Pifa4_hand4_1800	1753	-16,7	0,5	5,4	324	-11,36	0,33
Pifa4_hand5_900	862	-6,9	0,38	1,7	494	-3,83	2,32
Pifa4_hand5_1800	1777	-40	0,53	8,7	294	-17,54	0,08
Pifa4_hand6_900	893	-6,8	0,41	1,4	629	-5,2	1,56
Pifa4_hand6_1800	1782	19	0,56	11,2	159	-16,1	0,11

Table 43: PIFA1 performance at the top

Pifa Bi-band	Results						
	$f_R$ [MHz]	S11 [db]	$\eta$	Q	Bw [MHz]	S11 @ $f_0$	ML
Pifa3_900_freespace	958	-24,6	1,01	6,5	147	-	0,02
Pifa3_1800_freespace	1800	-14,3	1,01	14	129	-	0,16
Pifa3_bottom_hand1_900	840	-13,3	0,31	0,2	4646	-2,2	4,01
Pifa3_bottom_hand1_1800	1709	-10,8	0,35	2,9	596	-6,1	1,22
Pifa3_bottom_hand2_900	790	-10,5	0,25	2,4	334	-0,9	7,28
Pifa3_bottom_hand2_1800	1744	-34,6	0,40	8,6	202	-9,7	0,49
Pifa3_bottom_hand3_900	919	-18,7	0,48	4,1	225	-7,0	0,97
Pifa3_bottom_hand3_1800	1797	-16,0	0,46	13,5	133	-15,9	0,11
Pifa3_bottom_hand4_900	864	-6,5	0,37	1,6	549	-4,4	1,96
Pifa3_bottom_hand4_1800	1745	-14,5	0,44	4,6	375	-9,9	0,47
Pifa3_bottom_hand5_900	858	-6,4	0,38	1,7	503	-3,9	2,27
Pifa3_bottom_hand5_1800	1773	-30,9	0,50	9,0	196	-16,1	0,11
Pifa3_bottom_hand6_900	927	-7,6	0,46	1,0	898	-7	0,97
Pifa3_bottom_hand6_1800	1780	-19,8	0,54	11,3	158	-15,7	0,12

Table 44: PIFA1 performance at the bottom

## D.5. FICA

FICA	Results						
	$f_R$ [MHz]	S11 [db]	$\eta$	Q	Bw [MHz]	S11 @ $f_0$	Mismatch loss
FICA_hand1_900	779	-17,0	0,29	3,1	252	-2,0	4,33
FICA_hand1_1800	1811	-49,6	0,36	13,0	139	-22,9	0,02
FICA_hand2_900	833	-17,3	0,34	4,9	171	-3,2	2,83
FICA_hand2_1800	1799	-34,9	0,35	12,9	139	-31,1	0,00
FICA_hand3_900	806	-9,9	0,28	2,2	369	-2,3	3,86
FICA_hand3_1800	1785	-21,2	0,38	7,7	240	-16,8	0,09
FICA_hand4_900	835	-9,8	0,38	1,8	474	-5,5	1,44
FICA_hand4_1800	1789	-34,5	0,49	11,5	155	-20,3	0,04
FICA_hand5_900	851	-8,8	0,40	1,8	484	-5,8	1,33
FICA_hand5_1800	1784	-32,7	0,52	11,6	154	-17,2	0,08
FICA_hand6_900	832	-6,7	0,38	0,7	1139	-4,6	1,85
FICA_hand6_1800	1773	-25,7	0,55	9,7	183	-13,5	0,20

Table 45: PIFA1 performance at the top

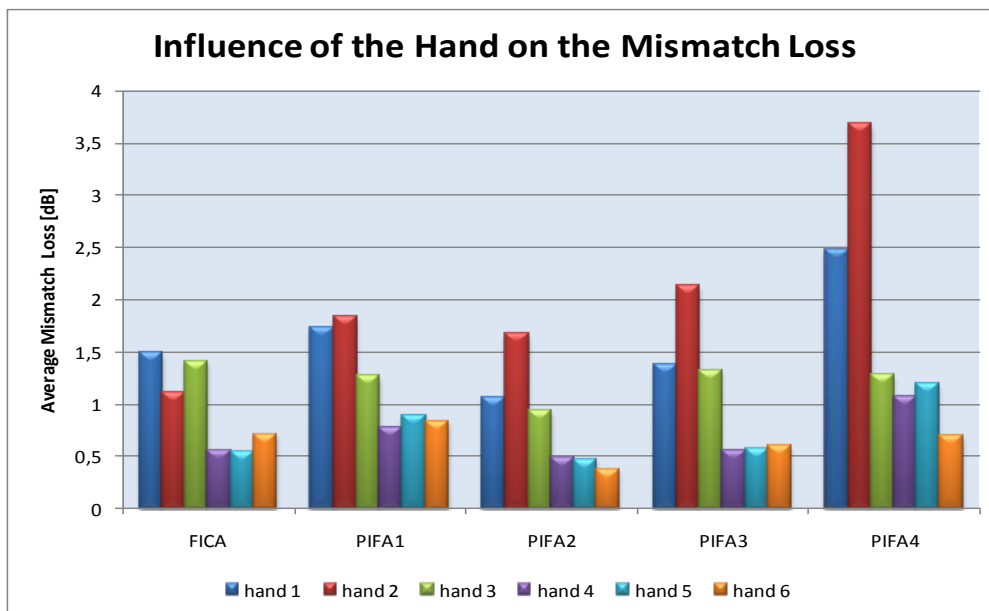
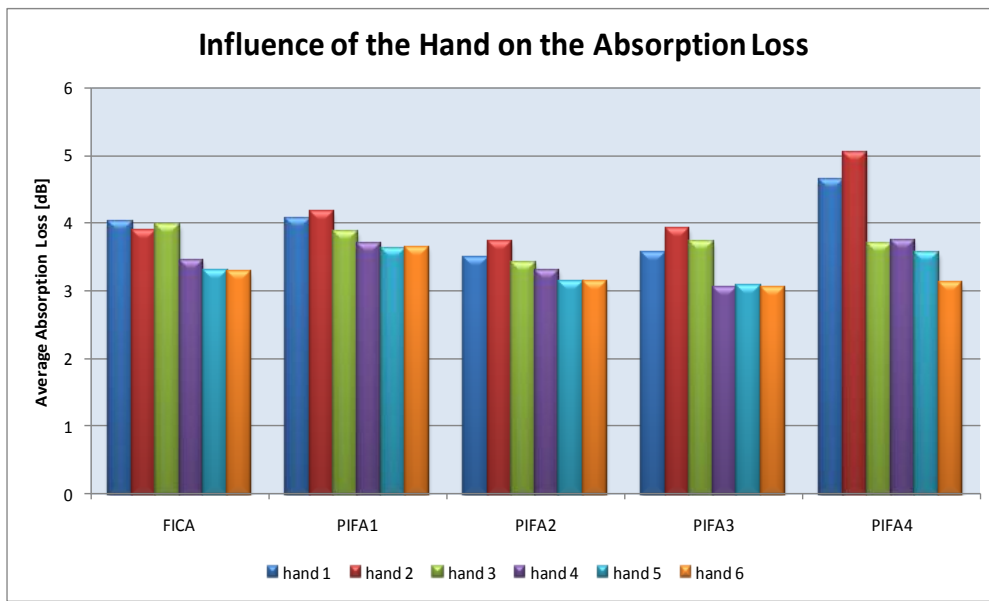
FICA	Results						
	$f_R$	S11	$\eta$	Q	Bw	S11 @	Mismatch
FICA_bottom_hand1_900	870	-24,2	0,51	9,8	892	-5,1	1,61
FICA_bottom_hand1_1800	1813	-29,7	0,47	10,1	179	-22	0,02
FICA_bottom_hand2_900	869	-24,1	0,51	9,8	888	-5,1	1,61
FICA_bottom_hand2_1800	1814	-30,8	0,46	10,2	178	-21,6	0,03
FICA_bottom_hand3_900	871	-22,6	0,52	10,2	858	-5,1	1,61
FICA_bottom_hand3_1800	1814	-31,4	0,47	10,2	177	-21	0,03
FICA_bottom_hand4_900	885	-11	0,4	2,9	309	-8,2	0,71
FICA_bottom_hand4_1800	1807	-24,2	0,56	21,8	141	-22,9	0,02
FICA_bottom_hand5_900	884	-10,7	0,41	2,7	325	-8,2	0,71
FICA_bottom_hand5_1800	1807	-25,2	0,56	12,5	144	-23,7	0,02
FICA_bottom_hand6_900	884	-10,8	0,42	2,8	318	-8,1	0,73
FICA_bottom_hand6_1800	1807	-24,7	0,56	12,6	144	-23,1	0,02

Table 46: PIFA1 performance at the bottom

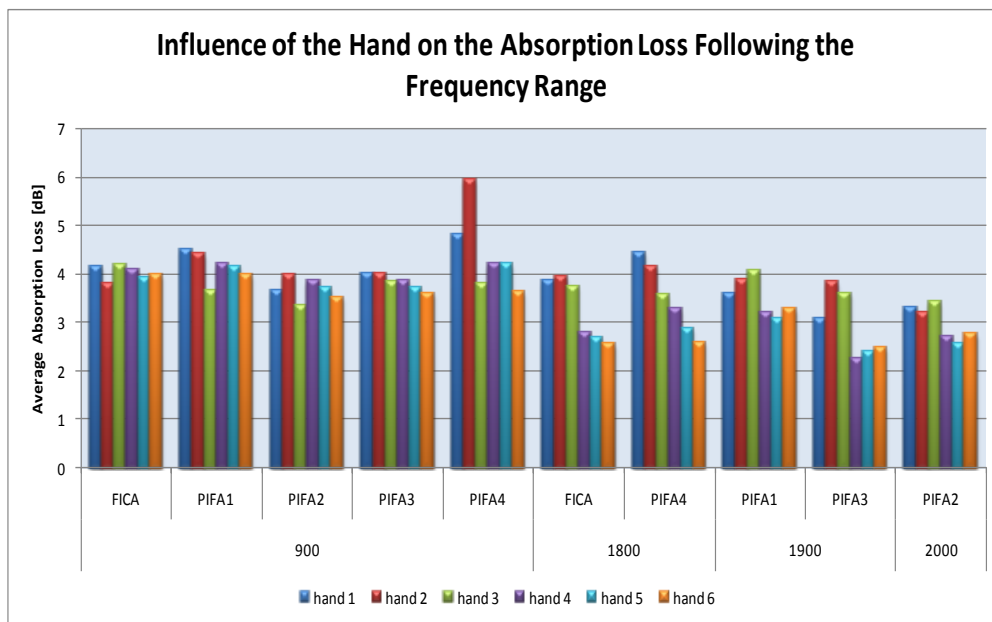
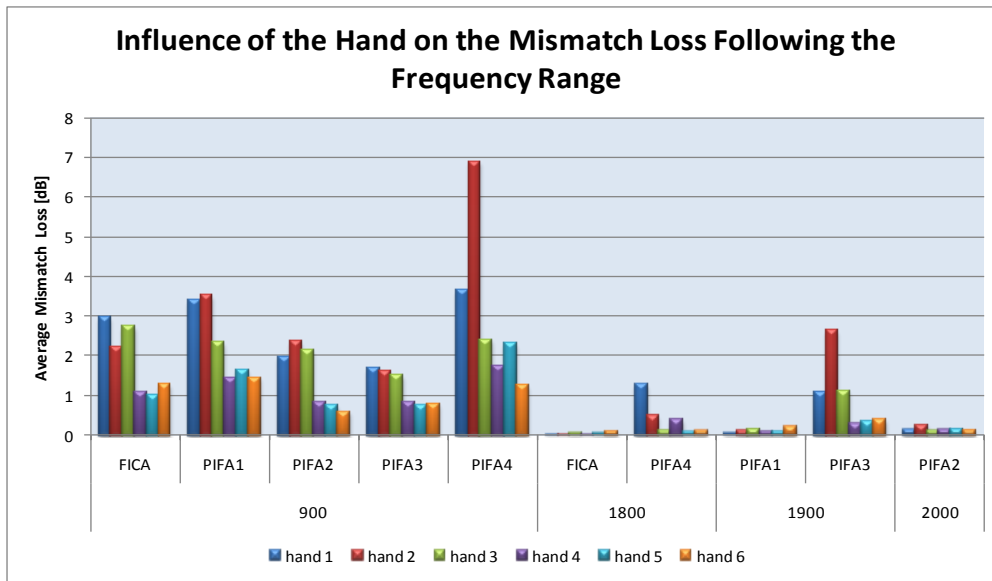
# APPENDIX E: COMPARATIVE STUDY

In this Appendix, the figures presented in the section 3.4 are displayed at a more visual scale.

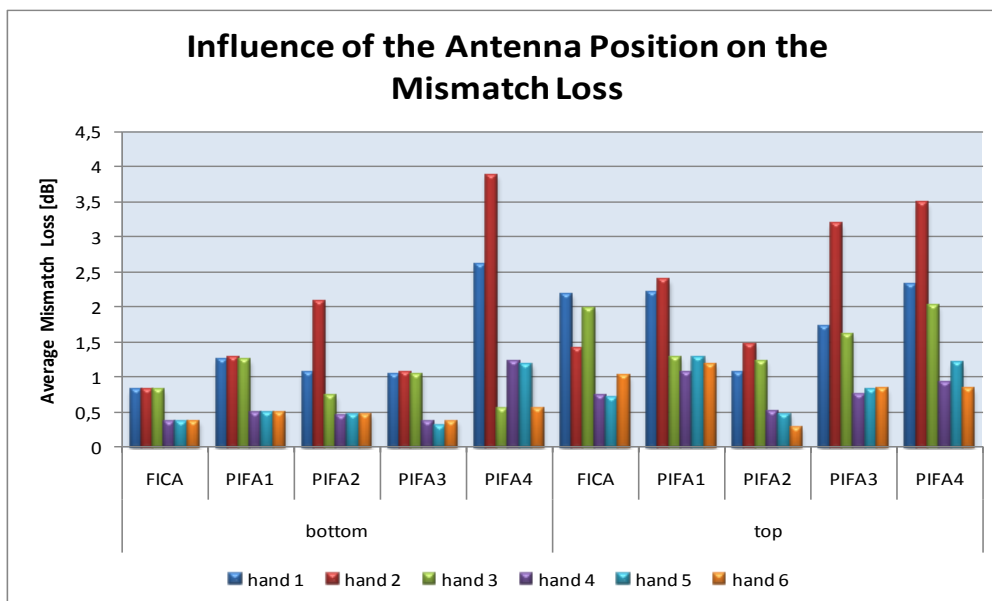
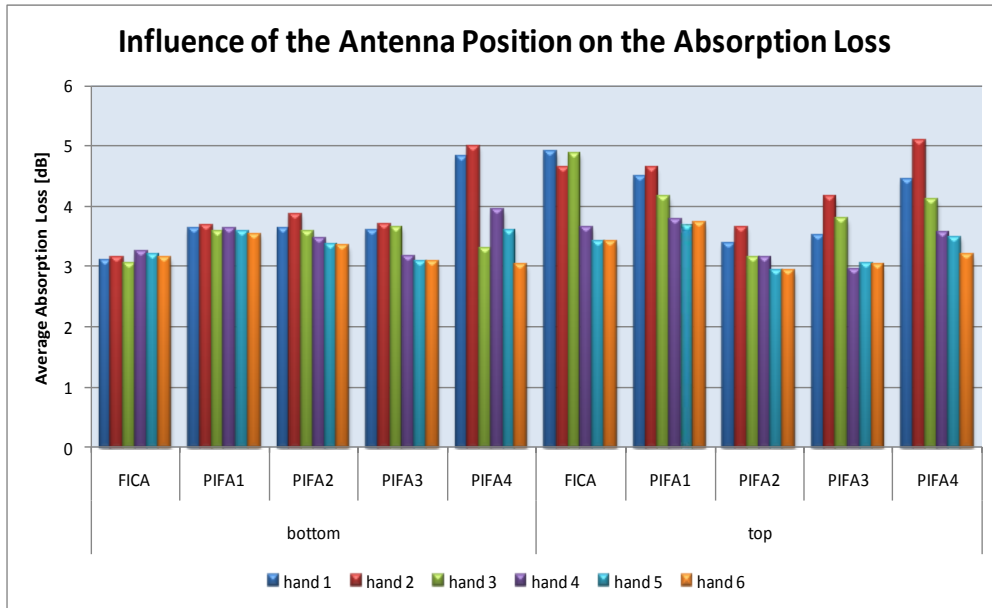
## 1) The six hand models comparison



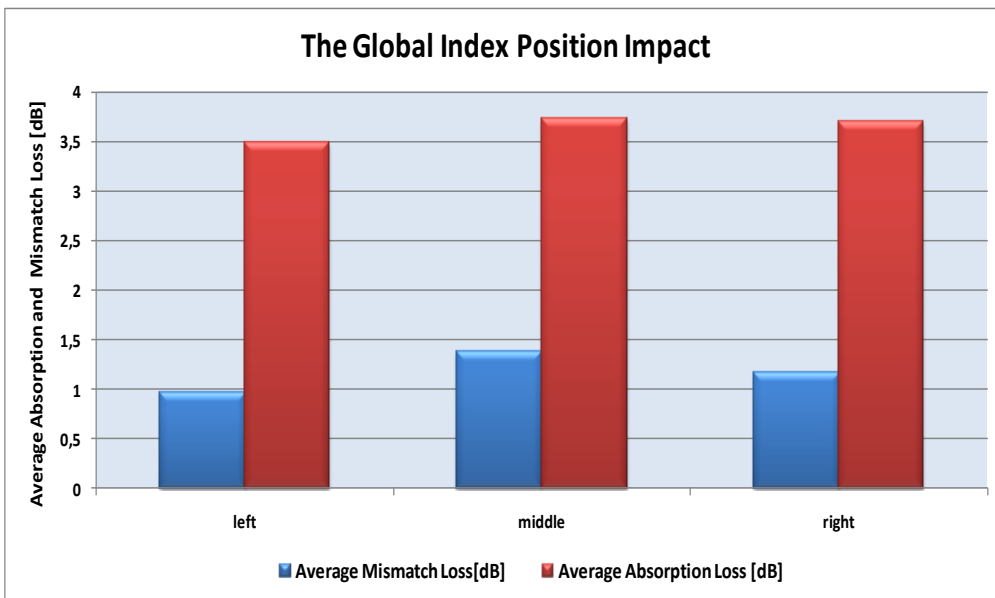
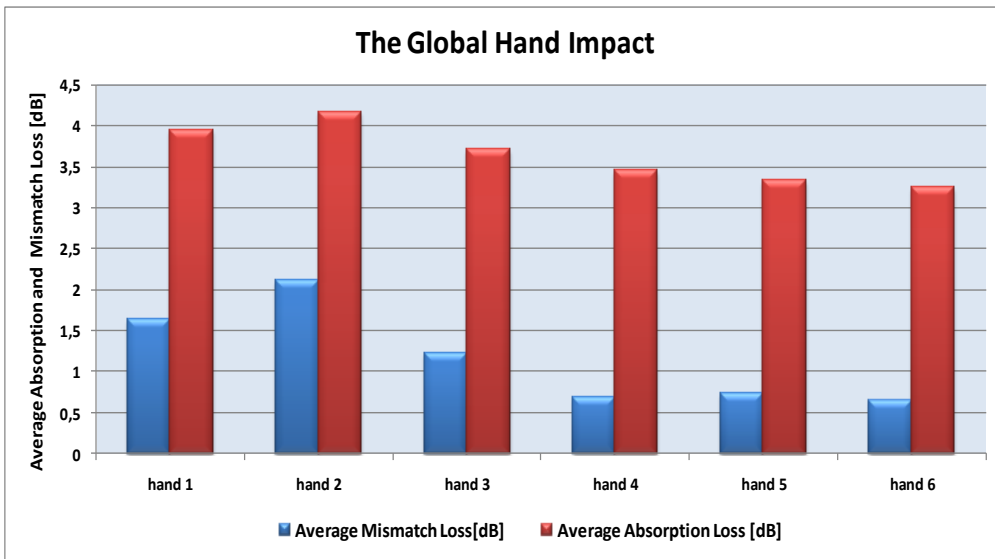
2) Hands influence study according to the frequency range



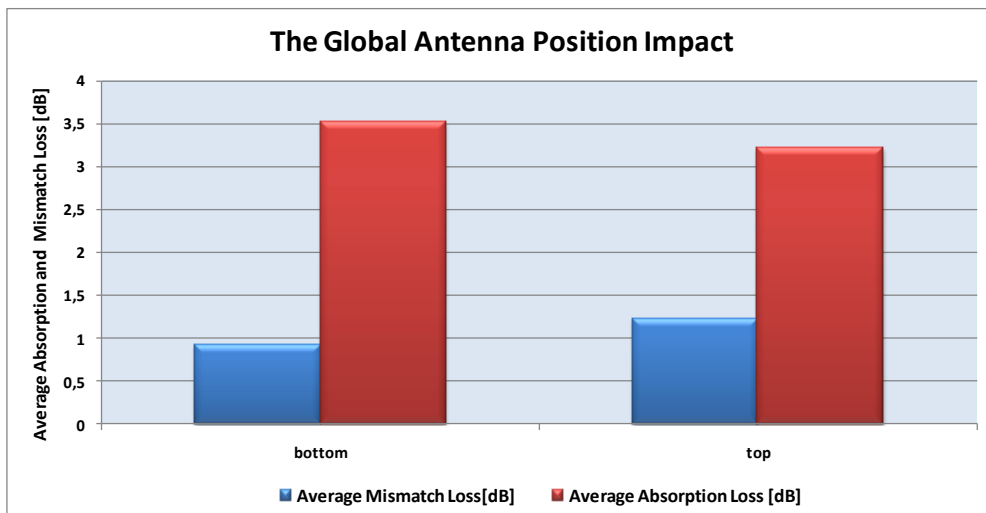
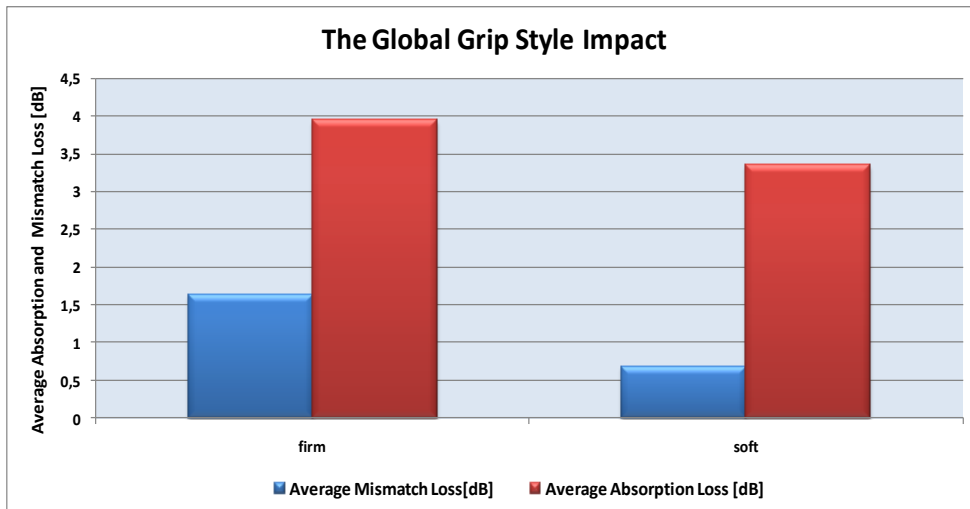
3) Antenna position (top or bottom localization) influence following the six hands



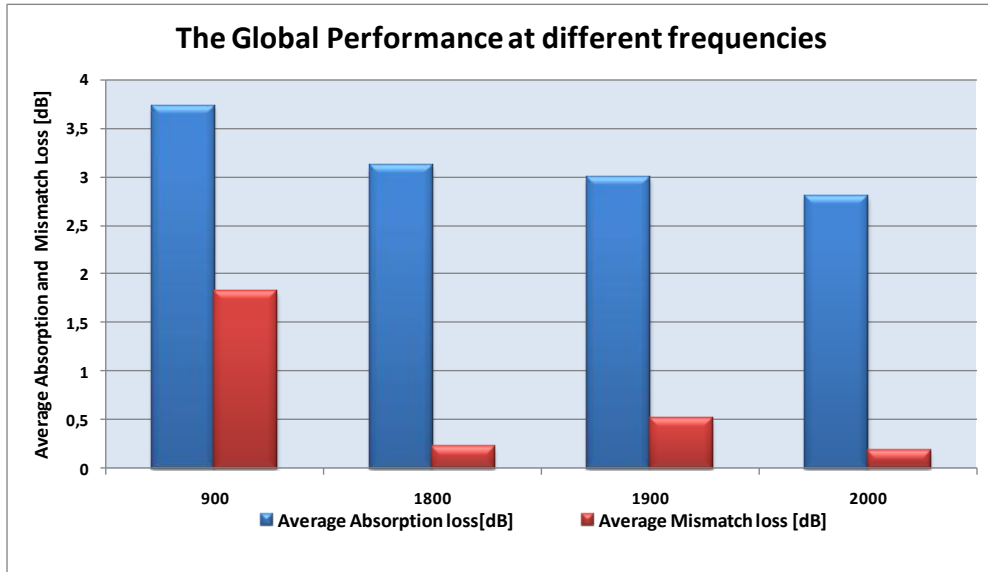
4) Hand position and Index Position impact on mismatch and absorption loss merged



5) Grip style and Antenna Position impact on mismatch and absorption loss merged



6) Global antenna performance on mismatch and absorption loss merged



# APPENDIX D: FREQUENCY BANDS USED IN WIRELESS PERSONAL COMMUNICATIONS

The chart following chart presents the general bands allocation, which may vary for different geographical regions.

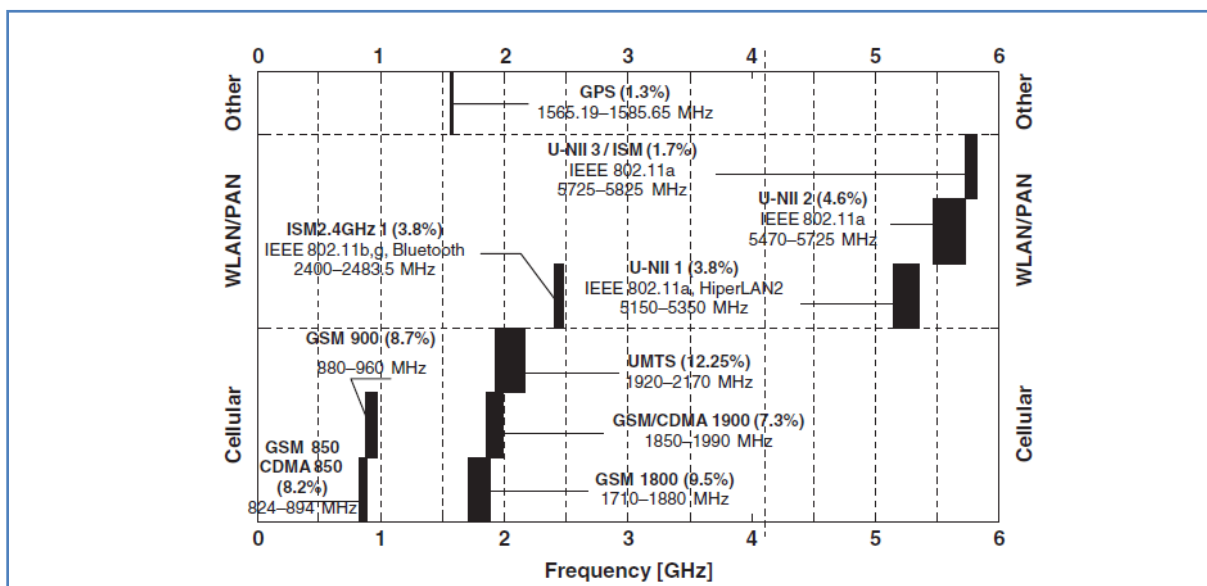


Figure 71: Overview of wireless bands widely used in wireless personal communications